TM No. 941015

NAVAL UNDERSEA WARFARE CENTER - DETACHMENT NEW LONDON
NEW LONDON, CONNECTICUT 06320

Technical Memorandum

ADAPTIVE-ADAPTIVE NARROWBAND SUBARRAY BEAMFORMING

Date: 10 February 1994

Prepared by: James A. Nuttall
James A. Nuttall
Advanced Engineering Division
Submarine Sonar Department

Report Documentation Page

Form Approved
OMB No. 0704-0188

1. REPORT DATE	2. REPORT TYPE	3. DATES COVERED
10 FEB 1994	**Technical Memorandum**	**10-02-1994 to 10-02-1994**

4. TITLE AND SUBTITLE	5a. CONTRACT NUMBER
Adaptive-Adaptive Narrowband Subarray Beamforming	5b. GRANT NUMBER
	5c. PROGRAM ELEMENT NUMBER
6. AUTHOR(S)	5d. PROJECT NUMBER
James Nuttall	5e. TASK NUMBER
	5f. WORK UNIT NUMBER
7. PERFORMING ORGANIZATION NAME(S) AND ADDRESS(ES)	8. PERFORMING ORGANIZATION REPORT NUMBER
Naval Undersea Warfare Center - Detachment New London,New London,CT,06320	**TM 941015**
9. SPONSORING/MONITORING AGENCY NAME(S) AND ADDRESS(ES)	10. SPONSOR/MONITOR'S ACRONYM(S)
Office of Naval Research	**ONR**
	11. SPONSOR/MONITOR'S REPORT NUMBER(S)

12. DISTRIBUTION/AVAILABILITY STATEMENT

Approved for public release; distribution unlimited

13. SUPPLEMENTARY NOTES

NUWC2015 This document was prepared as a Master's Thesis for a Master of Science of Electrical Engineering at the University of Connecticut, Storrs, CT.

14. ABSTRACT

A two-stage adaptive narrowband beamformer is introduced. Adaptive beamformers give high-resolution angle-of-arrival estimates, but at considerable computational cost. To reduce the computational cost, Abraham and Owsley have introduced a two-stage beamformer -- "conventional" first-stage, adaptive second-stage -- which gives near full adaptive resolution. This beamformer, however, can produce spatial aliases, or "false alarms," in the presence of dominant interferers. This memorandum introduces an adaptive-adaptive beamformer which does not produce false alarms, while maintaining near full adaptive resolution and low computational cost.

15. SUBJECT TERMS

beamformer; adaptive beamformer; adaptive-adaptive beamformer

16. SECURITY CLASSIFICATION OF:			17. LIMITATION OF ABSTRACT	18. NUMBER OF PAGES	19a. NAME OF RESPONSIBLE PERSON
a. REPORT	b. ABSTRACT	c. THIS PAGE			
unclassified	**unclassified**	**unclassified**	**Same as Report (SAR)**	**136**	

ABSTRACT

A two-stage adaptive narrowband beamformer is introduced. Adaptive beamformers give high-resolution angle-of-arrival estimates, but at considerable computational cost. To reduce the computational cost, Abraham and Owsley have introduced a two-stage beamformer — "conventional" first-stage, adaptive second-stage — which gives near full adaptive resolution. This beamformer, however, can produce spatial aliases, or "false alarms," in the presence of dominant interferers. This memorandum introduces an adaptive-adaptive beamformer which does not produce false alarms, while maintaining near full adaptive resolution and low computational cost.

ADMINISTRATIVE INFORMATION

This document was prepared as a Master's Thesis for a Master of Science of Electrical Engineering at the University of Connecticut, Storrs, CT. Technical advisers are Dr. P. Willett, Professor at University of Connecticut, Storrs, CT, Dr. C. Knapp, Professor at University of Connecticut, Storrs, CT, and Dr. N. Owsley, Senior Scientist at Naval Undersea Warfare Center, New London Detachment.

ACKNOWLEDGEMENTS

Appreciation is gratefully extended to Dr. D. Abraham, who reviewed the final draft of the text. This work was sponsored in part by the Office of Naval Research.

Reverse Blank

Contents

List of Tables

List of Figures

Chapter 1

Introduction

Narrowband adaptive beamforming using an array of sensors gives better resolution of two or more sources than conventional phase-adjust-and-sum beamforming techniques; this resolution improvement, however, requires a considerable increase in calculation burden. Since modern arrays can have numbers of sensors reaching into the hundreds, there is an interest in finding methods of reducing the numerical complexity of implementing adaptive algorithms. The most promising methods for decreasing the burden of adaptive algorithms involve techniques which reduce the numerical complexity of the adaptive problem, while maintaining performance near that of "full" narrowband beamforming. Note that the term "narrowband" refers to frequency band, not angular band.

Two general methods for reducing the size or dimension of the adaptive beamformer have been proposed: first, the effective number of sensors can be reduced [1], and, second, the dimension of the signal-subspace [2, 3] can be reduced. Both techniques can be used together to achieve even greater savings [1]. This thesis will concentrate on the first technique only.

Abraham and Owsley [1] have presented a technique, termed "subarray preprocessing" adaptive beamforming, for reducing the effective number of sensors. This method is a two-stage beamformer where the first stage performs conventional, Fourier-based (phase-adjust-and-sum) beamforming and the second stage performs adaptive beamforming. It is termed "subarray" beamforming because the first stage beamformer operates on segments of the full array termed "subarrays." The reduction in complexity is derived from the smaller dimension in the second stage adaptive beamformer. This beam-

former is termed a conventional subarray-adaptive full array (CSA/AFA) beamformer.

The CSA/AFA beamformer yields near optimal performance, in most scenarios, provided care is taken to preserve the "aperture" generated by the subarrays. In this thesis it is shown that the subarray processing reduces the effective aperture of the full array beamformer and, consequently, reduces the resolution capability of the adaptive beamformer. It is also shown that for the CSA/AFA beamformer most of the aperture can be retained, and that there is a tradeoff between effective aperture and algorithmic complexity.

This CSA/AFA beamformer is very promising, and it is natural to explore its extension to an adaptive-adaptive (ASA/AFA) scheme, one in which the subarray beamforming and full-array recombination are both adaptive. This is the subject of this thesis: how should an adaptive-adaptive subarray beamformer be implemented, and is there any advantage in its use? It will be shown that ASA/AFA is preferable to CSA/AFA because there is a reduced sensitivity to jammers, which can spatially alias through the sidelobes of a CSA/AFA subarray beamformer.

In comparison to CSA/AFA, the ASA/AFA beamformer increases the degrees of freedom for the adaptive problem, and it is important to gauge how computationally intensive this algorithm is. It is shown, for systems with nearly full effective aperture, that the ASA/AFA beamformer is roughly equivalent to CSA/AFA in numerical complexity and, as the effective aperture decreases below approximately 80%, that the CSA/AFA is less complex.

The most obvious approach to the design of an ASA/AFA beamformer is to use a Minimum Variance Distortionless Response (MVDR) technique at both the subarray and full array level; that is, to minimize the output power of all subarrays (subject to a "distortionlessness" constraint in the specified look-direction), and to do the same for the full array. It turns out that this performs very poorly in many cases of interest: qualitatively, what often happens, particularly when there is interference angularly close to the desired look direction, is that the subarray main beams become severely distorted and effective recombination is impossible.

An optimal two stage ASA/AFA scheme requires a time-consuming nonlinear joint optimization over the subarray filter weights and the full array filter weights; thus, it is not a likely candidate for a practical system. Its performance is worth examining, however, since it lends insight. From simulation results of an optimal two-stage adaptive beamformer, it has been

observed that the subarray beamformer naturally cancels angularly-distant interferers, while the full array beamformer cancels angularly-close interferers. Therefore, our design philosophy for an ASA/AFA beamforming system is to:

- at the subarray level, constrain the mainlobe to a constant shape, allowing adaptivity and noise cancellation in the sidelobes only, and
- at the full array level, constrain the beamformer in the look direction, allowing noise cancellation to occur everywhere else.

In this thesis we explore the following possible ways to achieve these goals:

- point-constraints on the main lobe shape (a generalization of the MVDR)
- an integral constraint on the main lobe (as in [4])
- a white-noise gain constraint

These may be used separately or together, and may be "hard" or applied via a penalty [5]. The most successful technique appears to use an integral mainlobe constraint, implemented via a penalty.

Chapter 2

Narrowband Beamforming

A general introduction to narrowband beamforming and motivation for its use are given in this section.

Background and notational development are covered in section 2.1. In section 2.2, a description of narrowband beamforming is discussed and the definitions of conventional and adaptive narrowband beamforming are presented. This discussion will focus on beamforming which uses sensor data for input. The response pattern and the beampattern are described in section 2.3. The response pattern and beampattern are tools for evaluating beamforming system performance. A technique termed "subarray beamforming" is described in section 2.4. Subarray beamforming is a two-stage beamformer which results in significant computational savings.

2.1 Background

Narrowband beamforming is the process by which a set of sensors "listen" to a single frequency source emanating from one spatial direction, in the presence of noise and interference arriving from many directions. There are many techniques for performing narrowband beamforming, but in its simplest form it first uses a temporal Fourier transform to listen to a single frequency, and then uses a second spatial Fourier transform to listen in one direction—narrowband beamforming can be viewed as a two-dimensional transform of the temporally and spatially sampled sensor data.

The availability of fast Fourier transforms (FFTs) permits the transfor-

mation of sensor data into the frequency domain and then into the spatial domain with minimal computational load and a minimum memory requirement. From a practical point of view, this makes narrowband beamforming attractive.

In the sections which follow, a model describing narrowband beamforming is given, and, using this model, the response of the an array of sensors to sources and noise is derived. These developments will be used extensively in the definition of narrowband beamforming

2.1.1 Narrowband Beamforming Model

In this section the "model" used for narrowband beamforming is defined. The model describes the type of source, the propagation of source energy to the sensors, and the physical placement of sensors. This model defines the basic set of assumptions used in beamforming in this paper.

A narrowband beamforming model is given in Figure 2.1. The figure shows a single source at angle θ emitting a sinusoidal tone at frequency f. The emitted wave travels through a propagation medium with speed v. The wavefront impinges on M equi-spaced sensors in a linear array with various delays due to the position of the sensors, the source location, the source's frequency, and the speed of propagation.

In the most general scenario, the sensors can have non-uniform sensitivities (or the paths from the source to each sensor may have non-uniform attenuation), the sensors can be arranged in a non-linear array, and the source may be placed close to the array. In this paper, the following assumptions will be made:

- The array will be considered linear,
- All sensors will have equal sensitivity,
- The propagation speed v between source and sensor is constant,
- The spacing between adjacent sensors d will be equal, and
- The source will be assumed distant enough from the array that, if lines were drawn from the source to any two sensors, then the lines would be considered parallel ("far-field").

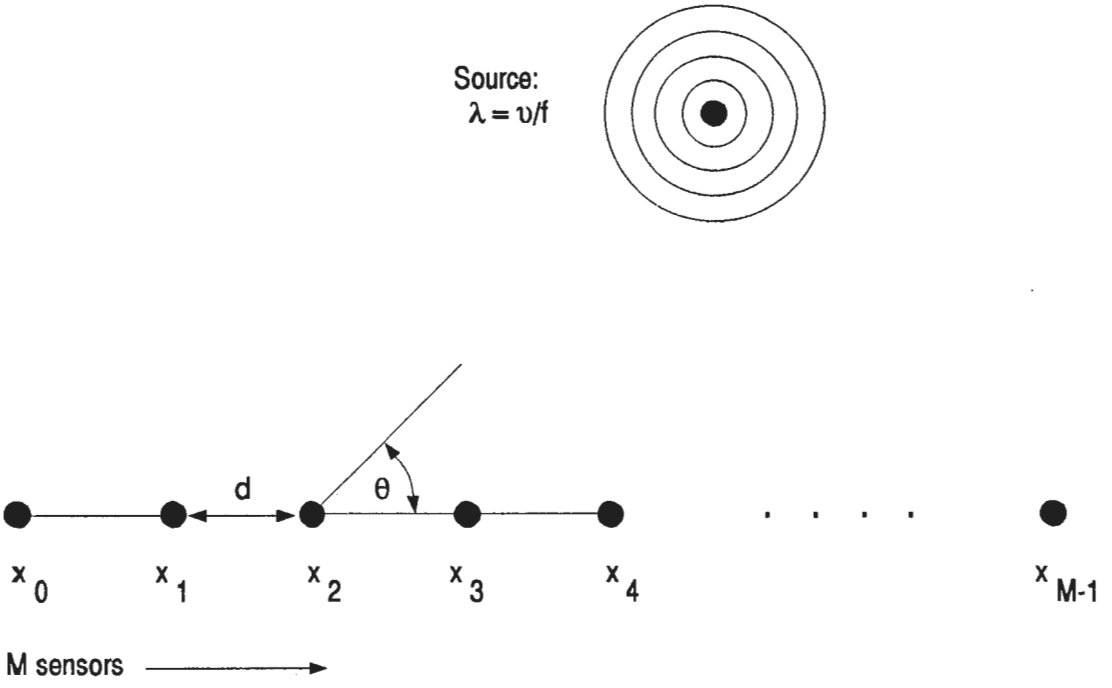

Figure 2.1: Narrowband Beamforming Model

These assumptions do not restrict the use of the techniques introduced in this paper, but the more general scenario is beyond the scope of this paper.

2.1.2 Narrowband Beamformer Array Response

In the previous section the model used in narrowband beamforming was presented. Using this model, it is desired to form an estimate of the waveform arriving from a given angle. In order to form this estimate, it is necessary to mathematically define the response of the array to external excitations. In this section, the response of an array of sensors to, first, a single source, and, second, to multiple sources and noise is given.

The single source of Figure 2.1 is emitting the signal

$$s(t) = A_0 \cos(2\pi f t + \gamma_0). \tag{2.1}$$

Here A_0 is the signal's maximum amplitude, and γ_0 is an arbitrary phase angle for the source.

In narrowband beamforming it is required to establish the relationship between the time domain signal $s(t)$ and the DFT coefficient at each sensor. To do this, the signal heard at each sensor and the Fourier Transform of that signal need to be formulated. Given the assumptions made above, it can be seen that the signal present at the m^{th} sensor will be the same signal emitted by the source, after accounting for the delay introduced by signal propagation from the source to signal. Defining a "bulk delay" as the time necessary to travel from the source to the first sensor, that is sensor 0, then the delay from the source to the m^{th} sensor is equal to the bulk delay plus the additional delay to the m^{th} sensor,

$$\begin{aligned} \tau_m &= \tau_{bulk} + \tau_{0m} \\ &= \tau_0 + \tau_{0m} \\ &= \tau_0 - md\cos\theta/v. \end{aligned} \tag{2.2}$$

Here

- d is the distance between adjacent sensors in an equi-spaced, linear array,
- τ_m is the delay from the source at θ to the m^{th} sensor,

- τ_{bulk} is the delay from the source at θ to the first sensor, and
- τ_{0m} is the additional delay required to reach the m^{th} sensor.

Using the delays of (2.2), the signal present at the m^{th} sensor is

$$\begin{aligned} s_m(t) &= A_0 \cos(2\pi f(t - \tau_m) + \gamma_0) \\ &= A_0 \cos(2\pi f(t - (\tau_{bulk} + \tau_{0m})) + \gamma_0) \\ &= A_0 \cos(2\pi f(t - \tau_{bulk} + md\cos\theta/v + \gamma_0). \end{aligned} \tag{2.3}$$

The narrowband coefficient for the m^{th} sensor can now be found from (2.3), but, first, in order to find a simple (and intuitive) expression for the narrowband coefficient, assume that:

- The source frequency f occurs at the center of a DFT, that is

$$f = \frac{k}{NT}, \tag{2.4}$$

  where k is an integer, N is the number of time samples taken, and T is the sampling interval.
- The source is uniformly sampled at time $t_n = nT$, where n is the time sample index.
- An N point DFT is used to calculate the narrowband coefficient at frequency f.

Using these assumptions and the time domain signal (2.3), the narrowband coefficient for the m^{th} sensor is

$$\begin{aligned} s_m(f,\theta) = s_m(\theta) &= \sum_{n=0}^{N-1} A_0 \cos(2\pi f(t_n - \tau_m) + \gamma_0) \exp(-j2\pi f t_n) \\ &= \sum_{n=0}^{N-1} A_0 \cos(2\pi kn/N - 2\pi f\tau_m + \gamma_0) \exp(-j2\pi kn/N) \\ &= A_0 \exp(-j(2\pi f\tau_m - \gamma_0))\frac{N}{2} \\ &= \frac{A_0 N}{2} \exp(j2\pi fmd\cos\theta/v) \exp(-j(2\pi f\tau_0 - \gamma_0)) \\ &= A\exp(j\gamma)\exp(j2\pi fmd\cos\theta/v) \\ &= \dot{A}\exp(j\Omega_\theta md), \end{aligned} \tag{2.5}$$

where

$$\begin{aligned} \gamma &\equiv \gamma_0 - 2\pi f \tau_0, \\ \Omega_\theta &\equiv 2\pi f \cos\theta / v \text{ and} \\ \dot{A} &\equiv A \exp(j\gamma). \end{aligned}$$

The narrowband coefficient's amplitude ($A = A_0 N/2$) is the signal's amplitude scaled by the constant gain of the DFT operation, and the arbitrary phase of arrival, γ, is equal to the source's phase, rotated by an amount proportional to the bulk propagation time (to sensor 0). The final term in (2.5) is the most important, because it depends on the spatial angle of arrival; it is this information that the beamformer will exploit.

It will be convenient to define a signal vector response for the narrowband coefficients,

$$\begin{aligned} \mathbf{s}(f,\theta) &= \mathbf{s}(\theta) \\ &= \left[\begin{array}{cccc} s_0(\theta) & s_1(\theta) & \cdots & s_{M-1}(\theta) \end{array} \right]^T \\ &= A \exp(j\gamma) \left[\begin{array}{cccc} 1 & \exp(j\Omega_\theta d) & \cdots & \exp(j(M-1)\Omega_\theta d) \end{array} \right]^T \\ &= \dot{A}\mathbf{d}(\theta) \end{aligned} \tag{2.6}$$

Here $\mathbf{d}$ is the $M \times 1$ array response vector to a *unit amplitude source* at θ (with zero phase referenced to the first sensor), and $\mathbf{s}$ is the $M \times 1$ array response to the source with amplitude A, phase of arrival γ, and angle of arrival θ. Vectors, shown as lower case boldface letters, are assumed to be columns, and the superscript "T" is the vector or matrix transpose operator.

The model of Figure 2.1 shows only one source. A more practical model includes multiple sources and also additive "white noise." Here white noise means the noise is uncorrelated from sensor to sensor; that is, the noise is spatially white. The multiple sources could represent, in the sonar environment for example, several cargo ships passing the array of sensors, and the white noise could represent omni-directional, independent, external noise or electronic noise internal to the sensors.

In the presence of multiple sources and additive noise, the narrowband coefficient for the m^{th} sensor is

$$x_m(f) = x_m = \sum_{s=1}^{S} s_{ms} + n_m \tag{2.7}$$

Here s_{ms} is the signal component of the s^{th} source at the m^{th} sensor, where it is assumed that there are a total of S sources, and n_m is the noise component of the m^{th} sensor. The dependence on frequency f is assumed, but will be suppressed for compactness of notation.

For notational convenience, vector responses for the signal and noise excitations are now defined. From (2.6), the signal vector for the s^{th} source is

$$\begin{aligned}
\mathbf{s}_s(f,\theta_s) &= \mathbf{s}_s(\theta_s) \\
&= \left[\, s_{0_s}(\theta_s) \;\; s_{1_s}(\theta_s) \;\; \cdots \;\; s_{M-1_s}(\theta_s) \,\right]^T \\
&= \dot{A}_s \left[\, 1 \;\; \exp(j\Omega_{\theta_s} d) \;\; \cdots \;\; \exp(j(M-1)\Omega_{\theta_s} d) \,\right]^T \\
&= \dot{A}_s \mathbf{d}(\theta_s) \qquad (2.8)
\end{aligned}$$

Each source is defined by its amplitude A_s, its phase of arrival γ_s, and its angle of arrival θ_s.

In Eqn. (2.8), $\mathbf{d}(\theta_s)$ is seen to be a discretely sampled complex sinusoidal signal. This is also referred to as a "steering vector," because it is used in beamforming to "electronically steer" the array sensor data in direction θ.

The noise vector response is defined as

$$\mathbf{n} = \left[\, n_0 \;\; n_1 \;\; \cdots \;\; n_{M-1} \,\right]^T. \qquad (2.9)$$

Defining the array vector response as

$$\mathbf{x} = \left[\, x_0 \;\; x_1 \;\; \cdots \;\; x_{M-1} \,\right]^T, \qquad (2.10)$$

and combining (2.7), (2.8), and (2.9) with (2.10), the array vector response is

$$\mathbf{x} = \sum_{s=1}^{S} A_s \exp(j\gamma_s)\mathbf{d}(\theta_s) + \mathbf{n}. \qquad (2.11)$$

The summation of (2.11) can be expressed in the compact matrix form

$$\sum_{s=1}^{S} A_s \exp(j\gamma_s)\mathbf{d}(\theta_s) = \left[\, \mathbf{d}(\theta_1) \;\; \mathbf{d}(\theta_2) \;\; \cdots \;\; \mathbf{d}(\theta_S) \,\right] \begin{bmatrix} A_1 \exp(j\gamma_1) \\ A_2 \exp(j\gamma_2) \\ \vdots \\ A_S \exp(j\gamma_S) \end{bmatrix}$$

$$= \mathbf{D} \begin{bmatrix} e_1 \\ e_2 \\ \vdots \\ e_S \end{bmatrix}$$
$$= \mathbf{De} \tag{2.12}$$

Here $\mathbf{D}$ is an $M \times S$ matrix, whose columns represent the unit amplitude response vectors (defined in (2.6)), and $\mathbf{e}$ is an $S \times 1$ vector comprised of the amplitude and phase of arrival for the sources. Eqn. (2.12) breaks the array response to sources into two components:

- The matrix $\mathbf{D}$ contains the deterministic information about the sources, and
- The vector $\mathbf{e}$ contains the unknown, and random, information about the sources. The vector $\mathbf{e}$ shall be called the "excitation" vector.

Inserting (2.12) into (2.11), the array vector response becomes

$$\mathbf{x} = \mathbf{De} + \mathbf{n}. \tag{2.13}$$

Eqn. (2.13) incorporates the array geometry, the signal environment, the noise environment, and the propagation medium to give the narrowband response of the array.

2.1.3 Spatial Undersampling and Aliasing

In section 2.1.2, the array response to a single source was presented and the response was seen to be a discretely sampled, complex sinusoid. As in temporal discrete signal processing, spatial signals must be sampled at or above a minimum rate to avoid aliasing. In this section, the conditions under which aliasing is avoided are investigated.

The m^{th} element of the array response to a unit amplitude source is:

$$\mathbf{d}(m, \theta) = \exp(j\Omega_\theta md), \tag{2.14}$$

where

$$\Omega_\theta \equiv 2\pi f \cos\theta / v.$$

Rearranging terms in (2.14), the element response can be represented as:

$$\mathbf{d}(m,\theta) = \exp\left[j2\pi(\cos\theta)m(d/\lambda)\right]. \tag{2.15}$$

In (2.15), λ is the signal's wavelength and the spatial equivalents of signal frequency and sampling interval can be identified as $\cos\theta$ and d/λ, respectively. Note that in this paper, spatial frequency and bandwidth refer to the cosine of arrival angle and width of cosine of arrival, respectively.

It is now possible to show when spatial aliasing will occur: spatial aliasing occurs when the magnitude of the phase differences of two consecutive samples in (2.15) exceeds π. When the phase differences exceed π, then a "positive" frequency ($\cos\theta > 0$) can not be distinguished from a "negative" frequency ($\cos\theta < 0$) and aliasing will occur. Mathematically, aliasing can be prevented provided:

$$\begin{aligned} 2\pi\left|\cos\theta\right|\frac{d}{\lambda} &\leq \pi, \\ d &\leq \frac{\lambda}{2\left|\cos\theta\right|}, \text{ or} \\ d &\leq \frac{\lambda}{2}. \end{aligned} \tag{2.16}$$

Eqn. (2.16) establishes a maximum temporal frequency

$$f \leq \frac{v}{2d} \tag{2.17}$$

which can be processed without spatial aliasing.

2.1.4 The Cross Spectral Density Matrix

In section 2.1.2, the array vector response was seen to be the summation of possibly several sinusoidal signals and noise. In beamforming applications [6] and equivalently in spectral applications [7], it is desired to form an optimal estimate of the "frequency" content of a signal. In order to form a "minimum-variance" estimate, it is necessary to calculate the second-order statistics of the array response. In this section the second-order statistics, known as the Cross Spectral Density Matrix (CSDM), are derived.

The array response of (2.13) is the output at frequency f from *one* DFT operation. That is, it is the response to data samples from one window in

time. It is desired to know the second order statistics of the array response, $\mathrm{E}[\mathbf{x}\mathbf{x}^H]$. This is known as the covariance matrix, and for narrowband data as the "cross-spectral density matrix" (CSDM) at a specific frequency,

$$\mathbf{R} = \mathrm{E}[\mathbf{x}\mathbf{x}^H]. \tag{2.18}$$

Here "E" is the statistical expectation operator, and the superscript "H" denotes the vector or matrix complex conjugate transpose operator. Matrices are shown as upper case bold letters.

Inserting (2.13) into the expectation of (2.18), the CSDM is

$$\begin{aligned} \mathbf{R} &= \mathrm{E}[\mathbf{x}\mathbf{x}^H] \\ &= \mathbf{D}\mathrm{E}[\mathbf{e}\mathbf{e}^H]\mathbf{D}^H + \mathbf{D}\mathrm{E}[\mathbf{e}\mathbf{n}^H] + \mathrm{E}[\mathbf{n}\mathbf{e}^H]\mathbf{D}^H + \mathrm{E}[\mathbf{n}\mathbf{n}^H]. \end{aligned} \tag{2.19}$$

Notice that the matrix $\mathbf{D}$ is deterministic and can be taken out of the expectation of (2.19).

With respect to (2.19), the following simplifying assumptions will be made:

- The amplitude and phase of a source are independent of the amplitude and phase of another source, that is

$$\begin{aligned} \mathrm{E}[e_s e_t] &= \begin{cases} \mathrm{E}[A_s^2] & s = t \\ 0 & s \neq t \end{cases} \\ &= \begin{cases} \sigma_s^2 & s = t \\ 0 & s \neq t \end{cases}. \end{aligned} \tag{2.20}$$

  Here e_s is the s^{th} element of the signal excitation vector, and σ_s^2 is the power of the s^{th} source.

  The excitation correlation matrix, the result of the expectation inside the first term in (2.19), becomes

$$\begin{aligned} \mathrm{E}[\mathbf{e}\mathbf{e}^H] &= \mathrm{diag}\left[\begin{array}{cccc} \sigma_1^2 & \sigma_2^2 & \cdots & \sigma_S^2 \end{array}\right] \\ &= \begin{bmatrix} \sigma_1^2 & 0 & \cdots & 0 \\ 0 & \sigma_2^2 & \ddots & \vdots \\ \vdots & \ddots & \ddots & 0 \\ 0 & \cdots & 0 & \sigma_S^2 \end{bmatrix} \equiv \mathbf{E} \end{aligned} \tag{2.21}$$

- The source's excitation is independent of the noise,

$$\mathrm{E}[[\mathbf{e}\mathbf{n}^H]_{ij}] = \mathrm{E}[[\mathbf{n}\mathbf{e}^H]_{ji}] = 0. \tag{2.22}$$

  Here $[\mathbf{e}\mathbf{n}^H]_{ij}$ is the element of the $S \times M$ matrix located in the i^{th} row and the j^{th} column. The independence of the excitation $\mathbf{e}$ and the noise $\mathbf{n}$ makes the second and third terms of (2.19) drop out.

- The noise at one sensor is independent of the noise at another sensor and the noise power is identical at each sensor,

$$\mathrm{E}[n_i n_j^*] = \begin{cases} \sigma_n^2 & i = j \\ 0 & i \neq j \end{cases}. \tag{2.23}$$

Combining (2.21), (2.22), and (2.23) in (2.19), the CSDM is expressed as

$$\begin{aligned} \mathbf{R} &= \mathrm{E}[\mathbf{x}\mathbf{x}^H] \\ &= \mathbf{D}\mathbf{E}\mathbf{D}^H + \sigma_n^2 \mathbf{I}_M, \end{aligned} \tag{2.24}$$

where $\mathbf{I}_M$ is an $M \times M$ identity matrix.

It must be noted that there are practical situations which do not fit the model of (2.24). Some examples are:

- Multi-path environments [8]: In a "multi-path" environment the signal emitted by a source will travel over two, or more, separate paths. The array will respond to the single source as if there were multiple sources, and the "sources" can be, if no signal distortion has occurred, completely correlated.

  The model can be extended to include correlated sources by putting off-diagonal terms in the excitation correlation matrix $\mathbf{E}$. However, it is beyond the scope of this paper to investigate the effects of correlated sources on narrowband beamforming.

- Angularly extended noise [9]: Angularly extended noise is generated from sources occupying a sector of space. The array response to an angularly extended source can be calculated by replacing the summation of (2.12) with an integral over space.

While it is possible to describe more general scenarios by modifying the model of (2.24), the assumptions of (2.21), (2.22), and (2.23) describe many practical environments.

2.2 Direct Narrowband Beamforming

In this section conventional and adaptive narrowband beamforming are described. These two types of beamforming systems combine the narrowband sensor data directly to form beamformer output. Here this type of system is referred to as a "direct" beamformer.

A narrowband beamforming system which could be either a conventional or adaptive beamformer is shown in Figure 2.2. In this figure, the following notation is used:

$$\begin{aligned} m &\equiv \text{sensor index,} \\ n &\equiv \text{time index,} \\ \theta &\equiv \text{angle of arrival,} \\ X_m(n) &\equiv \text{sensor time sample,} \\ x_m(f) &\equiv \text{sensor narrowband coefficient,} \\ w_m(f,\theta) &\equiv \text{beamforming coefficient, and} \\ y(\theta) &\equiv \text{beamforming output.} \end{aligned}$$

Narrowband beamforming, as shown in Figure 2.2, transforms the sensors' temporal data, phase adjusts the narrowband coefficients (compensating for spatial angle of arrival), amplitude adjusts based upon noise and signal powers, and forms a beam by coherently summing the phase and amplitude adjusted narrowband sensor data.

Two types of beamforming [10] shall be discussed in this paper:

- Direct, Full Array Beamforming: Direct beamforming combines all the sensors in the array into beams. The output shall be called a "full array beam," because the beam is formed using data from all sensors within the array. It is called "direct" beamforming because the full array beam output is created from the sensor data in one beamforming operation.

- Indirect or Subarray Beamforming: Indirect beamforming combines the sensors of the array into full array beams in two stages. The first stage of the beamforming combines a sub-part of the array's sensors, termed a "subarray", into a "subarray beam", and the second stage beamformer recombines the subarray beams into a full array beam.

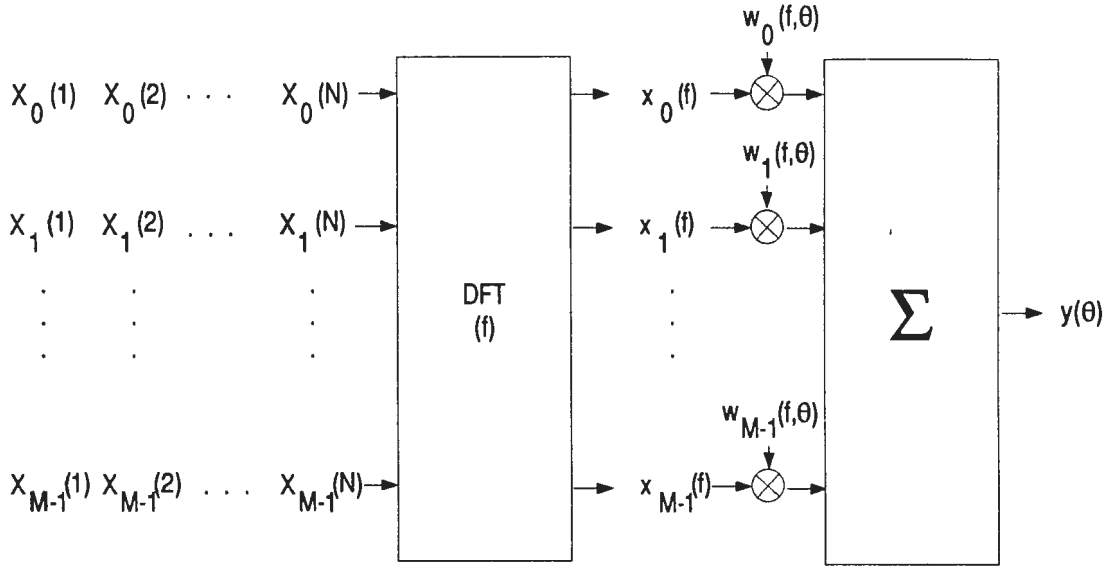

Figure 2.2: Narrowband Beamforming System

In the following sub-sections two types of "direct" beamforming are discussed:

- Direct Conventional Beamforming: Direct conventional beamforming is a spatial Fourier transform of the narrowband sensor data $\mathbf{x}$. Since it is a Fourier transform, is is computationally simple to perform. Because of its simplicity, this technique has historically been the beamformer of "choice," thus earning its name "conventional." Here the weights $w_i(f,\theta)$ in Figure 2.2 are fixed; that is, not data dependent.

- Direct Adaptive Beamforming: Direct adaptive beamforming combines the narrowband sensor data in an "optimal" fashion designed to minimize some criterion such as the power output of the operation, while maintaining a constant gain to a selected signal. In adaptive beamforming, the weights are data dependent and (as will be shown) computationally expensive to update.

2.2.1 Direct Conventional Narrowband Beamforming

Direct conventional narrowband beamforming forms an estimate of the energy arriving from a selected angle of arrival θ, by performing a spatial Fourier transform on the sensor's narrowband data. As mentioned earlier, the "direct" beamformer uses the entire set of sensor data (in one beamforming operation). As in spectral estimation, the spatial Fourier transform input data can be "windowed" to give lower sidelobe aliasing.

The spatial transform of the narrowband sensor data $\mathbf{x}$ is

$$\begin{aligned} y_c(\theta) &= \sum_{m=0}^{M-1} x_m \exp(-j2\pi f cos(\theta) md/v) \\ &= \sum_{m=0}^{M-1} x_m \exp(-j\Omega_\theta md). \end{aligned} \tag{2.25}$$

Borrowing from spectral estimation terminology, the "spatial frequency" of the transform is $\Omega_\theta = 2\pi f cos(\theta)/v$, the "spatial sampling frequency" of the signal is $1/d$, and the transform length is M. From (2.25), it is seen that narrowband beamforming is a two-dimensional transform of the original sensor data, where the first transform is from the time domain to the frequency domain and the second transform is to the spatial domain.

The spatial transform or beamforming operation of (2.25) can also be "windowed." A "window" is a set of weights $\{w_i\}_{i=0}^{M-1}$ applied to the transform input data, so that

$$y_c(\theta) = \sum_{m=0}^{M-1} x_m w_m \exp(-j\Omega_\theta md), \tag{2.26}$$

where window weights w_m satisfy the following symmetry rule:

$$w_i = w_{M-1-i}. \tag{2.27}$$

The window is used to lower the spatial sidelobes of the transform operation. Equation (2.25) is a special case of (2.26), where the window is termed the "rectangular" weighting. The summations of (2.25) and (2.26) can be expressed as the complex conjugate inner product of the sensor data and the signal steering vector at angle θ, with an optional weighting matrix W.

$$\begin{aligned} y_c(\theta) &= \begin{cases} \mathbf{d}^H(\theta)\mathbf{x} & \text{if rectangular window,} \\ \mathbf{d}^H(\theta)\mathbf{W}\mathbf{x} & \text{otherwise} \end{cases} \\ &= \tilde{\mathbf{d}}^H(\theta)\mathbf{x}, \end{aligned} \tag{2.28}$$

where the $M \times M$ diagonal weighting matrix is

$$\mathbf{W} = \text{diag}\left[\begin{array}{cccc} w_0 & w_1 & \cdots & w_{M-1} \end{array}\right]. \tag{2.29}$$

Another useful view of (2.28) is that of a correlation between the sensor data $\mathbf{x}$ and an assumed signal $\mathbf{s} = \mathbf{d}(\theta)$. Correlation "peaks" will occur where the data vector contains the embedded signal vectors $\{\mathbf{s}_i\}_{i=0}^{M-1}$. When the sensors are not equi-spaced, this view is more appropriate.

2.2.2 Direct Minimum Variance Narrowband Beamforming

Conventional beamforming systems such as (2.28) do not claim optimality except under very specific conditions. The minimum variance distortionless response (MVDR) beamformer seeks optimality in a general (least squares) sense. The MVDR beamformer uses an estimate of the surrounding environment in its calculation, and because of this estimate is known as an "adaptive" beamformer.

The MVDR beamformer is now derived. Suppose that the beamformer output is

$$y(\theta) = \mathbf{w}(\theta)^H \mathbf{x}. \tag{2.30}$$

Here $\mathbf{w}$ is the adaptive filter vector of dimension M, and $\mathbf{x}$ is the sensor data.

It is desired that the adaptive filter vector $\mathbf{w}$ satisfy two requirements:

- The expected power output of the filter is minimized.
- The signal gain at angle θ is constrained to a specific value.

It is clear that these two requirements formulate a maximum signal-to-noise ratio at the output y. Mathematically, the filter vector satisfies

$$\min_{\mathbf{w}} \left\{ \text{E}\left[|y|^2\right] \right\}, \text{ subj to } \left\{ \mathbf{w}^H \mathbf{d}(\theta) = M \right\}. \tag{2.31}$$

A signal gain of M is chosen (arbitrarily). Expanding the expected power in the beamformer output as

$$\text{E}\{|y|^2\} = \mathbf{w}^H \text{E}\left[\mathbf{x}\mathbf{x}^H\right] \mathbf{w} = \mathbf{w}^H \mathbf{R} \mathbf{w}, \tag{2.32}$$

prompts us to define the cross-spectral density matrix (CSDM),

$$\mathbf{R} = \mathrm{E}\left[\mathbf{x}\mathbf{x}^H\right]. \tag{2.33}$$

The CSDM, $\mathbf{R}$, is an $M \times M$ covariance matrix. Using the method of unknown Lagrangian multipliers, the adaptive filter vector which satisfies (2.31) is

$$\mathbf{w}(\theta) = \frac{M\mathbf{R}^{-1}\mathbf{d}(\theta)}{\mathbf{d}(\theta)^H\mathbf{R}^{-1}\mathbf{d}(\theta)}. \tag{2.34}$$

Interestingly, if the environment contains only "white noise" ($\mathbf{R} = \mathbf{I}$), then the optimal filter is identical to the conventional filter vector.

$$\mathbf{w}(\theta) = \frac{M\mathbf{d}(\theta)}{\mathbf{d}(\theta)^H\mathbf{d}(\theta)} = \mathbf{d}(\theta), \text{ if } \mathbf{R} = \mathbf{I}. \tag{2.35}$$

Equation (2.35) indicates that the conventional steering vector $\mathbf{d}(\theta)$ forms an optimal estimate in white noise. Intuitively, it also indicates that the conventional steering vector is nearly optimum in spatially white noise dominated environments.

To further analyze the adaptive filter vector, employ an eigenvector-eigenvalue decomposition of the CSDM.

$$\begin{aligned}
\mathbf{R} &= \mathbf{D}\mathbf{E}\mathbf{D}^H + \sigma_n^2\mathbf{I} = \mathbf{M}_s\mathbf{\Sigma}_s\mathbf{M}_s^H + \sigma_n^2\mathbf{I} \\
&= \begin{bmatrix} \mathbf{M}_s & \mathbf{M}_n \end{bmatrix} \begin{bmatrix} \mathbf{\Sigma}_s + \sigma_n^2\mathbf{I}_S & \mathbf{0} \\ \mathbf{0} & \sigma_n^2\mathbf{I}_{M-S} \end{bmatrix} \begin{bmatrix} \mathbf{M}_s & \mathbf{M}_n \end{bmatrix}^H \\
&= \mathbf{M}\mathbf{\Sigma}\mathbf{M}^H,
\end{aligned} \tag{2.36}$$

where

$\mathbf{M}_s \equiv$ Eigenvectors of the "signal space" ($\mathbf{D}$),
$\mathbf{\Sigma}_s \equiv$ Eigenvalues of the signal space, and
$\mathbf{M}_n \equiv$ Eigenvectors of noise space (orthogonal to signal space).

Now substitute the eigenvector-eigenvalue decomposition of the CSDM in (2.36) and the filter vector $\mathbf{w}$ of (2.34) into the beamformer output

$$y = \mathbf{w}^H\mathbf{x} = k\mathbf{d}^H\mathbf{R}^{-1}\mathbf{x} = k\mathbf{d}^H\mathbf{M}\mathbf{\Sigma}^{-1}\mathbf{M}^H\mathbf{x}. \tag{2.37}$$

where the constant $k = M/(\mathbf{d}^H(\theta)\mathbf{R}^{-1}\mathbf{d}(\theta))$.

It is clear that if a source (embedded in $\mathbf{x}$) projects onto an eigenvector associated with a large signal eigenvalue, then its power will be attenuated by the inverse of the signal eigenvalue, provided the signal eigenvalue is sufficiently larger than the noise power. Signals other than the desired signal $\mathbf{d}(\theta)$, termed interferences, can be cancelled with this filter; cancellation occurs when the interferer projects onto different eigenvectors than the desired signal. On the other hand, if the signal eigenvalues are much smaller than the noise power, then little signal attenuation will occur.

2.3 Response Pattern and Beampattern

The development of narrowband beamforming in section (2.2) focussed on the derivation of the conventional and adaptive filter vectors; in this section we turn our attention to the performance of these beamformers. The performance will be measured with two analysis tools:

1. The response pattern. The response plots the expected power response of the beamformer, as a function of look direction θ.

2. The beampattern. The beampattern plots the "leakage" of interfering sources into the beamformer output steered at angle θ, as a function of interference angle of arrival ϕ.

To facilitate the analysis of the response pattern and beampattern, the conventional beamformer output to a single source is developed.

$$
\begin{aligned}
&\mathbf{y}_c(\theta) = \\
&= \tilde{\mathbf{d}}(\theta)^H \mathbf{s}(\phi) \\
&= \dot{A} \begin{cases} \mathbf{d}^H(\theta)\mathbf{d}(\phi) & \text{if rectangular} \\ \mathbf{d}^H(\theta)\mathbf{W}\mathbf{d}(\phi) & \text{otherwise} \end{cases} \\
&= \dot{A} \begin{cases} \exp\left(\frac{j(\Omega_\phi - \Omega_\theta)d(M-1)}{2}\right) \frac{\sin((\Omega_\phi - \Omega_\theta)dM/2)}{\sin((\Omega_\phi - \Omega_\theta)d/2)} & \text{if rectangular} \\ \exp\left(\frac{j(\Omega_\phi - \Omega_\theta)d(M-1)}{2}\right) \sum_{m=0}^{M-1} w_m \cos\frac{(\Omega_\phi - \Omega_\theta)d(2m-M+1)}{2} & \text{otherwise} \end{cases} \\
&= \dot{A} H_M(\Omega_\phi - \Omega_\theta) \qquad (2.38)
\end{aligned}
$$

This response is the well known "Dirichlet kernel" function of spectral estimation (for the rectangular window). There is a large peak response to

sources arriving in the neighborhood of θ, often termed the "mainlobe", with the maximum point corresponding to the angle of the beamformer. A signal arriving from θ will be passed without phase change and a gain factor of M. Signals arriving from angles other than θ will be attenuated, but if the signal is spatially close to θ, the conventional beamformer response will contain considerable energy from that signal.

In realistic scenarios there are several signals arriving from different angles at the same time. The beamformer output of (2.38) becomes, by superposition, a summation of many sources,

$$\begin{aligned} y_c(\theta) &= \tilde{\mathbf{d}}(\theta)^H \mathbf{x} \\ &= \tilde{\mathbf{d}}(\theta)^H (\sum_{i=1}^{S} \mathbf{s}_i(\phi_i) + \mathbf{n}) \\ &= \tilde{\mathbf{d}}(\theta)^H (\mathbf{De} + \mathbf{n}) \end{aligned} \tag{2.39}$$

For any one look direction, spatially proximate sources will contribute a portion of their energy, however the response is an estimate of the energy arriving from the beamsteering direction. The response pattern plots the squared magnitude of the beamformer output (2.39), as a function of beamformer look direction θ.

$$\begin{aligned} r_c(\theta) &= \mathrm{E}\left[|\mathbf{y}_c|^2\right] \\ &= \tilde{\mathbf{d}}^H \mathrm{E}\left[\mathbf{x}\mathbf{x}^H\right] \tilde{\mathbf{d}} \\ &= \tilde{\mathbf{d}}^H \mathbf{R} \tilde{\mathbf{d}} \\ &= \tilde{\mathbf{d}}^H \mathbf{D}\mathbf{E}\mathbf{D}^H \tilde{\mathbf{d}} + \tilde{M}, \end{aligned} \tag{2.40}$$

where $\tilde{M} = \tilde{\mathbf{d}}^H \tilde{\mathbf{d}} \sigma_n^2$.

The conventional beamformer power output is seen to be a weighted summation of responses to individual source signals. The powers of individual sources weight the inner product of the filter vector and the signal steering vector. An additive white noise constant of $\tilde{M}$ is also present.

Similarly, the expected power output for the adaptive beamformer can be defined as

$$\begin{aligned} r(\theta) &= \mathrm{E}\left[|\mathbf{y}(\theta)|^2\right] \\ &= \mathbf{w}(\theta)^H \mathbf{R} \mathbf{w}(\theta) \end{aligned}$$

$$= \frac{M^2 \mathbf{d}^H \mathbf{R}^{-1} \mathbf{R} \mathbf{R}^{-1} \mathbf{d}}{(\mathbf{d}^H \mathbf{R}^{-1} \mathbf{d})^2}$$
$$= \frac{M^2}{\mathbf{d}^H \mathbf{R}^{-1} \mathbf{d}}. \tag{2.41}$$

When the expected beamformer power output is plotted as a function of angle of arrival the graph is termed a "response pattern." Both (2.40) and (2.41) depend on the CSDM, thus the response patterns will be data dependent. Figure 2.3 illustrates the adaptive and conventional response patterns for a 12 sensor array. The assumed scenario of sources and white noise are given in the figure. The small "x"s indicate the exact location of the sources on the plot. Noise power is assumed to be 0dB in all figures. From Figure 2.3, several observations can be made:

- The conventional response is wider than the adaptive response for the more powerful source. Put another way, the adaptive beamformer is able to cancel a spatially close source by steering nulls (in its beampattern) at it.
- The dominant source can mask the presence of the lesser source in conventional beamforming.
- The noise floor for the conventional, Hamming windowed beamformer is higher than the adaptive beamformer's noise floor.

The response pattern plots an estimate of the spatial power spectrum, much like the power of a Fourier transform can be used to plot the frequency spectrum of a time domain signal.

It was shown in (2.38) that the narrowband beamformer steered at θ will respond to a source at θ with no distortion to the source's phase of arrival (γ) and a constant gain to the source's power— that is, the narrowband beamformer exhibits the desirable characteristic that, within a constant gain factor, the output represents the true signal. It would also be desirable if the narrowband beamformer did not pass sources arriving from coordinates other than (f, θ). This will be an unattainable goal, but it is noteworthy that the beamformer discriminates well against "interfering" sources. The presence of interfering sources in the beamformer output is also called "leakage", because the interferer has leaked from its true location into the beamforming look

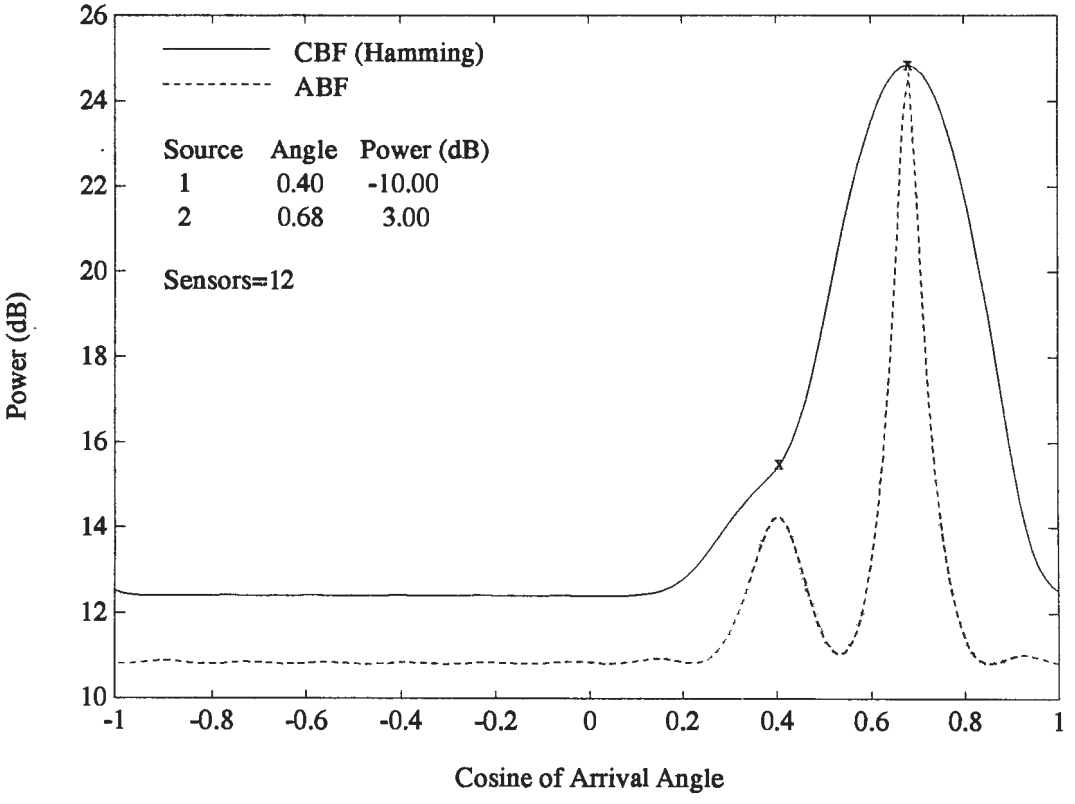

Figure 2.3: Response Patterns for ABF and CBF

direction. The beampattern measures the amount of leakage and from what direction the leakage is arriving.

Here the beampattern is defined as the magnitude squared transfer function of the beamformer steered at θ to a *unit amplitude source* arriving from ϕ, plotted as a function of ϕ. The value of the beampattern at a single angle ϕ is

$$b(\phi, \theta) = b(\phi) = |\mathbf{w}(\theta)^H \mathbf{d}(\phi)|^2. \tag{2.42}$$

$\mathbf{w}$ represents any $M \times 1$ filter vector and $\mathbf{d}$ is the interfering source's steering vector.

Figure 2.4 shows the beampattern for a Hamming windowed conventional beamformer and for an MVDR adaptive beamformer. The number of sensors plus the number and characteristics of the sources are indicated on the figure. The conventional beampattern has the following characteristics:

- The peak response to a single source occurs at the desired angle θ. The angle θ is denoted by a small circle on the beampattern.
- The response to the interferer at angle ϕ, denoted by a small 'x' on the conventional beampattern, is well above the sidelobe levels. This indicates that the interferer has leaked into the beamformer output—at levels much higher than desired.
- The sidelobe levels for the beampattern are uniformly 40 dB below the peak response. A sidelobe interferer will be rejected by no less than 40 dB.

2.4 Indirect or Subarray Narrowband Beamforming

The direct MVDR beamformer of section 2.2.2 is often termed a "fully adaptive" solution because all available degrees of freedom (the number of sensors in the array) are used in the solution of the filter vector. Fully adaptive systems can be impractical for several reasons:

- Providing the hardware resources necessary to calculate and invert the $M \times M$ CSDM, or calculate the inverse of the CSDM directly, can be prohibitive.

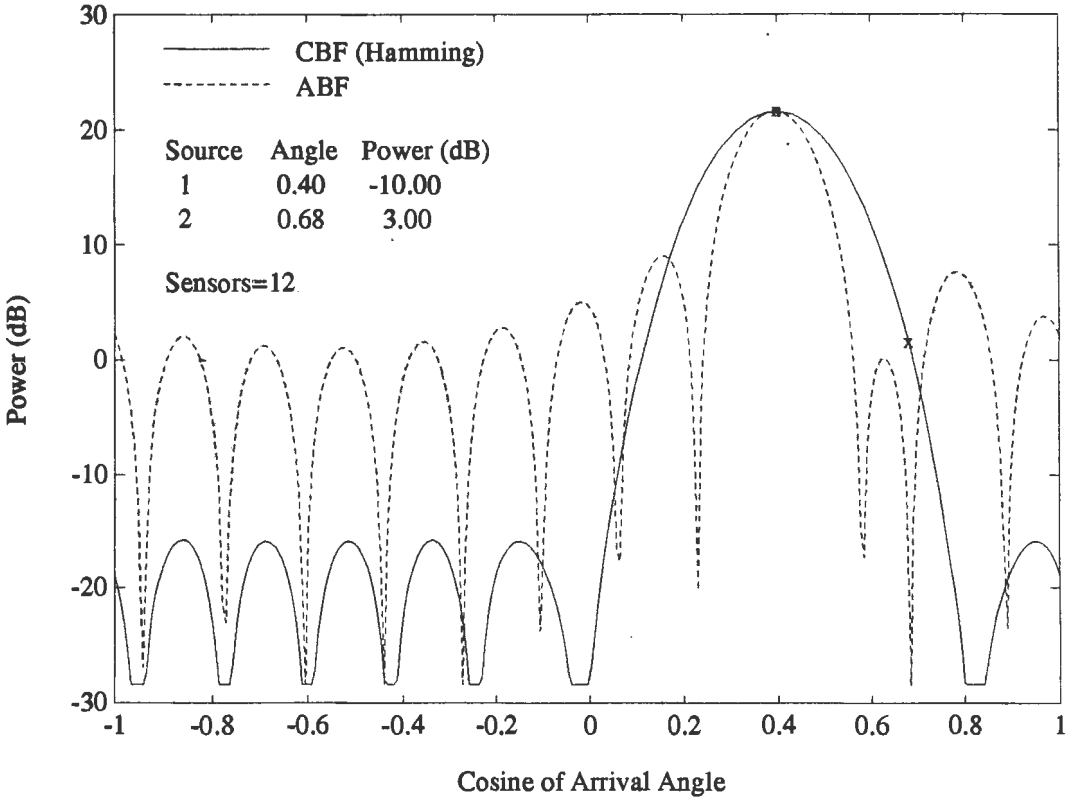

Figure 2.4: Beampatterns for ABF and CBF

- The quasi-stationarity of the environment may be of shorter time duration than the time required to create a full-rank CSDM estimate, and without a full rank matrix the adaptive weight vector can not be formed.

While a fully adaptive system does give optimal performance, in practice it is not a requirement. It has been found that considerably fewer degrees of freedom can yield nearly equal performance (in most realistic scenarios). Systems which employ fewer than the maximum number of available degrees of freedom [11] are termed "partially adaptive." It will be shown that the subarray technique is ideally suited for a partially adaptive solution to the narrowband beamforming problem.

Gray [12] has developed another partially adaptive solution to narrowband beamforming termed "beam-space" beamforming. Beam-space beamforming adaptively recombines the full array conventional beam outputs. This technique is mentioned because it is highly related to the subarray technique presented here; in fact, it can be viewed as an extension of the subarray technique.

Subarray processing is a two stage beamformer which "breaks" the problem down into two separate parts, where each part is considerably smaller than the equivalent direct method. The first stage beamforms sub-segments of the array, and the second stage "rebeamforms" by combining the outputs of the first stage beamformer.

The first stage beamformer, termed a "subarray beamformer," filters a broad spatial sector (in the vicinity of the subarray beam-steering direction), and the output of this stage is often characterized by a large mainlobe response and extremely low sidelobes. The low sidelobes are designed to suppress spatially distant sources. The second stage, or "full array," beamformer filters a narrow spatial sector within the mainlobe response of the subarray beamformer. This two stage process is an example of partitioning a problem into smaller more manageable sub-tasks by using a "global" strategy, followed by a "local" strategy: The global strategy, performed by the first stage, is to cancel spatially distant interference, while the local strategy, performed by the second stage, is to cancel spatially proximate interference.

As an aside, additional motivation for using subarray processing can be given when the assumed linear array is slightly perturbed. In this case, the array subsegments or subarrays can be treated as quasi-linear and beamformed

as previously mentioned, but the full array beamformer must compensate for subarray "phase center" perturbations. This process of accounting for the subarray phase center locations is referred to as "shape compensation." Shape compensation of subarray phase center locations is numerically simpler than shape compensation of each sensor.

In theory each stage of the subarray technique can be done using either conventional or adaptive beamforming, giving a total of four possible subarray beamformers. Each of the four "modes" is listed below, along with motivation for using each mode (The subarray beamforming technique is listed first):

- Conventional (SA)/Conventional (FA). This mode can be used when no strong interference is present.

- Conventional/Adaptive. This mode is useful when spatially distant interferences can be suppressed by low (conventional window) sidelobes in the subarray stage, and powerful interferences can be nulled by adaptive full array beamforming.

- Adaptive/Conventional. This mode is not useful: if adaptive subarrays are needed because of dominant interferences, then adaptive full array beamforming is also required.

- Adaptive/Adaptive. This mode is useful when spatially distant interferences can not be sufficiently suppressed (to avoid aliasing) by subarray beamforming sidelobes. This can happen in the presence of powerful interferences or in arrays of large numbers of sensors (when subarrays are made small). See section 4 for a discussion of this technique.

A detailed introduction to subarray formation and beamforming is covered in section 2.4.1. The subject of overlapped subarrays and spatial aliasing is discussed in section 2.4.2. Conventional/Conventional subarray beamforming is covered in section 2.4.3. Conventional/Adaptive subarray beamforming is covered in section 2.4.5.

2.4.1 Subarray Formation and Beamforming

Subarray narrowband beamforming, as shown in Figure 2.5, is a two-stage beamforming technique. The first stage is a series of beamformers $\{\text{SABF}(i,\beta)\}_{i=0}^{S-1}$. Each first stage beamformer selects as it input a subset of the vector of narrowband data vector $\mathbf{x}$. This subset $\mathbf{x}_i$, being a part of the whole array, shall be termed a "subarray". The first stage beamformers, or subarray beamformers, steer the subarrays in look direction β and produce the subarray outputs $\{z_i\}_{i=0}^{P-1}$. The second stage beamforming, accepting the subarray outputs as its input, produces a beam in look direction θ. The beam output $y(\theta)$ is termed a "full array beam" because the data from all sensors in the array has been utilized in its formation.

The discussion of the previous paragraph gave a brief overview of how subarray beamforming is performed. Attention is now given to the details of how the "subarrays" are created, beamformed, and, finally, rebeamformed (into full array beams). For a very thorough treatment of the temporal equivalent of narrowband subarray beamforming, see [13].

In subarray narrowband beamforming, or subarray processing, the array is logically broken into several separate arrays. Each separate array, comprised of a subset of the total set of sensors, is termed a "subarray". Figure 2.6 gives one illustration of how an array might be segmented into subarrays. In this example, an array of eight sensors is segmented into three subarrays. These subarrays consist of four adjacent sensors. Each subarray overlaps the next subarray by two sensors.

In general, subarrays are formed using the following rules.

- A subarray is comprised of adjacent sensors within the array.
- Each subarray has an identical number of sensors; this is not an absolute requirement, but its assumption will simplify later development.
- A subarray "overlaps" the next subarray in the array, either in the forwards or backwards direction. That is, the portion of the sensors on one subarray closest to the next subarray are, also, in the next subarray. For reasons that will be explained later in this section, there is typically fifty percent or more overlap between adjacent subarrays.
- The overlap between adjacent subarrays is identical across the entire array.

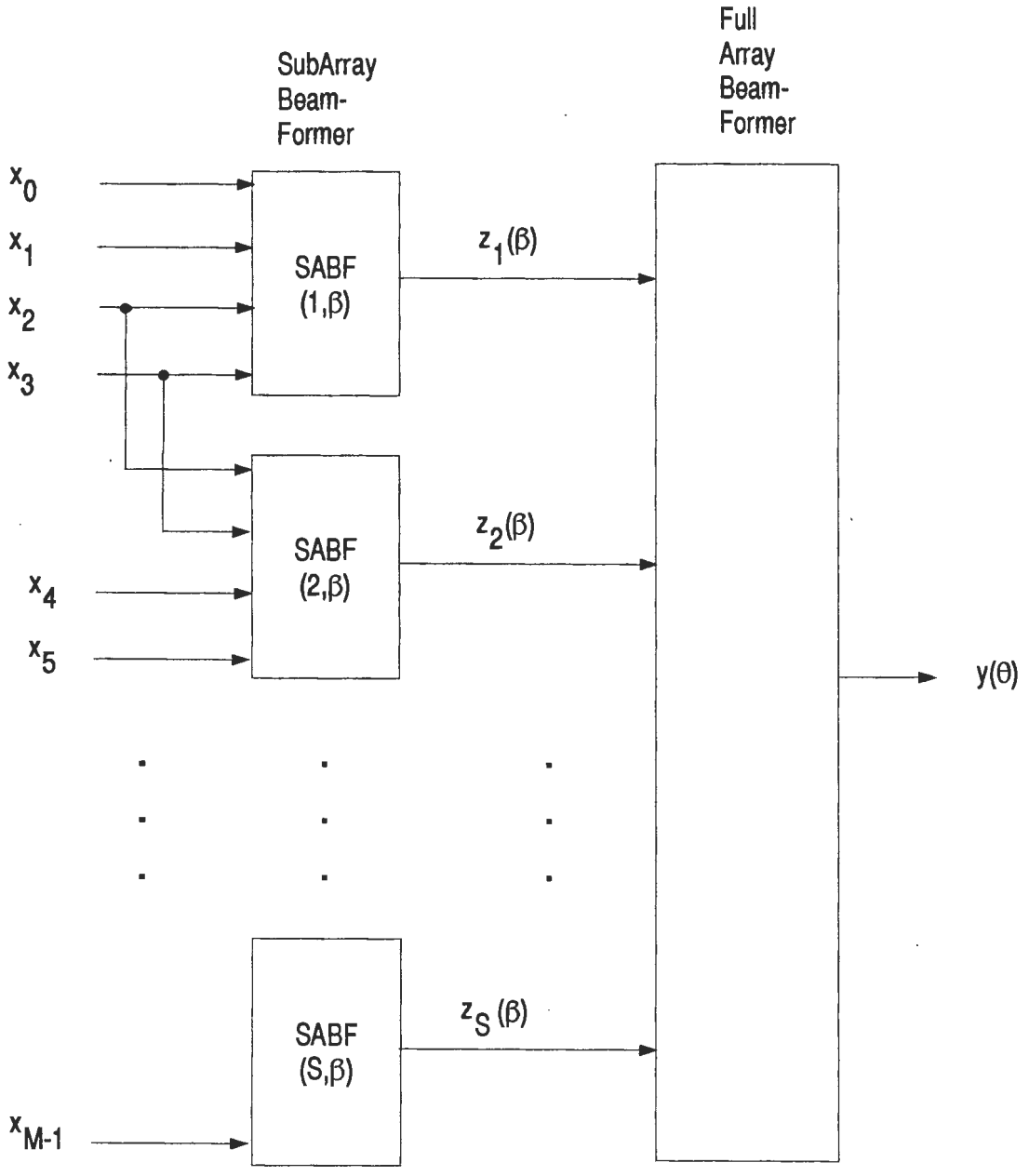

Figure 2.5: Subarray Beamforming System

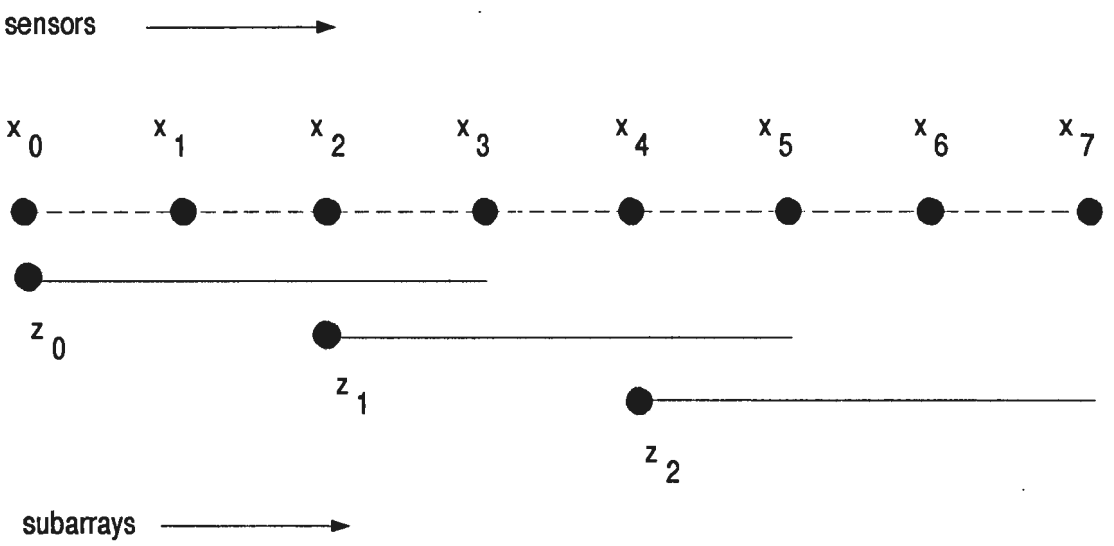

Some definitions:

M = 8 = Number of sensors per array
P = 4 = Number of sensors per subarray
S = 3 = Number of subarrays
Q = 2 = Number of sensors skipped between subarrays

Figure 2.6: Example of Subarray Formation

Using the definitions of Figure 2.6,

$$\begin{aligned} S &= \text{number of subarrays} \\ P &= \text{number of sensors per subarray and} \\ Q &= \text{number of sensors skipped between subarrays,} \end{aligned}$$

the elements of the i^{th} subarray can be expressed in the compact form

$$\begin{aligned} \mathbf{x}_i &= \left[\begin{array}{ccc} \mathbf{0}_{P\times iQ} & \mathbf{I}_P & \mathbf{0}_{P\times M-P-iQ} \end{array} \right] \mathbf{x} \\ &= \mathbf{S}_i\mathbf{x}. \end{aligned} \tag{2.43}$$

Here i ranges from 0 to $S-1$, $\mathbf{0}_{m\times n}$ is the m row $\times$ n column matrix of zeros, and I_P is the $P \times P$ identity matrix. From (2.43), the $P \times M$ matrix $\mathbf{S}_i$ is seen to select P adjacent sensors from the data vector $\mathbf{x}$ and place them in the $P \times 1$ subarray data vector $\mathbf{x}_i$. Note that the two adjacent subarray vectors $\mathbf{x}_i$ and $\mathbf{x}_{i+1}$ are uniformly overlapped by $P-Q$ sensors.

The subarray data vectors $\{\mathbf{x}_i\}_{i=0}^{S-1}$ are now input to the first stage, subarray beamformer. In this section we assume that the subarray beamformer is a conventional, windowed beamformer.

The output of the i^{th} conventional subarray beamformer is defined as:

$$\begin{aligned} z_i(\beta) &= \begin{cases} \mathbf{d}_s^H(\beta)\mathbf{x}_i & \text{if rectangular window,} \\ \mathbf{d}_s^H(\beta)\mathbf{W}_s\mathbf{x}_i & \text{otherwise} \end{cases} \\ &= \tilde{\mathbf{d}}_s^H(\beta)\mathbf{x}_i. \end{aligned} \tag{2.44}$$

Here $\tilde{\mathbf{d}}_s^H(\beta)$ is a $P \times 1$ conventional subarray filter vector steered at angle β, and $\mathbf{W}_s$ is a $P \times P$ diagonal subarray weighting matrix.

As in the full array filter vector case, the phase of the first sensor in the steering vector is zero. It is for this reason that the first sensor in a subarray is often called the *phase center* of the subarray.

The i^{th} subarray output $z_i(\beta)$ can also be expressed in terms of the original array data vector $\mathbf{x}$

$$\begin{aligned} z_i(\beta) &= \tilde{\mathbf{d}}_s^H(\beta)\mathbf{S}_i\mathbf{x} \\ &= \mathbf{a}_i^H(\beta)\mathbf{x}, \end{aligned} \tag{2.45}$$

where

$$\mathbf{a}_i^H(\beta) = \left[\begin{array}{ccc} \mathbf{0}_{1\times iQ} & \tilde{\mathbf{d}}_s^H(\beta) & \mathbf{0}_{1\times M-P-iQ} \end{array} \right]. \tag{2.46}$$

$\mathbf{a}_i$ is an $M \times 1$ vector. The two zero vectors of $\mathbf{a}_i$ "mask off" the sensors not the i^{th} subarray; the top zero vector excludes sensors from the start of the array up to, but not including, the first sensor in the subarray and the bottom zero vector excludes all sensors past the end of the subarray to the end of the array.

It will be convenient to express the set of subarray output $\{z_i\}_{i=0}^{S-1}$ in the vector form

$$\mathbf{z}(\beta) = \left[\begin{array}{cccc} z_0(\beta) & z_1(\beta) & \cdots & z_{S-1}(\beta) \end{array} \right]^T. \tag{2.47}$$

Inserting (2.45) in (2.47), the vector of subarray outputs becomes

$$\begin{aligned} \mathbf{z}(\beta) &= \left[\begin{array}{cccc} \mathbf{a}_0^H\mathbf{x} & \mathbf{a}_1^H\mathbf{x} & \cdots & \mathbf{a}_{S-1}^H\mathbf{x} \end{array} \right]^T \\ &= \left[\begin{array}{cccc} \mathbf{a}_0 & \mathbf{a}_1 & \cdots & \mathbf{a}_{S-1} \end{array} \right]^H \mathbf{x} \\ &= \mathbf{A}^H\mathbf{x}. \end{aligned} \tag{2.48}$$

$\mathbf{A}$ is an $M \times S$ filtering matrix applied to the array data vector $\mathbf{x}$. The i^{th} column of $\mathbf{A}$ spatially bandpass filters the i^{th} subarray in look direction β.

In equation (2.13), it was shown that the data vector $\mathbf{x}$ was a (weighted) summation of signal steering vectors. Later, in equation (2.28), it was shown that conventional beamforming attempts to correlate the signal steering vector, from an assumed direction of θ, with the signal steering vectors embedded in the array data vector $\mathbf{x}$. It is now important to show that the subarray data vector $\mathbf{z}(\beta)$ is a summation of "subarray phase center signal vectors." Once this has been shown, it will be clear how the conventional full array beamformer must recombine the subarray outputs; it must correlate the subarray data vector $\mathbf{z}(\beta)$ with a "subarray phase center (PC) signal vector." As will be seen, the full array re-beamformer assumes the subarray phase center signal vector is arriving from an angle in the neighborhood of β.

To find the "subarray phase center signal vector" mentioned in the previous paragraph, assume that the array data vector $\mathbf{x}$ is responding to only one source. The subarray data vector response to one signal,

$$\begin{aligned} \mathbf{s}_z(\phi, \beta) &= \mathbf{A}^H(\beta)\mathbf{s}(\phi) \\ &= \mathbf{A}^H\mathbf{s}, \end{aligned} \tag{2.49}$$

can now be investigated.

Each column of the filtering matrix **A** "picks off" part of the full array signal vector and bandpass filters it. The "selection" of the correct sensors for the subarray is done by the placement of two zero vectors in each column of **A**; these zero vectors mask out all signal data except the signal data received at one subarray.

Call the portion of the full array signal vector left unmasked, after the subarray selection, the subarray signal vector $\mathbf{r}(\phi)$. The subarray signal vector for the i^{th} subarray $\mathbf{r}_i(\phi)$ consists of P consecutive elements of the full array signal vector $\mathbf{s}(\phi)$. Using this definition and (2.6), the i^{th} subarray signal vector is

$$\begin{aligned} \mathbf{r}_i(\phi) &= \mathbf{S}_i\mathbf{s}(\phi) \\ &= \left[\exp(jiQ\Omega_\phi) \quad \cdots \quad \exp(j(iQ+P-1)\Omega_\phi) \right]^T . \end{aligned} \tag{2.50}$$

Factoring out the phase rotation between the first sensor in the array and the phase center of the subarray, the i^{th} subarray signal vector is

$$\begin{aligned} \mathbf{r}_i(\phi) &= \exp(jiQ\Omega_\phi) \left[1 \quad \exp(j\Omega_\phi) \quad \cdots \quad \exp(j(P-1)\Omega_\phi) \right]^T . \\ &= \exp(jiQ\Omega_\phi)\mathbf{d}_s(\phi) \end{aligned} \tag{2.51}$$

Each subarray signal vector is the product of the phase rotation between the first sensor in the array and the phase center of the subarray and the subarray steering vector at angle ϕ. To within a complex constant of phase rotation, the subarray signal vector is equal to the subarray filter vector steered at the same angle as the source.

For development of the subarray response to a single source, define a new vector containing the phase delays from each subarray's phase center to the first sensor in the array. This vector shall be referred to as the subarray phase center signal vector at angle ϕ,

$$\mathbf{d}_z(\phi) = \left[1 \quad \exp(jQ\Omega_\phi) \quad \cdots \quad \exp(jQ(S-1)\Omega_\phi) \right]^T , \tag{2.52}$$

because it steers the subarray phase centers to the source arriving from angle ϕ.

Combining (2.50) and (2.52) in (2.49), the subarray output response to a single source is

$$\mathbf{s}_z(\phi,\beta) = \mathbf{s}_z(\phi)$$

$$
\begin{aligned}
&= A\exp(j\gamma)\left[\begin{array}{ccc} \mathbf{r}_0(\phi) & \cdots & \mathbf{r}_{S-1}(\phi) \end{array}\right]^T \mathbf{d}_s^*(\beta) \\
&= A\exp(j\gamma)\left[\begin{array}{ccc} 1 & \cdots & \exp(jQ(S-1)\Omega_\phi) \end{array}\right]^T \mathbf{d}_s^T(\phi)\mathbf{d}_s^*(\beta) \\
&= A\exp(j\gamma)H_P(\Omega_\phi - \Omega_\beta)\mathbf{d}_z(\phi). \qquad (2.53)
\end{aligned}
$$

The subarray output response to a single source is equal to the subarray phase center signal vector $\mathbf{d}_z(\phi)$ multiplied by the signal excitation $A\exp(j\gamma)$ and by the filtering attentuation $H_P(\Omega_\phi - \Omega_\beta)$.

Equation (2.53) will be a central formula in the development of the subarray beamformer. It will be used to

- Describe subarray output as "directional" sensors,
- Reveal aliasing issues with subarrays which are insufficiently overlapped, and
- Determine the method by which subarray outputs can be rebeamformed into full array beams.

The filtering attenuation $H_P(\Omega_\phi - \Omega_\beta)$ is relatively constant in the neighborhood of β (at the top of the mainlobe response), and increases as the angle between the source ϕ and the subarray steering angle β increases. At a sufficient angular separation from the subarray steering direction β (in the "sidelobes"), the signal is considered to be rejected.

It is for reasons mentioned above that a subarray is also known as a "directional" sensor; sources arriving from the direction of β are "heard," while sources arriving from further away are not picked up. Viewed in this context, the rebeamforming of subarray outputs can be seen simply as the beamforming of sensors with directional sensitivity.

Figure 2.7 depicts this view of subarray outputs as directional sensors. Sources arriving at the top of the mainlobe, shown as region $\Psi(\beta)$ in the figure, are heard. The attenuation at the edge of the region $\Psi(\beta)$ defines the amount of signal loss deemed acceptable. Sources arriving in the mainlobe but not within $\Psi(\beta)$, or sources arriving in the sidelobes, are unwanted, interfering signals.

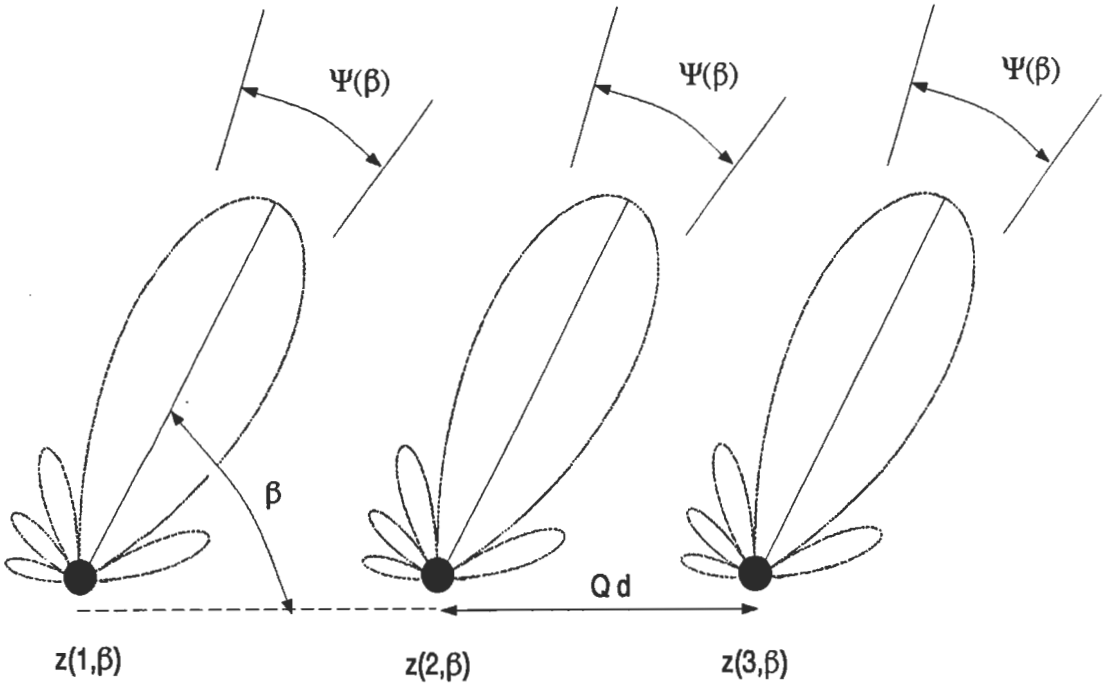

Figure 2.7: Subarray Beams as "Directional Hydrophones"

2.4.2 Subarray Beam Width and Subarray Aliasing

A set of "directional" sensors, such as the subarrays in this paper, spatially sample an impinging wavefront. In a manner completely analogous to temporal sampling or the spatial sampling by sensors (mentioned earlier), care must be taken not to undersample and cause aliasing of the signal.

To investigate exactly when aliasing occurs with subarrays, it is necessary to determine the spatial sampling frequency for the subarray phase center signal vector (2.52). Because the signal is a complex exponential sinusoid, the spatial sampling frequency is the maximum bandwidth which can be supported without aliasing. Therefore, if the bandwidth of the subarray phase center signal is less than the spatial sampling frequency, then aliasing will *not* occur. Of course, in practice a filter will always pass energy through the sidelobes, and this energy (however small) must alias. Figure (2.8) illustrates these concepts. If the spatial bandpass filter of width B_M cuts off the signals inside of the non-aliasing bandwidth B_F, then aliasing has been prevented.

To mathematically define the non-aliasing spatial bandwidth for subarrays, substitute the original definitions for Ω_ϕ back into (2.52), and express the m^{th} element of the subarray phase center signal vector as

$$\mathbf{d}_z(m,\phi) = \exp\left[2\pi\left(\cos\phi\right) m\left(\frac{Qd}{\lambda}\right)\right] \tag{2.54}$$

From (2.54), the spatial sampling interval is $\frac{Qd}{\lambda}$ and the non-aliasing bandwidth is

$$B_F = \frac{\lambda}{Qd}. \tag{2.55}$$

Recognizing from (2.53) that subarrays are a bandpass operation, the spatial band B_F must be centered at the subarrays' center frequency β with a width less than the non-aliasing band B_F; that is:

$$\begin{aligned} B_M &\leq B_F \\ 2\left|\cos\phi - \cos\beta\right| &\leq \frac{\lambda}{Qd} \\ \left|\cos\phi - \cos\beta\right| &\leq \frac{\lambda}{2Qd} \end{aligned} \tag{2.56}$$

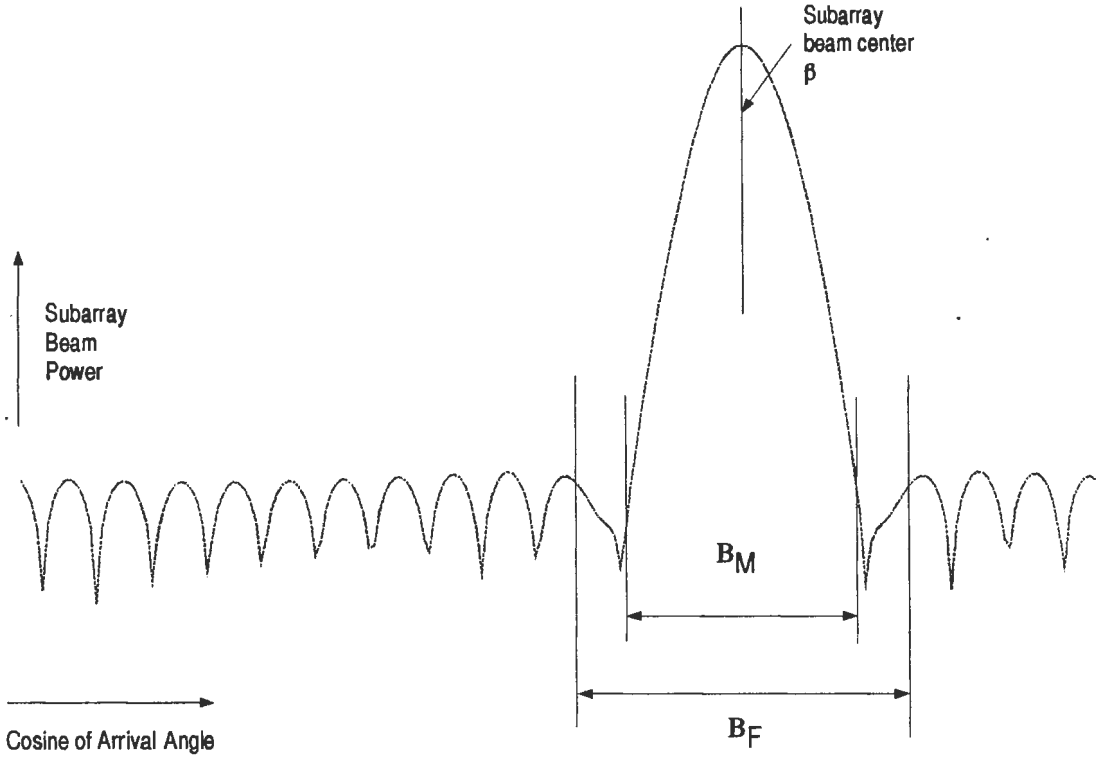

Figure 2.8: Subarray Bandpass Filter Width and Nyquist Cutoff

Spatial aliasing will occur if inequality (2.56) is not true. If aliasing should occur it is easily corrected by decreasing the skip Q between subarrays; that is, subarray aliasing is correctable by more frequent spatial sampling.

2.4.3 Conventional Subarray Rebeamforming

In this section, the conventional rebeamforming of conventional subarray output is discussed. The method of forming a single full array beam is given first, and then a general strategy for achieving full azimuthal coverage from individual full array beams is presented.

Conventional subarray rebeamforming is the process of combining subarray outputs into full arrays beams, using a coherent phase-adjust-and-sum (correlation) algorithm. This dual stage beamformer shall be termed a "conventional subarray/conventional full array" or "conventional/conventional" beamformer. Viewing the subarrays' outputs as directional sensors, the conventional subarray rebeamformer must choose the sensors "pointing" at the signal of interest, and then it can phase-adjust-and-sum these sensors for the assumed signal angle of arrival θ. The phase-adjust-and-sum operation is done using the subarray phase center steering vector.

Stated mathematically, the full array beam output is

$$\begin{aligned} y_{z_c}(\theta) &= \begin{cases} \mathbf{d}_z^H(\theta)\mathbf{z}(\beta) & \text{if rectangular window} \\ \mathbf{d}_z^H(\theta)\mathbf{W}_z\mathbf{z}(\beta) & \text{otherwise} \end{cases} \\ &= \tilde{\mathbf{d}}_z^H(\theta)\mathbf{z}(\beta), \end{aligned} \tag{2.57}$$

where, the full array look direction θ is inside the directional subarray beam; that is

$$\theta \in \Psi(\beta). \tag{2.58}$$

As seen in (2.58) and (2.57), a set of subarray beams focussed at β gives only partial azimuthal coverage. To obtain full azimuthal coverage, each subarray must be focussed at several angles. As suggested by Owsley [10], each subarray can be steered at a "fan" of angles evenly distributed in cosine of arrival angle. (The look directions are spaced evenly in cosine of angle because the bandpass filter width of a subarray beam is uniform in cosine of angle.)

To illustrate the concepts discussed above, Figure (2.9) plots the power response of (2.57) to white noise as a function of arrival. Referring to this

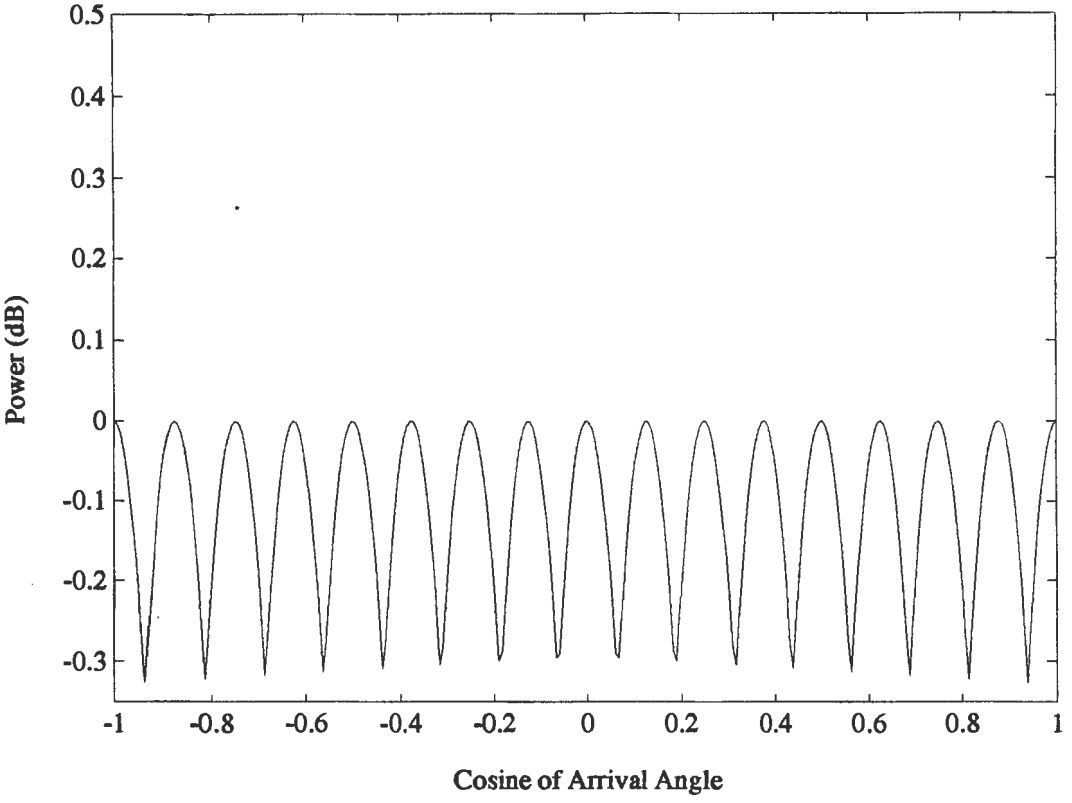

Figure 2.9: Full Azimuthal Coverage using 17 Subarray Beams

figure, the conventional subarray rebeamformer calculates full array beams in look directions ranging from $\cos\theta = +1$ ("forward-fire") to $\cos\theta = -1$ ("end-fire"), and typically the full array beams are spaced evenly in cosine space. In this example there are 17 subarray beams. At each subarray beam center the response reaches a maximum and between two subarray beam centers the response reaches a minimum.

The conventional full array beamformer is similar in form to the direct conventional beamformer, except that directional sensors are used as input.

2.4.4 Response Pattern using Conventional Subarray Processing

It is now possible to calculate the response pattern for a beamformer using subarray processing. It is of considerable interest to compare the performance of the subarray method with the performance of the "direct" beamformer of section (2.2.1).

In order to plot the response pattern, the expected beam output power as a function of look direction must be calculated. From (2.57), the expected beam output power is

$$\begin{aligned} r_{z_c}(\theta) &= \mathrm{E}\left[|y_{z_c}(\theta)|^2\right] \\ &= \mathbf{d}_z^H(\theta)\mathrm{E}\left[\mathbf{z}(\beta)\mathbf{z}^H(\beta)\right]\mathbf{d}_z(\theta) \\ &= \mathbf{d}_z^H(\theta)\mathbf{A}^H\mathrm{E}\left[\mathbf{x}\mathbf{x}^H\right]\mathbf{A}\mathbf{d}_z(\theta) \\ &= \mathbf{d}_z^H(\theta)\mathbf{A}^H\mathbf{R}\mathbf{A}\mathbf{d}_z(\theta). \end{aligned} \tag{2.59}$$

Figure 2.10 plots the response pattern for a direct conventional beamformer and a subarray conventional beamformer. It is clear, by observation, that the two responses are approximately equal, but there are some minor differences:

- Sources arriving at the subarray maximum response axis (MRA) do not suffer power loss. The source at $\cos\theta = 0.38$ illustrates a signal arriving at a subarray MRA; it has no power loss relative to the direct beamformer method.

- Sources arriving off the subarray MRA experience a signal loss corresponding to the subarray beams' scalloping loss. The source at $\cos\theta = 0.69$ arrives off a subarray MRA and is shown experiencing a small power loss.

- The white or omni-directional noise is subject to scalloping loss, in a manner similar to the power loss of the "point" sources mentioned above. To illustrate the noise scalloping caused by subarray processing, consider the three subarrays centered at -0.75, -0.625, and -0.5. In this region of the plot, because the sources at 0.38 and 0.69 can have no significant contributions to the response pattern (40 dB sidelobes of the Hamming window), the response is due primarily to the noise. Notice

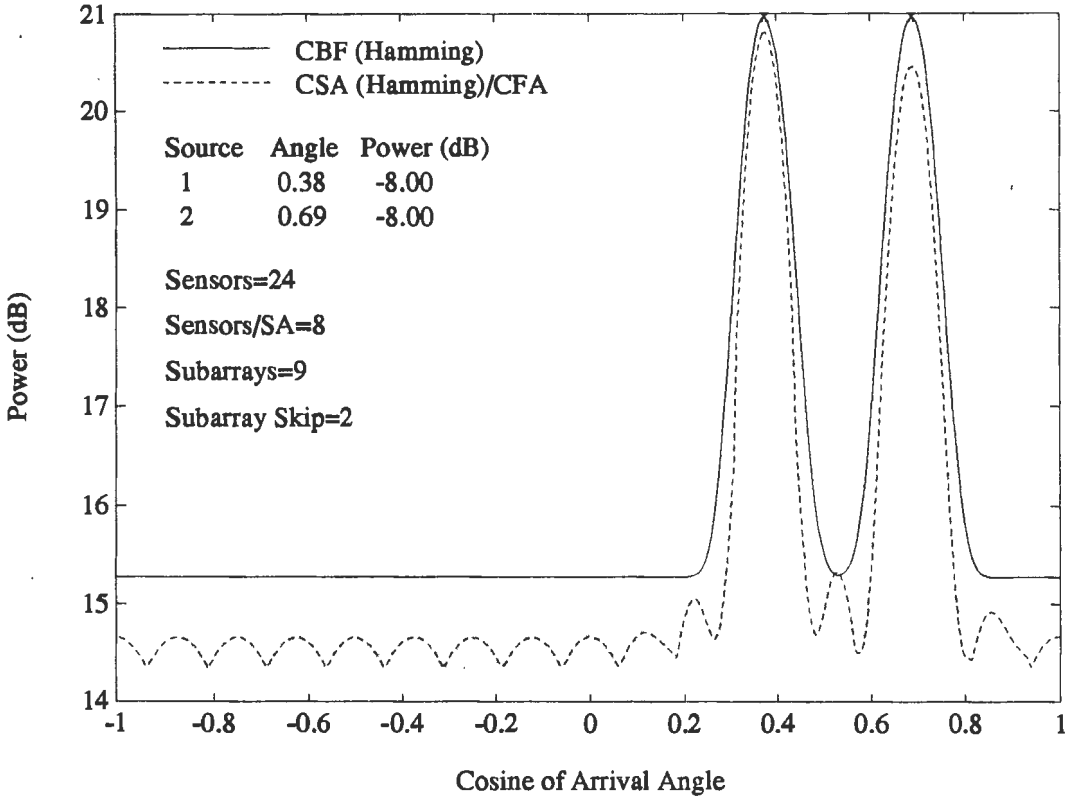

Figure 2.10: Response Pattern for Conventional Subarray Beamforming

that the noise response at the indicated subarray MRAs is at a maximum, and the maximum scalloping loss is exhibited at the midpoints between the subarray MRAs.

- The noise level in the CSA/CFA plot is lower because the second stage uses an "unwindowed" subarray recombination. The unwindowed subarray recombination also leads to signal sidelobes.

The scalloping losses can be alleviated by compensating for the bandpass filter attenuation, but generally this is not done because the attenuation is considered insignificant.

2.4.5 Adaptive Beamforming using Conventional Subarrays

In this section the MVDR adaptive rebeamforming of conventional subarray beam outputs is derived. It is seen that the AFA beamformer is nearly identical in form to the MVDR solution.

In deriving the direct MVDR filter vector $\mathbf{w}$, the criterion for optimality was a constant gain to the signal of interest, while achieving a minimum expected power output. Applying the same criterion to the subarray rebeamformer requires that the subarray MVDR filter $\mathbf{w}_z$ has a constant gain to the subarray phase center signal vector $\mathbf{d}_z(\theta)$, while realizing a minimum expected power output. Defining the full array output $y_z(\theta)$ to be the complex conjugate inner product of a filter vector $\mathbf{w}_z$ with the subarray data, that is

$$y_z(\theta) = \mathbf{w}_z^H \mathbf{z}, \tag{2.60}$$

the optimum filter vector must satisfy

$$\mathbf{w}_z(\theta) = \min_{\mathbf{w}} \left\{ \mathrm{E}\left[|y_z(\theta)|^2 \right] \right\}, \text{ subj to } \left\{ \mathbf{w}^H \mathbf{d}_z(\theta) = M/P \right\}. \tag{2.61}$$

The constraint $\mathbf{w}^H \mathbf{d}_z(\theta) = M/P$ ensures that the subarray rebeamformer has the same signal gain as the direct beamformer.

Expanding the expected power in (2.61),

$$\mathrm{E}\left[|y_z|^2 \right] = \mathbf{w}_z^H \mathbf{A}^H \mathbf{R} \mathbf{A} \mathbf{w}_z, \tag{2.62}$$

and defining a "subarray CSDM"

$$\mathbf{R}_z = \mathbf{A}^H \mathbf{R} \mathbf{A}, \tag{2.63}$$

the filter vector $\mathbf{w}_z$ must satisfy

$$\mathbf{w}_z = \min_{\mathbf{w}} \left\{ \mathbf{w}^H \mathbf{R}_z \mathbf{w} \right\}, \text{ subj to } \left\{ \mathbf{w}^H \mathbf{d}_z(\theta) = M/P \right\}. \tag{2.64}$$

The solution to (2.64), obtained by using the well known method of Lagrangian multipliers, is

$$\mathbf{w}_z = \frac{(M/P)\mathbf{R}_z^{-1} \mathbf{d}_z}{\mathbf{d}_z^H \mathbf{R}_z^{-1} \mathbf{d}_z}. \tag{2.65}$$

It is clear that the AFA output is formed in a manner completely analagous to that of the direct adaptive beamformer. The AFA beamformer is, however, much easier to implement because the CSDM $\mathbf{R}_z$ is of smaller dimension.

Chapter 3

Alternative Minimum Variance Beamforming Techniques

The MVDR solutions of (2.34) and (2.65) are designed to pass one signal of interest and cancel, within the limits of the filter's capabilities, all other signals. If the objective of the filter were changed to pass a narrow spatial sector, then this type of single or "point" constraint is not an optimum method. In this section, several techniques are introduced which guarantee a signal "bandwidth."

A solution which maximizes signal-to-noise ratio over a continuum of signal space is often termed "robust," because it is relatively insensitive to small pointing direction errors [4]. Besides direction of arrival errors, robust solutions are desired for other practical situations. For instance, imperfectly known sensor locations or propagation speed [14] are two examples where robust solutions are sought. The methods of this section can be used to achieve a variety of optimum, robust solutions.

In section 3.1 the minimum variance solution with a point and zero-slope/derivative constraint is discussed, in section 3.2 the minimum variance solution with multiple point constraints is given, and in section 3.3 the minimum variance solution with a continuous (integral) constraint is given.

The solutions introduced in this section present techniques to constrain the mainlobe response of an adaptive beam. With modifications, these techniques will be used in specifying constraints for shaping the mainlobe in adaptive subarray processing; specifically, an extension of the unity gain integral constraint to a "mainlobe integral" constraint will be used extensively

in Chapter 4 to form adaptive subarray beams.

3.1 MVDR Beamforming with a Slope Constraint

The MVDR solution guarantees that a source arriving at the beam steering direction θ will pass through the filter, but it can cancel sources which are very close to the look direction. In this section, an alternative optimal filter is designed to alleviate the need to point exactly at a source: the slope of the beampattern response at the beam focussing direction is constrained [15] to zero.

Recall that the MVDR solution requires a "distortionless response" at look direction θ. If it is also specified that the slope of the beampattern at θ be zero, then sources arriving in the immediate neighborhood of the point constraint will have nearly equal magnitude and phase responses, as compared to a source at the point constraint. It is for this reason that a slope constraint is termed "robust" to small pointing errors. However, it is important to note that the slope constraint does not guarantee a near-uniform response.

To set the slope of the beampattern to zero, calculate the derivative of the beampattern, with respect to spatial angle of arrival, and set the derivative to zero. Since the beampattern width is uniform in cosine space, define a variable $u = \cos\theta$, and take the derivative of the beampattern with respect to u:

$$\begin{aligned}
\frac{d}{du}|b(u)|^2 &= \frac{d}{du}\mathbf{w}^H\mathbf{d}(u)\mathbf{d}(u)^H\mathbf{w} \\
&= \frac{d}{du}\sum_{k=0}^{M-1}\sum_{l=0}^{M-1} w_k^* w_l \exp(j\bar{\omega}u(k-l)) \\
&= \sum_{k=0}^{M-1}\sum_{l=0}^{M-1} w_k^* w_l j\bar{\omega}(k-l)\exp(j\bar{\omega}u(k-l)) \\
&= j\bar{\omega}\left(\mathbf{w}^H\bar{\mathbf{d}}\mathbf{d}^H\mathbf{w} - \mathbf{w}^H\mathbf{d}\bar{\mathbf{d}}^H\mathbf{w}\right). \qquad (3.1)
\end{aligned}$$

Here

$$\left[\bar{\mathbf{d}}(u)\right]_k = k\exp(j2\pi f\cos\theta kd/v)$$

$$
\begin{aligned}
&= k\exp(j\bar{\omega}uk), \\
u &= \cos\theta, \text{ and} \\
\bar{\omega} &= 2\pi f d/v.
\end{aligned}
$$

Substituting the distortionless constraint ($\mathbf{w}^H\mathbf{d} = N$) into (3.1), the spatial derivative is

$$\frac{d}{du}|b(u)|^2 = -\bar{\omega}N2\Im(\mathbf{w}^H\bar{\mathbf{d}}), \tag{3.2}$$

where $\Im()$ is the imaginary part of the operand. It is clear that the spatial derivative is zero if $\Im(\mathbf{w}^H\bar{\mathbf{d}}) = 0$.

The optimal filter vector which gives a constant gain to a source at θ and nearly constant gain to sources in the neighborhood of θ must satisfy the set of constraints

$$
\begin{aligned}
\mathbf{w}^H\mathbf{d} &= N \text{ and} \\
\Im(\mathbf{w}^H\bar{\mathbf{d}}) &= 0.
\end{aligned} \tag{3.3}
$$

It is convenient to define these constraints in terms of real numbers as

$$
\begin{aligned}
\Re(\mathbf{w}^H\mathbf{d}) &= N, \\
\Im(\mathbf{w}^H\mathbf{d}) &= 0, \text{ and} \\
\Im(\mathbf{w}^H\bar{\mathbf{d}}) &= 0
\end{aligned}
$$

or

$$\left[\begin{array}{ccc} \hat{\mathbf{d}} & \check{\mathbf{d}} & \check{\bar{\mathbf{d}}} \end{array}\right]^T \hat{\mathbf{w}} = \hat{\mathbf{D}}^T\hat{\mathbf{w}} = \left[\begin{array}{c} N \\ 0 \\ 0 \end{array}\right] = \hat{\mathbf{c}}. \tag{3.4}$$

Here

$$
\begin{aligned}
\hat{\mathbf{w}} &= \left[\begin{array}{c} \Re(\mathbf{w}) \\ \Im(\mathbf{w}) \end{array}\right], \\
\hat{\mathbf{d}} &= \left[\begin{array}{c} \Re(\mathbf{d}) \\ \Im(\mathbf{d}) \end{array}\right], \\
\check{\mathbf{d}} &= \left[\begin{array}{c} \Im(\mathbf{d}) \\ -\Re(\mathbf{d}) \end{array}\right], \text{ and} \\
\check{\bar{\mathbf{d}}} &= \left[\begin{array}{c} \Im(\bar{\mathbf{d}}) \\ -\Re(\bar{\mathbf{d}}) \end{array}\right].
\end{aligned}
$$

In order to formulate the optimal filter, the expected beam power must also be expressed in real quantities as:

$$\begin{aligned} \mathbf{w}^H \mathbf{R} \mathbf{w} &= \hat{\mathbf{w}}^T \hat{\mathbf{R}} \hat{\mathbf{w}} \\ &= \hat{\mathbf{w}}^T \begin{bmatrix} \Re(\mathbf{R}) & -\Im(\mathbf{R}) \\ \Im(\mathbf{R}) & \Re(\mathbf{R}) \end{bmatrix} \hat{\mathbf{w}}. \end{aligned} \tag{3.5}$$

The filter vector that minimizes the expected power output in (3.5) subject to the constraints of (3.4), obtained by the method of undetermined Lagrangian multipliers, is

$$\hat{\mathbf{w}} = \hat{\mathbf{R}}^{-1} \hat{\mathbf{D}} \left[\hat{\mathbf{D}}^T \hat{\mathbf{R}}^{-1} \hat{\mathbf{D}}^T \right]^{-1} \hat{\mathbf{c}}. \tag{3.6}$$

Figure 3.1 shows a beampattern obtained by using the filter vector of (3.6). The filter response is flat in the vicinity of the beam steer direction. In this same figure, the beampattern for an MVDR filter is shown. The MVDR filter response is not flat at the beam steer direction. Instead it is "sloped," so as to cancel the proximate source at $\cos\phi = 0.22$.

The MVDR filter tends to cancel proximate sources, making it necessary to steer directly at the source to avoid cancellation. The zero-slope beampattern does not cancel the close sources (as much), allowing beam steering directions to be spaced further apart. For this reason, the zero-slope beamformer is termed "robust" to small pointing errors.

As the signal interference power increases, the zero-slope solution will tend to cancel close sources; the zero-slope constraint only guarantees "robustness" exactly at the beam steering direction. This beamformer provides weak mainlobe control.

An additional second derivative constraint can ensure the correct "acceleration" of the mainlobe, giving further control of the mainlobe's shape. But these "slope" and "acceleration" constraints, and any more derivative constraints, only control mainlobe shape at the beam steering direction (with certainty). It is clear, however, that increasing the number of derivative constraints will tend to provide increasing robustness.

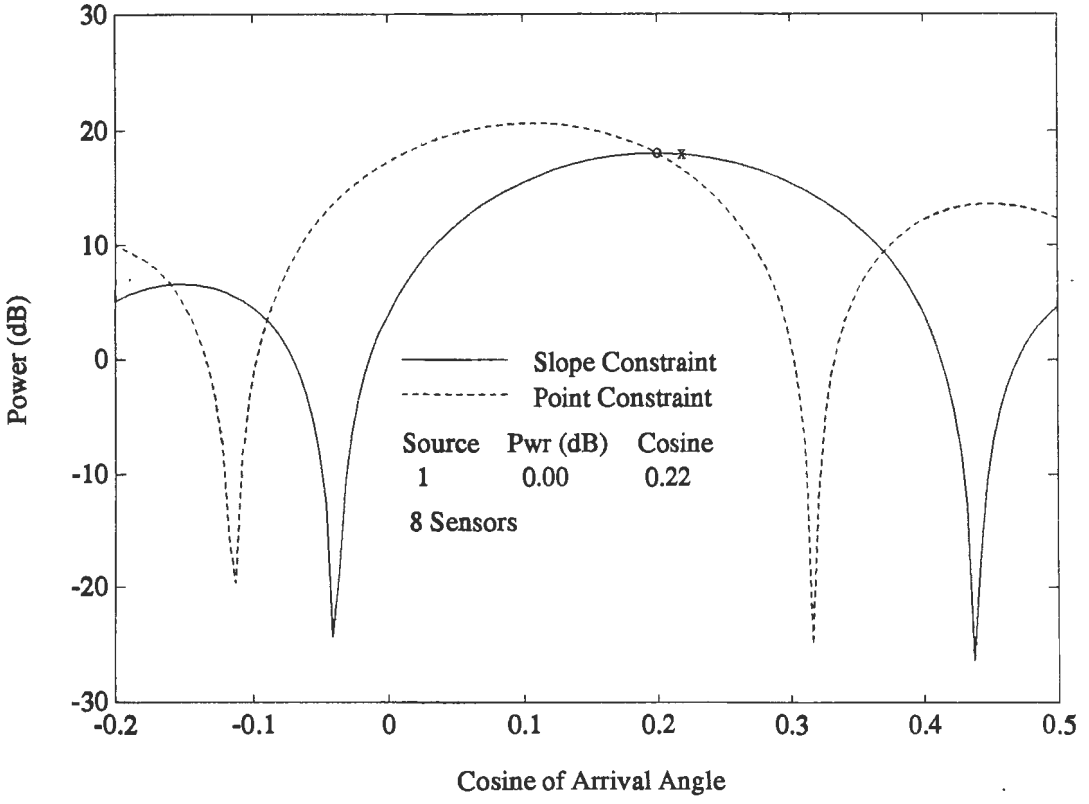

Figure 3.1: Beampattern for Minimum Variance Derivative Constrained Beamforming

3.2 MVDR Beamforming with Multiple Point Constraints

The MVDR solution of (2.34) guarantees a constant gain for a signal arriving at the beam steering direction θ, but it does not ensure the gain for a source arriving very close to the beam steer direction. This can lead to signal cancellation— even when beam steering directions are spaced relatively closely. One method of combatting signal cancellation (for close sources) is to specify more than one constraint [16]; that is, form a minimum variance solution with a "distortionless response" for several angles of arrival. This solution shall be called an MVDR beamformer with "multiple point constraints."

If the object of a multiple constraint beamformer is to pass a spatial region centered about the look direction θ, then constraints must be placed "at the top" of the beampattern's mainlobe response. In addition to constraint location, a choice arises as to the nature of the constraint: that is, what are the exact magnitude and phase constraints to be imposed? In this paper, the constraints shall be equal to the response of a (selected) conventional filter at the specified constraint points. This approach has the desirable features of linear phase shift and a known, realizable mainlobe (magnitude) shape.

To present a concrete example, assume that three constraints are imposed on the MVDR solution at angles θ_1, θ_2 and θ_3, and that the desired response is equal to the conventional filter response at look direction θ to sources at those angles. The set of constraints is expressed as:

$$\begin{aligned} \left[\begin{array}{ccc} \mathbf{d}(\theta_1) & \mathbf{d}(\theta_2) & \mathbf{d}(\theta_3) \end{array}\right]^H \mathbf{w}_L &= \left[\begin{array}{ccc} \mathbf{d}(\theta_1) & \mathbf{d}(\theta_2) & \mathbf{d}(\theta_3) \end{array}\right]^H \mathbf{d}(\theta) \\ \mathbf{D}_L^H \mathbf{w}_L &= \mathbf{c}_L. \end{aligned} \tag{3.7}$$

Here the $M \times 3$ matrix $\mathbf{D}_L$ contains the steering vectors for the source's angles of arrival and the 3×1 constraint vector $\mathbf{c}_L$ contains the desired responses. In general, if there are L constraints, $\mathbf{D}_L$ would be an $M \times L$ matrix and $\mathbf{c}_L$ would be an $L \times 1$ vector.

The desired MVDR solution must minimize the expected output power subject to the constraints (3.7). That is, it must satisfy

$$\mathbf{w}_L = \min_{\mathbf{w}} \left\{ \mathbf{w}^H \mathbf{R} \mathbf{w} \right\}, \text{ subj to } \left\{ \mathbf{D}_L^H \mathbf{w} = \mathbf{c}_L \right\}. \tag{3.8}$$

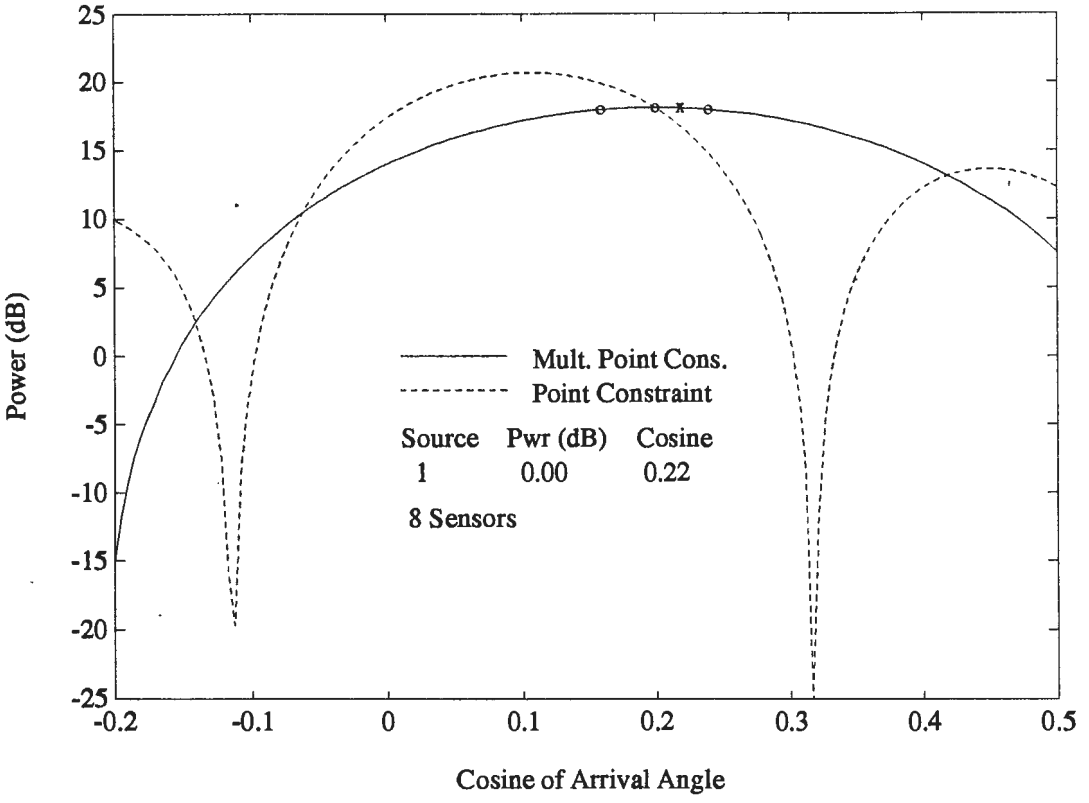

Figure 3.2: Beampattern for Minimum Variance Multiply Constrained Beamforming

The solution to (3.8), obtained by the method of undetermined Lagrangian multipliers, is

$$\mathbf{w}_L = \mathbf{R}^{-1}\mathbf{D}_L \left[\mathbf{D}_L^H \mathbf{R}^{-1}\mathbf{D}_L\right]^{-1} \mathbf{c}_L. \tag{3.9}$$

Figure 3.2 plots beampatterns for the multiple point constraint and the single point constraint (MVDR) techniques. In this figure, the point constraints are indicated by small circles (o's) and a single source location is indicated by a small cross (x). Referring to this illustration, notice that the multiple point constraint does not attempt to null this source, while the single point MVDR partially cancels it.

If the object of the set of constraints were to pass a "larger" spatial region,

unlike the narrow region of the previous example, then more constraints could be specified across the entire mainlobe. Used in this way, the set of constraints can provide strong control of the mainlobe, but (because of the nature of point constraints) the control is not absolute.

A drawback of using multiple point constraints for mainlobe shape control is the loss of degrees of freedom. Many degrees of freedom are lost to mainlobe control, potentially leaving few for interference cancellation. This problem can be addressed by making low rank approximations [4] to the steering vector constraint matrix $\mathbf{D}_L$.

3.3 MVDR Beamforming with a Continuous Constraint

An alternative to the "point" constraints suggested for zero-slope and multiple angle of arrival problems is a continuous (integral) constraint [4]. In this method the response of the beamformer can be (almost) specified on a continuum, thus achieving a robust solution across a specified region.

The continuous constraint is achieved by integrating the magnitude squared difference between the actual response to a source at angle ϕ with the desired response to that source, and then setting the integrated differences (nearly) equal to zero. In [4], the desired response was chosen to be unity. The total magnitude squared error is

$$\begin{aligned} e^2 &= \frac{1}{\Delta}\int_{\phi=\theta-\Delta/2}^{\theta+\Delta/2} \left| 1 - \mathbf{w}^H\mathbf{d}(\phi) \right|^2 d\phi \\ &= 1 - \mathbf{w}^H\mathbf{p} - \mathbf{p}^H\mathbf{w} + \mathbf{w}^H\mathbf{Q}\mathbf{w} \\ &= (\mathbf{w}_0 - \mathbf{w})^H\mathbf{Q}(\mathbf{w}_0 - \mathbf{w}), \end{aligned} \tag{3.10}$$

where

$$\begin{aligned} \mathbf{p} &= \frac{1}{\Delta}\int_{\phi=\theta-\Delta/2}^{\theta+\Delta/2} \mathbf{d}(\phi)d\phi, \\ \mathbf{Q} &= \frac{1}{\Delta}\int_{\phi=\theta-\Delta/2}^{\theta+\Delta/2} \mathbf{d}(\phi)\mathbf{d}(\phi)^H d\phi, \text{ and} \\ \mathbf{w}_0 &= \begin{bmatrix} 1 & 0 & \cdots & 0 \end{bmatrix}^T. \end{aligned} \tag{3.11}$$

It is not always possible to set the error in (3.10) to zero, except in the trivial case of $\mathbf{w} = \mathbf{w}_0$, therefore the optimum filter vector must satisfy

$$\mathbf{w} = \min_{\mathbf{w}} \left\{ \mathbf{w}^H \mathbf{R} \mathbf{w} \right\}, \text{ subj to } \left\{ (\mathbf{w}_0 - \mathbf{w})^H \mathbf{Q} (\mathbf{w}_0 - \mathbf{w}) = \epsilon \right\}, \tag{3.12}$$

where $0 < \epsilon < 1$ defines the range of meaningful error deviations.

The solution to (3.12), obtained using unknown Lagrangian multipliers, is

$$\mathbf{w}(\theta) = \lambda \left(\mathbf{R} + \lambda \mathbf{Q} \right)^{-1} \mathbf{p}, \tag{3.13}$$

where λ satisfies

$$\lambda \mathbf{p}^H \left[(\mathbf{R} + \lambda \mathbf{Q})^{-1} + (\mathbf{R} + \lambda \mathbf{Q})^{-1} \mathbf{R} (\mathbf{R} + \lambda \mathbf{Q})^{-1} \right] \mathbf{p} = 1 - \epsilon. \tag{3.14}$$

In Figure 3.3, a beampattern is shown for a filter which satisfies (3.13). Referring to this figure, the left and right ends of the constrained region are indicated by small circles (placed on the response). The beampattern response is indeed "flat" in the region of interest, but the response does not fall off immediately outside of the constrained region. In fact, the response increases just outside of the constrained region, and, though not shown in this figure, it also has very high sidelobe behavior.

The poor characteristics of the filter of (3.13) is a direct consequence of the unity gain; the causal filter is attempting to create a passband which has zero phase shift, and this may be considered an error on the part of the authors. A slight modification to the desired (unity) response will alleviate the undesirable response of this filter: make the desired response have unity magnitude with a linear phase shift. The integrated error now becomes

$$\begin{aligned} e^2 &= \frac{1}{\Delta} \int_{\phi=\theta-\Delta/2}^{\theta+\Delta/2} \left| \exp(j(\Omega_\phi - \Omega_\theta)(M-1)/2) - \mathbf{w}^H \mathbf{d}(\phi) \right|^2 d\phi \\ &= 1 - \mathbf{w}^H \bar{\mathbf{p}} - \bar{\mathbf{p}}^H \mathbf{w} + \mathbf{w}^H \mathbf{Q} \mathbf{w} \\ &= (\bar{\mathbf{w}}_0 - \mathbf{w})^H \mathbf{Q} (\bar{\mathbf{w}}_0 - \mathbf{w}) + \alpha, \end{aligned} \tag{3.15}$$

where

$$\begin{aligned} \bar{\mathbf{p}} &= \frac{1}{\Delta} \int_{\phi=\theta-\Delta/2}^{\theta+\Delta/2} \exp(-j(\Omega_\phi - \Omega_\theta)(M-1)/2) \mathbf{d}(\phi) d\phi, \\ \mathbf{Q} &= \frac{1}{\Delta} \int_{\phi=\theta-\Delta/2}^{\theta+\Delta/2} \mathbf{d}(\phi) \mathbf{d}(\phi)^H d\phi, \\ \bar{\mathbf{w}}_0 &= \mathbf{Q}^{-1} \bar{\mathbf{p}}, \text{ and} \\ \alpha &= 1 - \bar{\mathbf{w}}_0^H \mathbf{Q} \bar{\mathbf{w}}_0. \end{aligned}$$

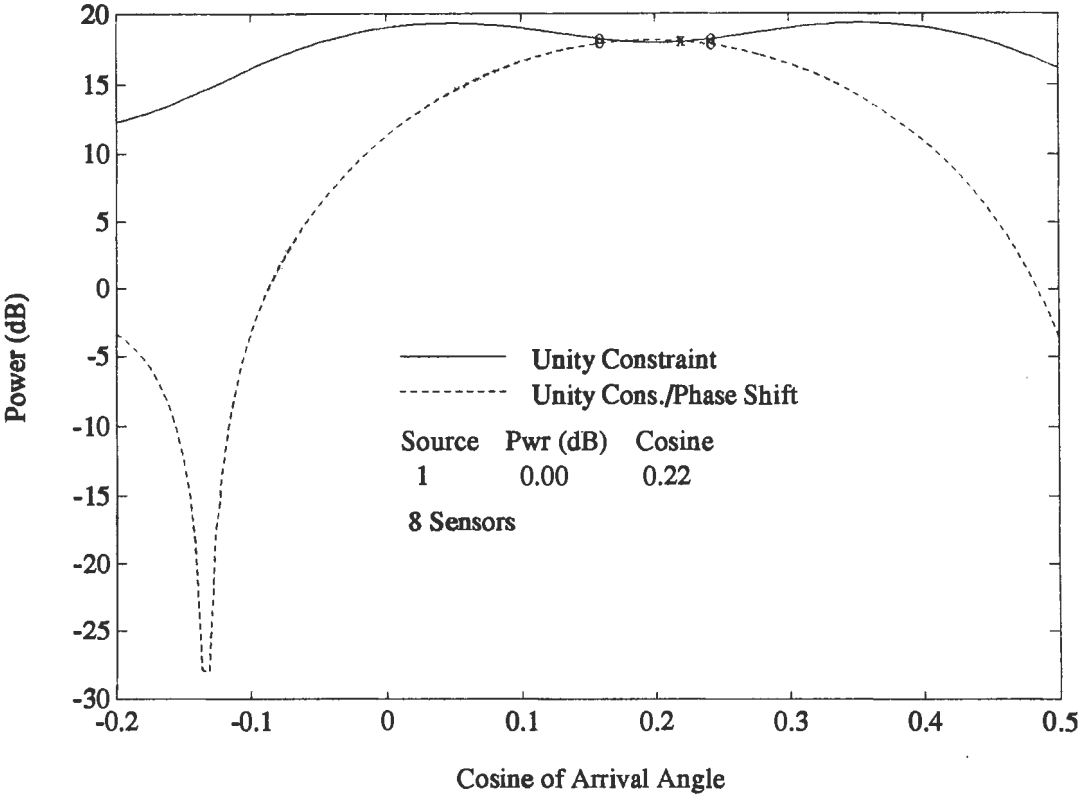

Figure 3.3: Beampatterns for Minimum Variance Continuously Constrained Beamforming

Note that the $M \times 1$ filter vector $\bar{\mathbf{w}}_0$ minimizes the total error in (3.15), and that the minimum error, unlike the unity response of (3.10), is not zero, but $\alpha = 1 - \bar{\mathbf{w}}_0^H \mathbf{Q} \bar{\mathbf{w}}_0$. This minimum error is very small for spatial bandwidths of approximately the width of the mainlobe, and only becomes large when the constrained bandwidth approaches the full spatial bandwidth.

The filter vector must then satisfy

$$\mathbf{w}(\theta) = \min_{\mathbf{w}} \left\{ \mathbf{w}^H \mathbf{R} \mathbf{w} \right\}, \text{ subj to} \left\{ (\bar{\mathbf{w}}_0 - \mathbf{w})^H \mathbf{Q} (\bar{\mathbf{w}}_0 - \mathbf{w}) = \epsilon \right\}, \qquad (3.16)$$

where $\alpha < \epsilon < 1$ defines the range of meaningful error deviations.

The solution to (3.16), obtained using unknown Lagrangian multipliers, is

$$\mathbf{w} = \lambda \left(\mathbf{R} + \lambda \mathbf{Q} \right)^{-1} \bar{\mathbf{p}}, \qquad (3.17)$$

where λ satisfies

$$\lambda \bar{\mathbf{p}}^H \left[\left(\mathbf{R} + \lambda \mathbf{Q} \right)^{-1} + \left(\mathbf{R} + \lambda \mathbf{Q} \right)^{-1} \mathbf{R} \left(\mathbf{R} + \lambda \mathbf{Q} \right)^{-1} \right] \bar{\mathbf{p}} = 1 - \epsilon. \qquad (3.18)$$

In Figure 3.3, a beampattern is shown for a filter which satisfies (3.17). Referring to Figure 3.3, the left and right ends of the constrained region are indicated by small circles placed on the beampattern response. It can be seen that the response is flat across the region of interest, and, unlike the unity response, the mainlobe response drops off immediately. Although not shown in this figure, the sidelobes are also satisfactorily low.

The "modified" integral constraint (3.16) is a good method for controlling the "top" of the beampattern's mainlobe, but it can not be used to maintain the shape of an entire mainlobe (the mainlobe has non-unity magnitude as it drops off). In Chapter 4, a further modification to the integral constraint is given which allows full mainlobe control.

Chapter 4

Adaptive Subarray Processing

In section 2.4 the subarray pre-processor was developed. The main emphasis was to describe a conventional subarray pre-processor which would "feed" a full array recombination stage. In this section several techniques are derived which form an adaptive beam suitable for use as a subarray pre-processor. The methods are termed adaptive subarray/adaptive full array (ASA/AFA) techniques.

From Figure 2.7, it is seen that a subarray processor must spatially band-pass a region of interest, designated as $\Psi(\beta)$, centered about the subarray focussing direction β, while rejecting sources arriving from outside the region of interest. The conventional subarray processor discriminates against interfering sources with very low and static sidelobes. But it does so at the expense of a "wide" transition band and a "narrow" region of interest. The adaptive subarray processor seeks to have a wider region of interest, for a given stopband width, or a narrower transition bandwidth, for a given passband width, while adaptively nulling sidelobe interferers. The wider subarray beam passband would be selected to decrease the total number of required subarray beams and their corresponding subarray output CSDMs.

The central issue in adaptive subarray beamforming is to decide at what stage to cancel the proximate sources. In section 4.1, an optimal two-stage beamformer is presented, and it is shown that the proximate interferers are *not* cancelled at the first stage, but at the second stage. In fact, occasionally, proximate interferers are amplified at the first stage. This result is surprising because it "contradicts" single stage MVDR, which must cancel an interfering source immediately. The reason that the two stage beamformer does not

cancel the close interferers is related to white noise amplification, also referred to as noise gain: the tradeoff between interference cancellation and noise gain (inherent in a minimum power output solution) is much more expensive at the first stage than at the second stage. Conceptually, the first stage beamformer has to "strain" to cancel a proximate source, while the second stage beamformer can cancel them quite easily; this makes it much more efficient to "divide" the adaptive cancellation work, so that:

1. The subarray beamformer cancels subarray sidelobe interferers and "shapes" a broad passband, and

2. The full array cancels all remaining signals (arriving from the subarray mainlobe), except for the single source of interest.

In forming the subarray beam it is necessary to either maintain the mainlobe shape or ignore sources in the mainlobe; accordingly, two approaches to calculating adaptive subarrays are then investigated:

1. The first approach constrains the response, to be equal to a specified conventional response, in the entire mainlobe, and

2. The second approach explicitly constrains the noise gain of the subarray beamformer, while passing the region of interest. This approach tends to ignore sources in the mainlobe.

A method for performing the latter, termed a "noise gain constraint" technique, is given in section 4.3. It is an effective but, computationally, very expensive method. Two methods for performing the former, termed "full mainlobe constraint" techniques, are given in sections 4.2 and 4.4. The approaches do not mathematically exclude subarray noise gain, but, for practical situations, they perform with little excess noise gain. Both full mainlobe constraint methods are much simpler to calculate than the noise gain constraint method.

As an aside, the relationship between the subarray beamformers of this section and the spatially constrained beamformers of section 3 is discussed. In section 3, a variety of techniques were introduced which adaptively beamformed with "local" or "narrow" spatial constraints. Because of the noise gain concerns discussed above, such techniques, though highly related to the methods of this section, are inadequate as subarray pre-processors.

The subarray beams of sections 4.2–4.4 are constrained so that the response in the "region of interest" is equal to the conventional response of a bandpass filter. For the mainlobe constrained beamformers, the effect of this constraint is to conventionally beamform the subarray mainlobe, adaptively cancel in the subarray sidelobe, and, at the second stage, to adaptively cancel the subarray mainlobe signals.

In summary, this section establishes several adaptive beamformer techniques designed to limit noise gain and conventionally pass a region of interest. The emphasis of this section will be to demonstrate that these methods can avoid the noise gain "pitfalls" and perform *as well as* a conventional subarray pre-processor; the issue of enhanced adaptive subarray beamformer performance (in the presence of dominant interferers or "jammers") is examined in section 5.

4.1 Non-Linear Optimum Subarray Processing

In this section the problem of calculating a subarray filter which minimizes the full array output power (subject to a signal gain constraint) is investigated. It is shown that calculating an optimum subarray filter vector is a non-linear process, involving the simultaneous manipulation of the full array and subarray filter vectors. By example, the "strategy" of the simultaneous solution can be seen, and then, from observation of this strategy, a suboptimal approach is suggested.

Perhaps the most obvious criterion for a subarray filter vector is that it should produce a minimum output power at the subarray level. If this were the case, then the full array filter would cancel any remaining signals left after the first stage cancellation. The weakness of this approach is that the subarray filter attempts to do all the "work" itself, leaving little for the full array filter to cancel. Cancelling signals in the first stage beamformer in itself is not a problem, but the (unnecessary) white noise gain introduced by doing so can not be compensated for by the second stage; basically, the white or omni-directional noise power, enhanced at the subarray output, can not be cancelled by the full array filter. In this section, the concepts of noise gain and the constraint of same are also investigated.

Recall that the adaptive subarray filter was constrained to pass a region of space, and that a separate adaptive full array filter must be calculated for each look direction within a subarray's beam. For this method, it would be very difficult to calculate a globally optimum subarray filter because it would involve a joint optimization of the subarray filter with all full array filters. Accordingly, in this section the adaptive subarray filter and *one* adaptive full array filter will be constrained to pass a single signal. This approach will provide useful insight into the "strategy" of an optimal two-stage adaptive beamformer.

The globally optimum subarray/full array beamformer seeks to simultaneously calculate the subarray and full array filters so as to minimize the full array output, subject to signal constraints at the subarray and full array output; that is:

$$y(\theta) = \min_{\mathbf{u},\mathbf{w}} \left\{ \mathbf{w}^H \mathbf{A}(\mathbf{u})^H \mathbf{R} \mathbf{A}(\mathbf{u}) \mathbf{w} \right\}, \text{ subject to } \left\{ \begin{array}{l} \mathbf{u}(\theta)^H \mathbf{d}_s(\theta) = P, \\ \mathbf{w}^H \mathbf{d}_z(\theta) = M/P \end{array} \right\} \quad (4.1)$$

Here

$$\begin{aligned} \mathbf{w}(\theta) = \mathbf{w} &= \text{the } S \times 1 \text{ full array filter,} \\ \mathbf{u}(\theta) = \mathbf{u} &= \text{the } P \times 1 \text{ subarray filter,} \\ \mathbf{A}(\mathbf{u}) = \mathbf{A} &= \text{the } M \times S \text{ subarray preprocessing matrix (see (2.48)),} \\ \mathbf{d}_s(\theta) &= \text{the } P \times 1 \text{ subarray signal steering vector, and} \\ \mathbf{d}_z(\theta) &= \text{the } S \times 1 \text{ subarray phase center steering vector.} \end{aligned}$$

To allow for further developments, rewrite the optimum beamformer output in terms of the subarray filter and a "full array" preprocessing matrix as

$$y(\theta) = \min_{\mathbf{u},\mathbf{w}} \left\{ \mathbf{u}^H \mathbf{B}(\mathbf{w})^H \mathbf{R} \mathbf{B}(\mathbf{w}) \mathbf{u} \right\}, \text{ subject to } \left\{ \begin{array}{l} \mathbf{u}(\theta)^H \mathbf{d}_s(\theta) = P, \\ \mathbf{w}^H \mathbf{d}_z(\theta) = M/P \end{array} \right\}. \quad (4.2)$$

Here the $M \times P$ "full array" preprocessing matrix $\mathbf{B}(\mathbf{w}) = \mathbf{B}$ satisfies the equality

$$\mathbf{B}(\mathbf{w})\mathbf{u} = \mathbf{A}(\mathbf{u})\mathbf{w}. \quad (4.3)$$

The full array preprocessing matrix is found by rearranging the vector $\mathbf{A}(\mathbf{u})\mathbf{w}$ in terms of the vector $\mathbf{u}$ and the matrix $\mathbf{B}$.

From (4.1) or (4.2), it is clear that there are fourth order terms (of the individual filter elements) in the beamformer output y, making a direct, linear solution impossible; hence, an alternative solution is sought. An iterative, two-stage linear solution is now proposed:

1. Assign a conventional filter vector to the subarray filter $\mathbf{u}$, for initialization.

2. Solve for the full array filter with the subarray filter fixed, subject only to the full array constraint,

$$y(\theta) = \min_{\mathbf{w}} \left\{ \mathbf{w}^H \mathbf{A}(\mathbf{u})^H \mathbf{R} \mathbf{A}(\mathbf{u}) \mathbf{w} \right\}, \text{ subject to } \left\{ \mathbf{w}^H \mathbf{d}_z(\theta) = M/P \right\}. \tag{4.4}$$

3. Solve for the subarray filter with the full array fixed, subject only to the subarray constraint,

$$y(\theta) = \min_{\mathbf{u}} \left\{ \mathbf{u}^H \mathbf{B}(\mathbf{w})^H \mathbf{R} \mathbf{B}(\mathbf{w}) \mathbf{u} \right\}, \text{ subject to } \left\{ \mathbf{u}(\theta)^H \mathbf{d}_s(\theta) = P \right\} \tag{4.5}$$

4. Repeat steps 2 and 3, until convergence. Here, convergence is defined to have occurred at iteration k if the power output at the current iteration $y(k)$, is only a small percentage less than the previous iteration $y(k-1)$; that is, if

$$\frac{y(k-1) - y(k)}{y(k-1)} < \epsilon, \tag{4.6}$$

then convergence has occured. Steps 2 and 3, each finding a global minimum for their respective problems, are guaranteed to descend, until "convergence."

This shall be called the "iterative ASA/AFA" algorithm. It is of interest to investigate the performance of this iterative subarray/full array filter set with the performance of competing approaches. The metric used here is the full array power output: the goal of a subarray processor is to approach the global minimum obtained by the fully adaptive processor.

Two specific interference/noise scenarios are of general importance:

1. Interference signal impinging close to a selected look direction.

   By "close," it is meant that the signal angle of arrival falls on the mainlobe of a conventional windowed subarray beampattern.

2. Interference signal impinging relatively far away from the selected look direction (signal angle of arrival falling in the sidelobes of a conventional windowed subarray beampattern).

Also, three methods for calculating the subarray and full array filters shall be compared (for the above two interference scenarios):

1. Iterative ASA/AFA: Iterative adaptive subarray/adaptive full array filter set, obtained by iterative solution of (4.1). This is the "optimal" solution.

2. Sequential ASA/AFA: The subarray filter is obtained by minimizing the subarray output, subject to a subarray signal constraint,

$$y_z(\theta) = \min_{\mathbf{u}} \left\{ \mathbf{u}^H \mathbf{R}_s \mathbf{u} \right\}, \text{ subject to } \left\{ \mathbf{u}(\theta)^H \mathbf{d}_s(\theta) = P \right\}, \tag{4.7}$$

   where $\mathbf{R}_s$ is the $P \times P$ CSDM embedded on the diagonal of the CSDM $\mathbf{R}$.

   Next, using the subarray filter from the first step, the full array filter is obtained by minimizing the full array output power, subject to the subarray phase center signal constraint; that is,

$$y(\theta) = \min_{\mathbf{w}} \left\{ \mathbf{w}^H \mathbf{A}(\mathbf{u})^H \mathbf{R} \mathbf{A}(\mathbf{u}) \mathbf{w} \right\}, \text{ subject to } \left\{ \mathbf{w}^H \mathbf{d}_z(\theta) = M/P \right\}. \tag{4.8}$$

3. CSA/AFA: The subarray filter is a selected (Hanning windowed) conventional filter $\tilde{\mathbf{d}}_s(\theta)$, and the full array filter minimizes the full array output power; that is,

$$y(\theta) = \min_{\mathbf{w}} \left\{ \mathbf{w}^H \mathbf{A}(\tilde{\mathbf{d}}_s)^H \mathbf{R} \mathbf{A}(\tilde{\mathbf{d}}_s) \mathbf{w} \right\}, \text{ subject to } \left\{ \mathbf{w}^H \mathbf{d}_z(\theta) = M/P \right\}. \tag{4.9}$$

Before evaluating the selected beamformers, the concept of "noise gain" must be introduced. Noise gain or white noise amplification is defined here to be ratio of output power due to white noise divided by the input power due to white noise

$$\text{NG} \equiv \frac{\text{Noise Power}_{\text{out}}}{\text{Noise Power}_{\text{in}}}, \tag{4.10}$$

or, assuming unity input power,

$$\mathrm{NG} \equiv \mathbf{w}^H \mathbf{A}(\mathbf{u})^H \mathbf{A}(\mathbf{u}) \mathbf{w}. \tag{4.11}$$

As defined in (4.11), it measures the power due to white noise, and will be useful in discriminating whether signal and/or noise power has been passed into the beamformer output. When evaluating a beampattern, the noise gain of the beamformer can be judged by the relative width and heights of the sidelobes; large sidelobes (possibly larger than the mainlobe) lead to significant increases in noise gain.

To help evaluate the performance of the candidate beamformers, the subarray beampatterns for a "close" interferer are plotted in Figure 4.1 and for a "distant" interferer in Figure 4.2. The beamformer look direction is indicated by a small circle, and the interferer location is indicated by a small "x." Interference scenario 2 of Table 4.4 is used, and the subarrays are setup according to Eqn. 4.12 below:

$$\begin{aligned} P &= 8 \equiv \text{sensors per subarray}, \\ M &= 20 \equiv \text{sensors in array, and} \\ S &= 5 \equiv \text{number of subarrays}. \end{aligned} \tag{4.12}$$

Referring to Figure 4.1, the following observations can be made:

- The iterative ASA/AFA beamformer does not place a null in the direction of the close interferer in the first stage, subarray beamformer, but defers the work of cancelling the close interferer until the second stage full array beamformer. It is noteworthy that the mainlobe is moved *towards* the interferer, giving a signal amplification at the subarray stage, instead of cancellation. Evidently, the beamformer can afford to amplify the signal because it "knows" (from the recursion) that the signal will be cancelled.

  The distant interferer is cancelled by the first stage beamformer by manipulating the sidelobes and placing a null at the source location. The mainlobe does "move" but, for distant interferers, not always towards the source. Most likely, the freedom to move the mainlobe a little allows for better sidelobe structure (if, for a single interferer, a slight shift/amplification of the entire "quiescent" beampattern placed the

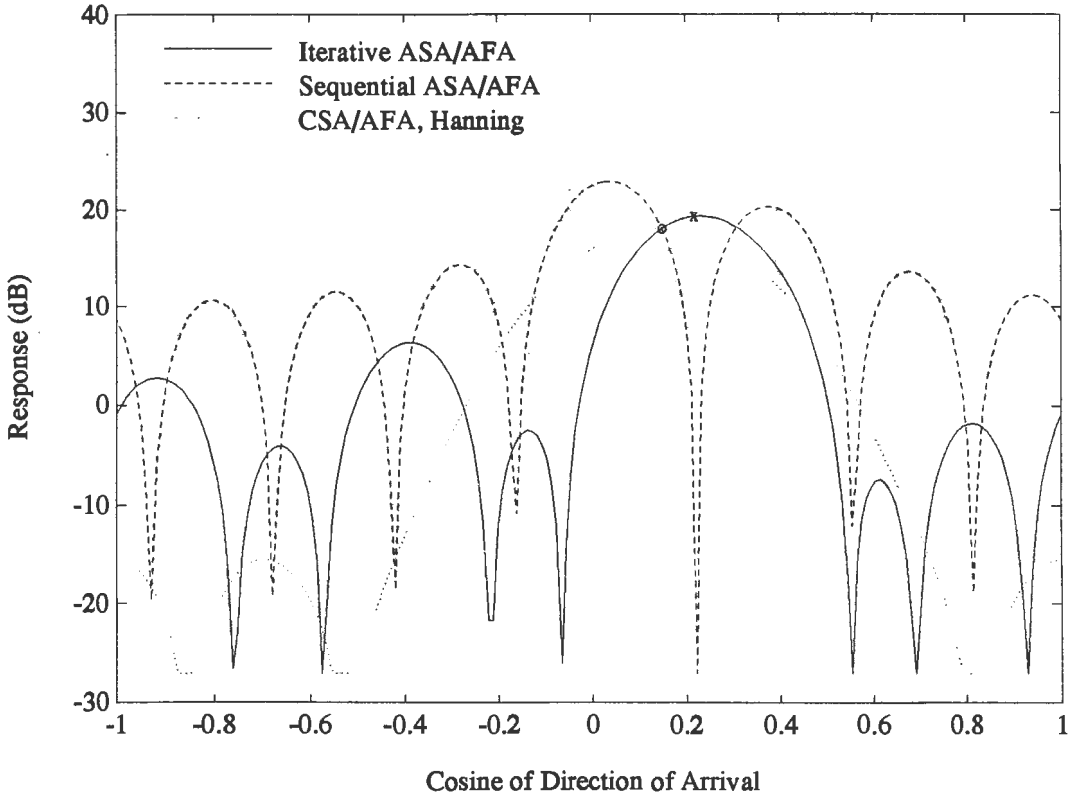

Figure 4.1: Subarray Beampatterns for a Close Interferer

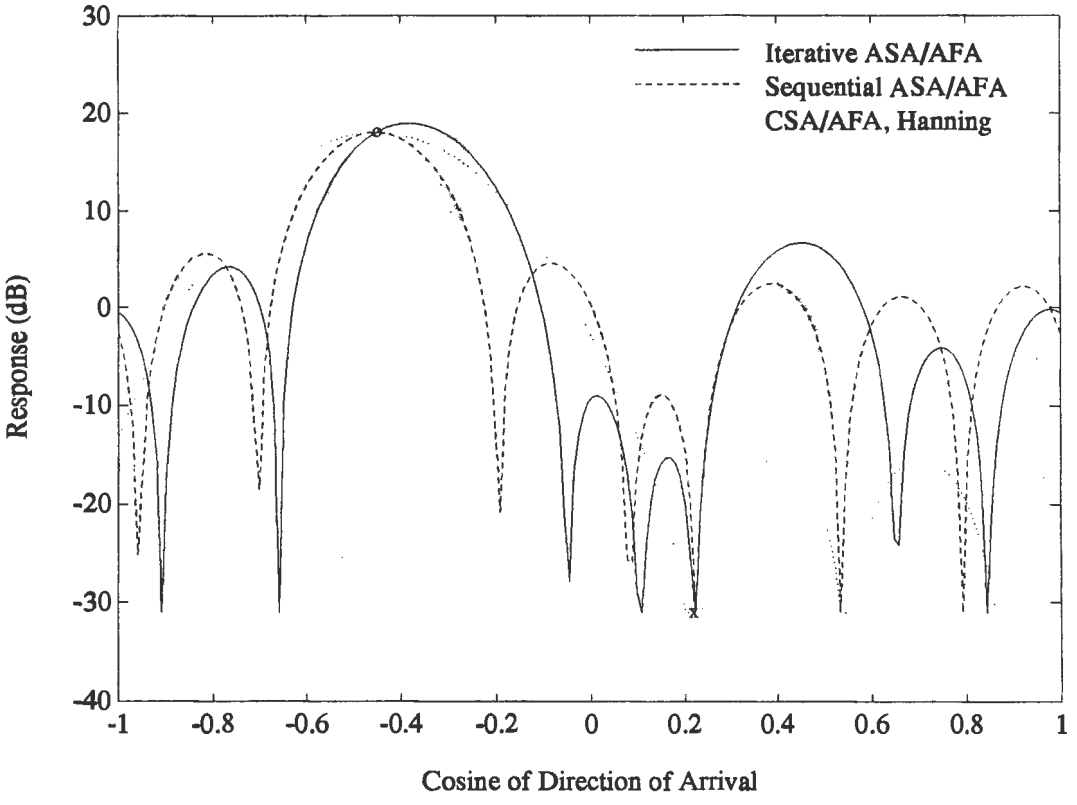

Figure 4.2: Subarray Beampatterns for a Distant Interferer

Table 4.1: Power Outputs and Noise Gains for Subarray Processors

Method	Beamform at 0.15		Beamform at -0.45	
	$\text{Power}_{\text{out}}$	NG	$\text{Power}_{\text{out}}$	NG
Fully Adaptive	23.1	23.0	20.0	20.0
Iterative ASA/AFA	24.2	24.1	20.6	20.6
Sequential ASA/AFA	40.5	31.4	21.3	21.2
CSA/AFA	32.3	32.1	23.6	23.6
Conv. Full Array	191.9	20.0	22.7	20.0

interferer in a null, then near optimal noise discrimination will occur, while cancelling the source entirely.).

Another less obvious observation is the fact that the sidelobes of the subarray beampattern are "picketed"; that is, every other sidelobe is smaller than its neighbor. The beamformer is using this sidelobe structure to achieve noise cancellation.

- The sequential ASA/AFA cancels the close interferer immediately in the first stage subarray beamformer and does no further signal cancellation in the full array beamformer. It does cancel the interferer, but it is clear that significant white noise amplification or gain has also occured.

  This beamformer also cancels the distant interferer with, apparently, little more than the minimum noise gain.

- The CSA/AFA subarray beamformer suppresses the proximate interferer at the subarray beamformer stage (with -40 dB sidelobes) and uses a "quiescent" beampattern to cancel the noise at the full array stage.

The output powers and noise gains for the two interference scenarios and three algorithms are given in the Table 4.1:

In reference to the above Table 4.1, the following observations can be made:

- The iterative ASA/AFA method performs nearly optimally, whether the interference is close in or far away.

From the beampatterns, it is clear that this beamformer "decides" whether to cancel an interferer based on the overall expense of the operation; when the interferer is close to the beamformer look direction, it is advantageous to cancel the signal at the full array stage, avoiding excessive noise gain. And, conversely, when the interferer is distant, this beamformer can afford to cancel the source at the first stage.

- The sequential ASA/AFA method performs nearly optimally when the interfering source is not close, but does poorly when the interferer is proximate.

  From the beampatterns, it is clear that the excessive subarray beamformer noise gain can not be compensated for by the full array beamformer. It is interesting to note that there is a measurable signal power remaining, for the close interferer scenario (as evidenced by the difference between the power out and the noise gain), and that the full array beamformer makes no effort to cancel it— the noise power has become so dominant that the response is basically "conventional." This could be viewed as an (inadvertently created) adaptive subarray/conventional full array beamformer.

- For the low-level examples used here, the CSA/AFA technique performs nearly optimally for the distant interferer and reasonably well for the close interferer. When the interferer is close, the full array beamformer is able to cancel the interferer, but at the expense of a measurable increase in noise gain.

  It will be shown, however, that CSA/AFA can produce "false alarms" due to spatial aliasing through the subarray beam's sidelobes.

From observing the beampatterns for the iterative ASA/AFA there are several features that an adaptive subarray beamformer would ideally adopt– such as "intelligent" mainlobe placement and signal cancellation and "picketed" sidelobe structure– but pursuit of these features in a sequential SA/FA beamformer seems impractical. Instead, a sub-optimal approach is now proposed:

- Constrain the mainlobe of the subarray response, well down towards the sidelobes, to be equal to that of a specified (bandpass) filter response,

- Allow the subarray beamformer to cancel signals in the sidelobes, and
- Allow the full array beamformer to cancel all signals, subject to a point constraint for the particular signal of interest.

This beamformer would not in general suffer from excessive subarray noise gain (because the mainlobe has not been "misshapen" from adaptive cancellation of close sources), and would cancel close interferers. Additionally, the constrained mainlobe guarantees a signal bandwidth (about the mainlobe peak), which is a required subarray beamformer characteristic.

The sub-optimal approach of subarray mainlobe constraint does not absolutely guarantee a low noise gain, and in some extreme cases an additional (inequality) noise gain constraint can be imposed on the beamformer. This option is investigated in section 4.3.

The iterative ASA/AFA technique, as presented in this section, is excessively costly in terms of computational burden. Other algorithmic approaches, such as reduced-rank signal-subspace representations [2, 3] of the CSDM, may reduce the computational load, making this method more attractive.

4.2 Mainlobe Constrained Subarray Processing

In section 4.1, the non-linear adaptive subarray beamforming solution was investigated, and it was shown that optimal performance is achieved when signals arriving in the quiescent beampattern's mainlobe are not cancelled by the subarray beamformer. In this section, a beamformer which constrains the response across the entire mainlobe is introduced, and it is shown that this beamformer (in most cases) avoids excessive noise gain.

The derivation of the full mainlobe constraint presented here follows very closely that of the integral constraint of section 3.3, except that here the desired response in the mainlobe is set equal to the response of a conventional beamforming filter [5]. The conventional beamforming filter chosen here has linear phase, nearly flat magnitude, and (acceptably) low sidelobes. The adaptive filter must match the response of the conventional beamforming filter or "model" filter in the constrained region and adjust the sidelobe

response to minimize power output. The advantage of using a model filter is that an adaptive filter can match the desired response and still have low sidelobes.

In this thesis the Parks-McClellan equi-ripple filter is used as the model filter. This flexible filter is chosen because mainlobe width, passband ripple, and stopband sidelobe levels can be adjusted. This will prove useful in selecting a subarray configuration which has maximal subarray beamwidth, low sidelobes, and does not exhibit spatial aliasing. The topic of choosing a model filter, other than the Parks-McClellan filter, which is "optimal" is not pursued in this thesis.

To constrain the response of the subarray beamformer across a spatial region, the difference or error between the actual response and a specified, realizable response is integrated, and the total error is set to zero. The integrated error is

$$\begin{aligned} e^2 &= \int_{\phi=\theta-\Delta/2}^{\theta+\Delta/2} \left|\mathbf{u}^H\mathbf{d}(\phi) - \mathbf{e}^H(\theta)\mathbf{d}(\phi)\right|^2 \mathrm{d}\phi \\ &= \int_{\phi=\theta-\Delta/2}^{\theta+\Delta/2} \left(\mathbf{u}^H\mathbf{d}\mathbf{d}^H\mathbf{u} - \mathbf{u}^H\mathbf{d}\mathbf{d}^H\mathbf{e} - \mathbf{e}^H\mathbf{d}\mathbf{d}^H\mathbf{u} + \mathbf{e}^H\mathbf{d}\mathbf{d}^H\mathbf{e}\right) \mathrm{d}\phi, \end{aligned} \tag{4.13}$$

where

$$\begin{aligned} \theta &\equiv \text{the subarray focussing direction,} \\ \Delta &\equiv \text{the mainlobe width,} \\ \mathbf{d}(\phi) = \mathbf{d} &\equiv \text{the } M \times 1 \text{ steering vector at angle } \phi, \\ \mathbf{e}(\theta) = \mathbf{e} &\equiv \text{The } M \times 1 \text{ conventional filter, or "model," vector, and} \\ \mathbf{u} &\equiv \text{the } M \times 1 \text{ subarray adaptive filter vector.} \end{aligned}$$

Defining the $M \times M$ matrix $\mathbf{D}_\theta$,

$$\mathbf{D}_\theta = \int_{\phi=\theta-\Delta/2}^{\theta+\Delta/2} \mathbf{d}\mathbf{d}^H \mathrm{d}\phi, \tag{4.14}$$

and substituting the eigenvector-eigenvalue decomposition of $\mathbf{D}_\theta$,

$$\mathbf{D}_\theta = \mathbf{M}\Sigma\mathbf{M}^H, \tag{4.15}$$

the integrated error (4.13) becomes

$$\begin{aligned} e^2 &= \mathbf{u}^H\mathbf{D}_\theta\mathbf{u} - \mathbf{u}^H\mathbf{D}_\theta\mathbf{e} - \mathbf{e}^H\mathbf{D}_\theta\mathbf{u} + \mathbf{e}^H\mathbf{D}_\theta\mathbf{e} \\ &= \mathbf{u}^H\mathbf{M}\Sigma\mathbf{M}^H\mathbf{u} - \mathbf{u}^H\mathbf{M}\Sigma\mathbf{M}^H\mathbf{e} - \mathbf{e}^H\mathbf{M}\Sigma\mathbf{M}^H\mathbf{u} + \mathbf{e}^H\mathbf{D}\Sigma\mathbf{M}^H\mathbf{e}. \end{aligned} \tag{4.16}$$

It is clear that if

$$\mathbf{M}^H\mathbf{u} = \mathbf{M}^H\mathbf{e}, \tag{4.17}$$

then the error (4.16) is zero, and the adaptive filter $\mathbf{u}$ *exactly* matches the conventional response of the filter vector $\mathbf{e}$— in the specified region $\theta - \Delta \leq \phi \leq \theta + \Delta$. It is noteworthy that a set of linear point constraints can be used to satisfy an integral constraint. It is, however, not practical to use (4.17) as a set of linear constraints, because, noting that the matrix $\mathbf{M}$ is full-rank, the constraints would consume all available degrees of freedom.

To allow for the greatest number of degrees of freedom (in a least squares, adaptive solution), form a lower-rank approximation to the matrix $\mathbf{D}_\theta$,

$$\mathbf{D}_\theta \approx \mathbf{D}_r = \mathbf{M}_r\Sigma_r\mathbf{M}_r^H, \tag{4.18}$$

where r is the rank of the approximation matrix $\mathbf{D}_r$, the $M \times r$ matrix $\mathbf{M}_r$ contains the r eigenvectors associated with the r largest eigenvalues of $\mathbf{D}_\theta$, and the $r \times r$ diagonal matrix Σ_r contains the r largest eigenvalues of $\mathbf{D}_\theta$. The rank of $\mathbf{D}_r$ determines the degree to which the integral constraint is met. (In the example that follows, six eigenvectors are used, spanning 99.99% of the total eigenvalue power.)

The adaptive filter $\mathbf{u}$ which (approximately) matches the desired conventional response in the mainlobe, while producing minimum expected power output, satisfies the equation

$$y(\theta) = \min_{\mathbf{u}} \left\{ \mathbf{u}^H\mathbf{R}\mathbf{u} \right\}, \text{ subj to } \left\{ \mathbf{M}_r^H\mathbf{u} = \mathbf{M}_r^H\mathbf{e} \right\}. \tag{4.19}$$

The solution to (4.19) is

$$\mathbf{u} = \mathbf{R}\mathbf{M}_r \left(\mathbf{M}_r^H\mathbf{R}^{-1}\mathbf{M}_r \right)^{-1} \mathbf{M}_r^H\mathbf{e}. \tag{4.20}$$

As an aside, the issue of the computational burden of calculating (4.20) is discussed, with regards to a complex Hermitian Toeplitz CSDM. If the elements of a subarray are (considered) evenly and linearly spaced, the subarray CSDM is a complex Hermitian Toeplitz matrix. The benefits of the CSDM structure are:

- The CSDM estimate involves estimating M quantities, instead of the $\frac{M(M+1)}{2}$ quantities in a general $M \times M$ CSDM. And the M CSDM quantities, using a DFT convolution, can be estimated very quickly.

- A complex Hermitian Toeplitz matrix inverse can be calculated in order M^2 steps, as compared to order M^3 steps for a general $M \times M$ matrix.

- The statistical information in a CSDM estimate can be increased by using all the sensors in the array to form one subarray CSDM estimate. (The single CSDM estimate can be used to form the adaptive filter vector for all subarrays.) This increases the computational burden slightly, but affords greater stability in the estimate.

It is noted that assuming a Hermitian Toeplitz structure precludes applications where the array is not assumed linear.

To illustrate the integral constraint subarray beamformer, Figures 4.4 — 4.5 show the subarray and overall full array beampatterns, respectively, for a close interferer, and Figures 4.6 — 4.7 show the same beampatterns for a distant interferer. For the integrally constrained responses, the rank r was selected so as to include 99.99% of the energy of the matrix $\mathbf{D}$, using six eigenvectors (out of nine available). For comparison, the CSA/AFA responses are plotted, where the conventional subarray filter of the mainlobe constraint method is used. Interference scenario 2 of Table 4.4 is used, and the subarrays are setup according to 4.52.

In the examples described above, the subarray "model" filter $\mathbf{e}$ used is a Parks-McClellan equi-ripple filter. Figure 4.3 shows the beampattern for this filter and that of a Hamming window. The Parks-McClellan window is a bandpass filter, with a stop bandwidth roughly equal to that of the Hamming window. (The subarray overlap percentages are the same, but fewer subarray beams are required.)

Figure 4.4 shows the subarray beampattern for the close interferer. The limits of the integral constraint are indicated by two circles, placed on the beampattern. The response of the approximate integral constraint filter and the conventional filter are seen to be almost identical in the mainlobe, differing only slightly at the "tails" of the mainlobe. Figure 4.5 shows the overall full array beampattern for the close interferer. It is clear that the source is cancelled at the full array stage.

Table 4.2: Power Outputs for Mainlobe Constrained Subarray Processor

Method	Beamform at 0.10			Beamform at -0.50		
	P_{out}	NG	PI (dB)	P_{out}	NG	PI (dB)
Fully Adaptive	21.73	21.72	0.00	21.05	21.05	0.00
ML Constrained SA	28.76	28.76	1.22	28.58	28.58	1.33
CSA/AFA	28.68	28.68	1.21	28.58	28.56	1.33

Figure 4.6 shows the subarray beampattern for the far interferer. The limits of the integral constraint are indicated by two circles, placed on the beampattern. It is clear that the source is cancelled at the subarray stage. Figure 4.7 shows the overall full array beampattern for the far interferer.

Using the integrally constrained subarray beamformer, the full array beam power output for the distant and close interferer cases are slightly higher than the optimal, direct beamformer. In Table 4.2, the power outputs and noise gains for the fully adaptive, the mainlobe constrained SA/adaptive FA, and conventional SA/adaptive FA beamformers are given. Also, a measure of the power increase, defined as

$$\mathrm{PI} \equiv \frac{P_{out}}{P_{out_{MVDR}}}, \tag{4.21}$$

is included. The power increase (PI) compares the output power for a selected beamformer with the minimum power output of the direct, MVDR solution. The power increases of the mainlobe constrained beamformer, for the close and distant interferer cases, are approximately equal and acceptably low.

The increase in the output power is a consequence of the reduced number of degrees of freedom at the full array stage and the (spatially) wide subarray beam: the subarray beam is very wide (approximately one half of the total spatial bandwidth) and the full array stage must cancel the white noise in this large bandwidth with a small number of degrees of freedom. It is inevitable that there is a small increase in noise gain. If a decrease in noise gain is sought, the number of subarrays can be increased and/or the spatial bandwidth of the subarray beam can be decreased.

The integrally constrained subarray beamformer is a good choice for an adaptive first stage. It performs nearly optimally and does not introduce a large computational burden (linear solution, using the Hermitian Toeplitz

property). In section 4.4, another very similar technique is introduced which yields nearly identical performance, with significantly less computational burden.

4.3 Noise Gain Constrained Subarray Processing

In section 4.1, it was shown that a linearly constrained subarray beamformer which attempts to cancel strong proximate sources will produce significant increases in noise gain in the subarray output (and the full array output). An alternative subarray beamformer would cancel interfering sources, subject to (linear) signal constraints, provided that the noise gain did not exceed a specified threshold [16]. Accordingly, in this section, the minimization of the subarray beamformer power output subject to a (white) noise gain constraint and other linear constraints is investigated.

The noise gain has been defined as the ratio of the beamformer output from white noise to input power from white noise. Here subarray noise gain

$$\mathrm{NG_{sa}} = \frac{\mathbf{u}^H \sigma_n^2 \mathbf{I} \mathbf{u}}{\sigma_n^2} = \mathbf{u}^H \mathbf{u}. \tag{4.22}$$

is defined as the gain against white noise in the subarray stage beamformer.

Because of the signal gain constraint of P at the subarray focussing point, the noise gain constraint must be greater than or equal to P to be realizable. For practical purposes, an upper bound on the noise gain is set a fraction higher than the noise gain of the conventional subarray filter vector (after which the signal constraints are modeled). This establishes the limits on the subarray beamformer noise gain of

$$P \leq \mathbf{u}^H \mathbf{u} \leq k \mathbf{e}^H \mathbf{e} \equiv k P_e \ (k > 1\ ), \tag{4.23}$$

where $P_e \equiv \mathbf{e}^H \mathbf{e}$ is the subarray noise gain of the "model" filter vector $\mathbf{e}$. The value of k used is determined by how much excess noise is considered acceptable. As an aside, if k is set to less than unity, then the "quiescent" beampattern is altered, producing a narrower mainlobe and higher sidelobes. (Here quiescent [17] refers to the response to white noise only.)

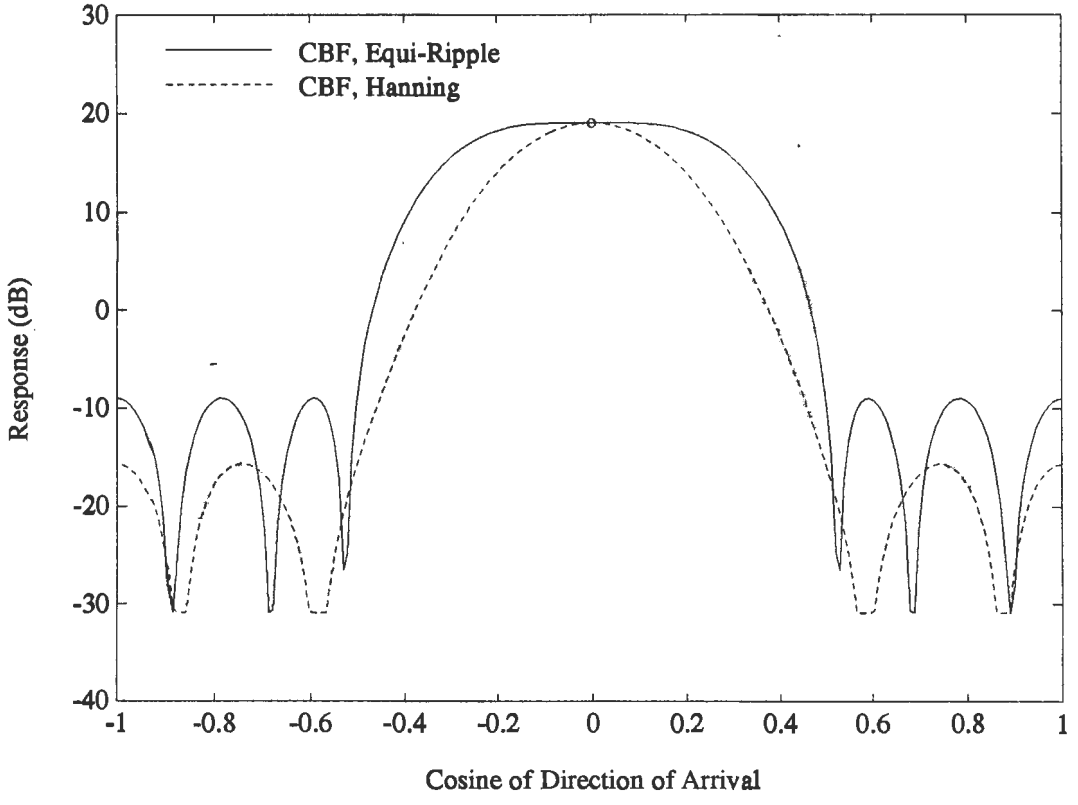

Figure 4.3: Subarray Beampatterns for Selected Conventional Windows

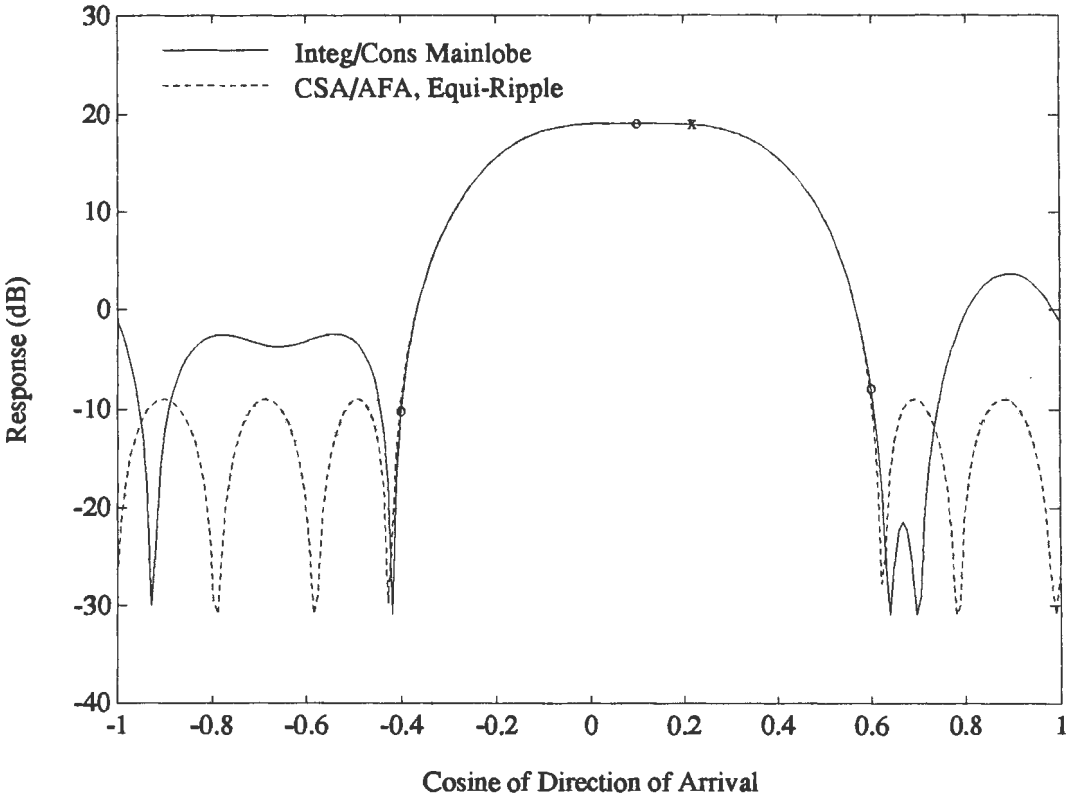

Figure 4.4: Mainlobe Constrained Subarray Beampatterns for a Close Interferer

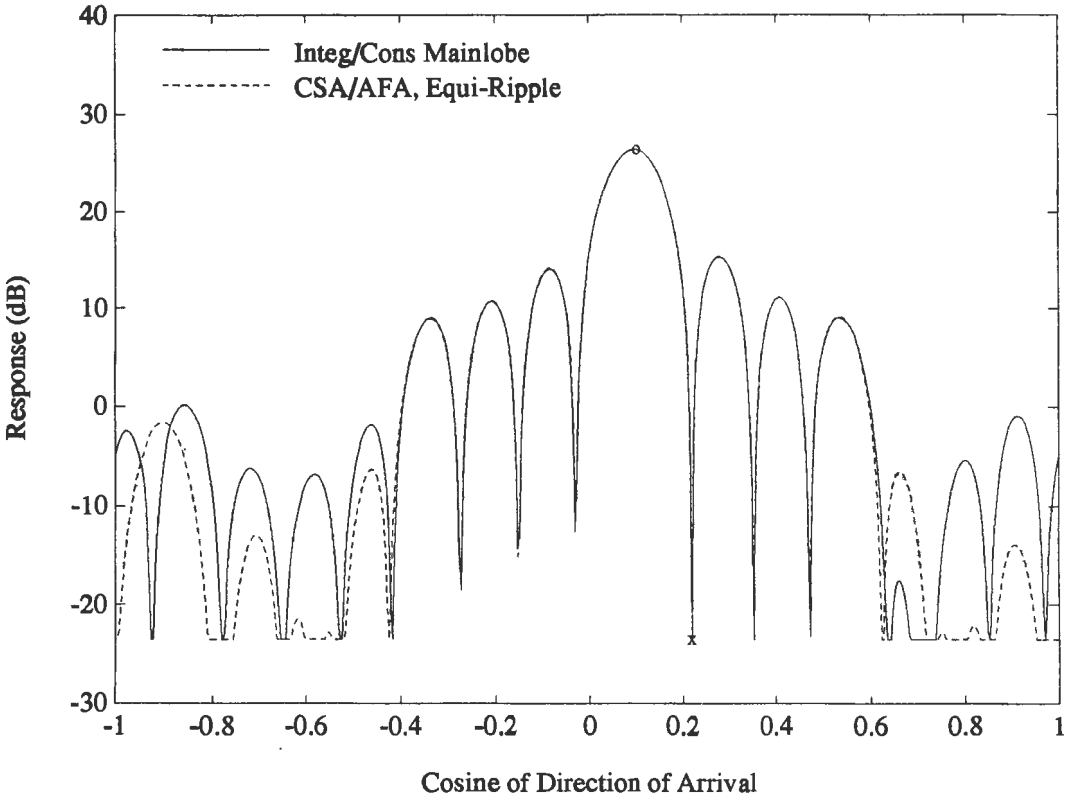

Figure 4.5: Mainlobe Constrained Overall Full Array Beampatterns for a Close Interferer

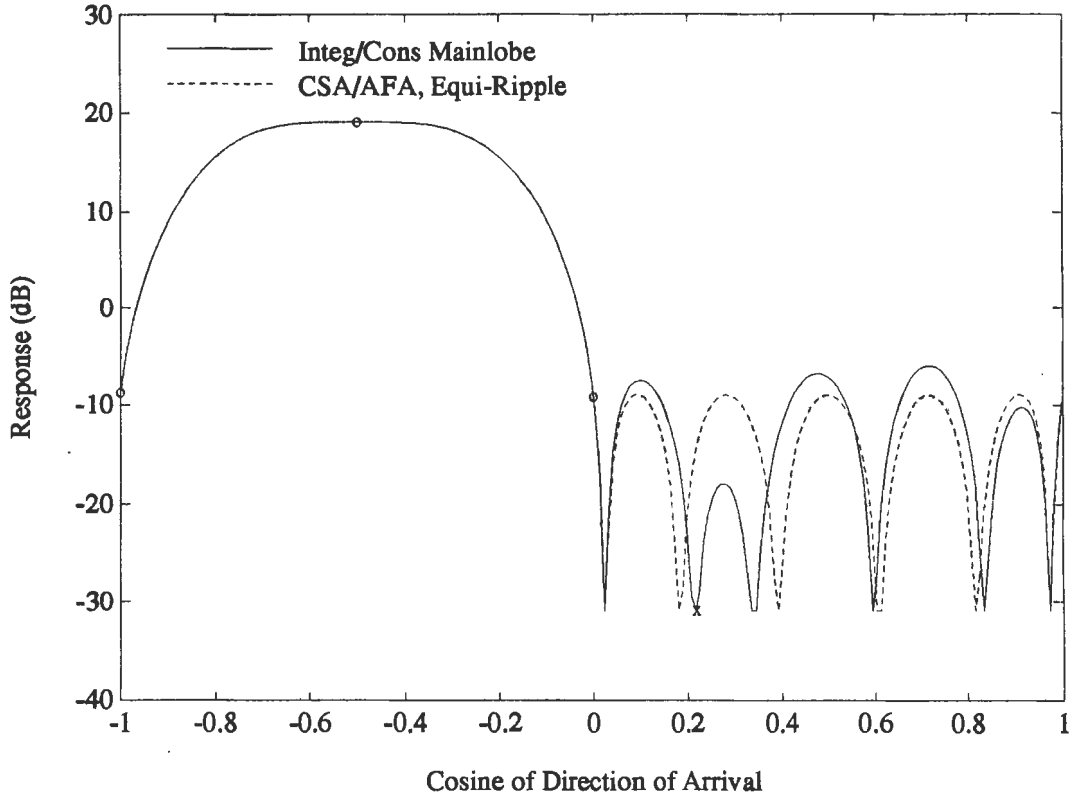

Figure 4.6: Mainlobe Constrained Subarray Beampatterns for a Distant Interferer

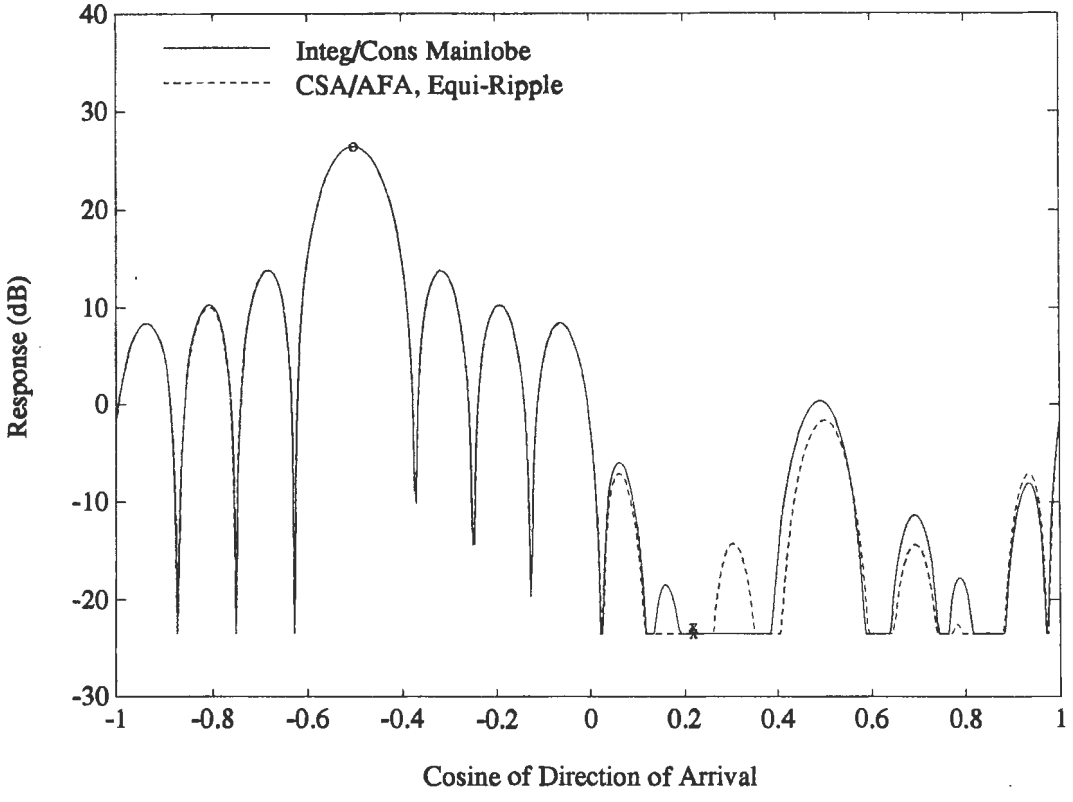

Figure 4.7: Mainlobe Constrained Overall Full Array Beampatterns for a Distant Interferer

The subarray beamformer which minimizes the power output, subject to multiple linear signal constraints and a noise gain constraint, must satisfy

$$y = \min_{\mathbf{u}} \left\{ \mathbf{u}^H \mathbf{R} \mathbf{u} \right\}, \text{ subj to } \left\{ \mathbf{u}^H \mathbf{u} \leq k P_e, \mathbf{D}^H \mathbf{u} = \mathbf{b} \right\}. \tag{4.24}$$

Here k is chosen to be slightly greater than unity and the $P \times C$ matrix $\mathbf{D}$ contains the signal vectors of interest, and the $C \times 1$ vector $\mathbf{b}$ contains the signal constraints. The signal vector matrix $\mathbf{D}$ and its corresponding signal constraint vector $\mathbf{c}$ could represent a set of point constraints, integral constraints, or any other set of meaningful linear signal constraints.

To avoid solving both constraints simultaneously, a rotation matrix $\mathbf{B}$ is sought which satisfies the following two equations:

$$\mathbf{D}^H \mathbf{B} = \begin{bmatrix} \mathbf{I}_C & \mathbf{0} \end{bmatrix} \text{ and} \tag{4.25}$$

$$\mathbf{B}^H \mathbf{B} = \begin{bmatrix} \tilde{\mathbf{B}} & \mathbf{0} \\ \mathbf{0} & \mathbf{I}_{P-C} \end{bmatrix}, \tag{4.26}$$

where the $C \times C$ matrix $\tilde{\mathbf{B}}$ is to be a specified, non-singular matrix.

As will be seen the two conditions on $\mathbf{B}$, as represented by (4.25) and (4.26), will allow the solution of (4.24) to be found with regard to the noise-gain constraint only, knowing that the linear constraints must be satisfied.

To find a matrix $\mathbf{B}$ which satisfies (4.25) and (4.26), perform the following singular value decomposition on the constraint vectors $\mathbf{D}$:

$$\mathbf{D}^H = \mathbf{U}\mathbf{S}\mathbf{V}^H = \mathbf{U} \begin{bmatrix} \mathbf{S}_D & \mathbf{0} \end{bmatrix} \begin{bmatrix} \mathbf{V}_D & \mathbf{V}_0 \end{bmatrix}^H = \mathbf{U}\mathbf{S}_D\mathbf{V}_D^H. \tag{4.27}$$

Here the $C \times C$ matrix $\mathbf{U}$ contains the left-hand singular vectors. The $C \times P$ matrix $\mathbf{S}$ of singular values is partitioned into the $C \times C$ matrix $\mathbf{S}_D$ of non-zero singular values and the $C \times P - C$ matrix of zeros. And the $P \times P$ matrix $\mathbf{V}$ of right-hand singular vectors is partitioned into an $P \times C$ matrix $\mathbf{V}_D$ and an $P \times P - C$ matrix $\mathbf{V}_0$.

Then, if the rotation matrix $\mathbf{B}$ is defined as

$$\mathbf{B} = \begin{bmatrix} \mathbf{V}_D \mathbf{S}_D^{-1} \mathbf{U}^H & \mathbf{V}_0 \end{bmatrix}, \tag{4.28}$$

it is clear that

$$\mathbf{D}^H \mathbf{B} = \mathbf{U}\mathbf{S}\mathbf{V}_D^H \begin{bmatrix} \mathbf{V}_D \mathbf{S}_D^{-1} \mathbf{U}^H & \mathbf{V}_0 \end{bmatrix} = \begin{bmatrix} \mathbf{I}_C & \mathbf{0} \end{bmatrix} \tag{4.29}$$

and that

$$\begin{aligned}\mathbf{B}^H\mathbf{B} &= \begin{bmatrix} \mathbf{U}\mathbf{S}_D^{-1}\mathbf{V}_D^H \\ \mathbf{V}_0^H \end{bmatrix} \begin{bmatrix} \mathbf{V}_D\mathbf{S}_D^{-1}\mathbf{U}^H & \mathbf{V}_0 \end{bmatrix} \\ &= \begin{bmatrix} \mathbf{U}\mathbf{S}_D^{-2}\mathbf{U}^H & \mathbf{0} \\ \mathbf{0} & \mathbf{I}_{P-C} \end{bmatrix} = \begin{bmatrix} \tilde{\mathbf{B}} & \mathbf{0} \\ \mathbf{0} & \mathbf{I}_{P-C} \end{bmatrix}. \end{aligned} \tag{4.30}$$

Therefore equation (4.28) satisfies (4.25) and (4.26).

Given a rotation matrix $\mathbf{B}$ from (4.28), the linear constraints become

$$\begin{aligned}\mathbf{D}^H\mathbf{u} &= \mathbf{D}^H\mathbf{B}\mathbf{v} = \mathbf{D}^H\mathbf{B}\begin{bmatrix} \mathbf{v}_c \\ \mathbf{v}_a \end{bmatrix} \\ &= \begin{bmatrix} \mathbf{I}_C & \mathbf{0} \end{bmatrix}\begin{bmatrix} \mathbf{v}_c \\ \mathbf{v}_a \end{bmatrix} = \mathbf{v}_c = \mathbf{b}. \end{aligned} \tag{4.31}$$

Here the rotated filter vector $\mathbf{v}$ has been partitioned into a $C\times 1$ "constrained" filter vector $\mathbf{v}_c$ and a $P-C\times 1$ "adaptive" filter vector $\mathbf{v}_a$. Note, from (4.31), that the vector $\mathbf{v}_c$ must be equal to the constraints $\mathbf{b}$, leaving the vector $\mathbf{v}_a$ "free" for use in minimization.

Substituting (4.31) and (4.30) into the original constrained problem and minimizing with respect to the free variables $\mathbf{v}_a$, the minimum output power must satisfy

$$\begin{aligned} y &= \min_{\mathbf{v}_a}\left\{ \begin{bmatrix} \mathbf{v}_c \\ \mathbf{v}_a \end{bmatrix}^H \mathbf{B}^H\mathbf{R}\mathbf{B}\begin{bmatrix} \mathbf{v}_c \\ \mathbf{v}_a \end{bmatrix} \right\}, \\ &\quad \text{subj to } \left\{ \begin{bmatrix} \mathbf{v}_c \\ \mathbf{v}_a \end{bmatrix}^H \mathbf{B}^H\mathbf{B}\begin{bmatrix} \mathbf{v}_c \\ \mathbf{v}_a \end{bmatrix} \le kP_e \right\} \text{or} \\ &= \min_{\mathbf{v}_a}\left\{ \begin{matrix} \mathbf{v}_c^H\tilde{\mathbf{R}}_{11}\mathbf{v}_c + \mathbf{v}_c^H\tilde{\mathbf{R}}_{12}\mathbf{v}_a + \\ \mathbf{v}_a^H\tilde{\mathbf{R}}_{21}\mathbf{v}_c + \mathbf{v}_a^H\tilde{\mathbf{R}}_{22}\mathbf{v}_a \end{matrix} \right\}, \\ &\quad \text{subj to } \left\{ \mathbf{v}_c^H\tilde{\mathbf{B}}\mathbf{v}_c + \mathbf{v}_a^H\mathbf{v}_a \le kP_e \right\}. \end{aligned} \tag{4.32}$$

Here the $P\times P$ matrix $\tilde{\mathbf{R}}$ is defined as

$$\tilde{\mathbf{R}} = \mathbf{B}^H\mathbf{R}\mathbf{B} = \begin{bmatrix} \tilde{\mathbf{R}}_{11} & \tilde{\mathbf{R}}_{12} \\ \tilde{\mathbf{R}}_{21} & \tilde{\mathbf{R}}_{22} \end{bmatrix}, \tag{4.33}$$

where $\tilde{\mathbf{R}}_{11}$ is a $C\times C$ matrix, $\tilde{\mathbf{R}}_{12}$ and $\tilde{\mathbf{R}}_{21}^T$ are $C\times P-C$ matrices, and $\tilde{\mathbf{R}}_{22}$ is a $P-C\times P-C$ matrix.

The optimum adaptive filter $\mathbf{v}_a$, obtained using the method of undetermined Lagrangian multipliers, is

$$\mathbf{v}_a = -\left(\tilde{\mathbf{R}}_{22} + \lambda \mathbf{I}\right)^{-1} \tilde{\mathbf{R}}_{21} \mathbf{v}_c, \tag{4.34}$$

and substituting this filter into the noise gain constraint the solution is found for a positive value of λ satisfying

$$\mathbf{v}_c^H \tilde{\mathbf{R}}_{12} \left(\tilde{\mathbf{R}}_{22} + \lambda \mathbf{I}\right)^{-2} \tilde{\mathbf{R}}_{21} \mathbf{v}_c + \mathbf{v}_c^H \tilde{\mathbf{B}} \mathbf{v}_c = k P_e. \tag{4.35}$$

If a positive λ can be found then the noise gain equality constraint is in effect, otherwise (4.32) can be solved without the noise gain constraint [18].

To facilitate numerical solution of (4.35), perform the following eigenvalue-eigenvector decomposition on the hermitian Toeplitz matrix $\tilde{\mathbf{R}}_{22}$,

$$\tilde{\mathbf{R}}_{22} = \mathbf{M} \mathbf{\Lambda} \mathbf{M}^H, \tag{4.36}$$

where the $P - C \times P - C$ matrix $\mathbf{M}$ contains the eigenvectors of $\tilde{\mathbf{R}}_{22}$ and the $P - C \times P - C$ matrix $\mathbf{\Lambda}$ contains the eigenvalues of $\tilde{\mathbf{R}}_{22}$.

Substituting the decomposition of (4.36) into (4.35), the desired value of λ must satisfy

$$\begin{aligned} \mathbf{v}_c^H \tilde{\mathbf{R}}_{12} \mathbf{M} \left(\mathbf{\Lambda} + \lambda \mathbf{I}\right)^{-2} \mathbf{M}^H \tilde{\mathbf{R}}_{21} \mathbf{v}_c &= k P_e - \mathbf{v}_c^H \tilde{\mathbf{B}} \mathbf{v}_c, \\ \tilde{\mathbf{v}}_c^H \left(\mathbf{\Lambda} + \lambda \mathbf{I}\right)^{-2} \tilde{\mathbf{v}}_c &= \acute{P}, \text{ or} \\ \sum_{i=1}^{P-C} \frac{|\tilde{\mathbf{v}}_{c_i}|^2}{\left(\Lambda_i + \lambda\right)^2} &= \acute{P}. \end{aligned} \tag{4.37}$$

Here the constant $\acute{P}$ is equal to $k P_e - \mathbf{v}_c^H \tilde{\mathbf{B}} \mathbf{v}_c$ and the $P - C \times 1$ vector $\tilde{\mathbf{v}}_c$ is defined as $\mathbf{M}^H \tilde{\mathbf{R}}_{21} \mathbf{v}_c$.

In (4.37) it is clear that there are poles at $\{\lambda = -\Lambda_i\}_{i=1}^{P-C}$ and that the left hand side of the equation goes, monotonically, to zero as the absolute value of λ goes to infinity. Therefore, the desired value of λ lies on the positive side of the largest pole; that is

$$\lambda > -\min\left(\{\Lambda_i\}_{i=1}^{P-C}\right) \equiv \Lambda_{min}, \tag{4.38}$$

$$\Lambda_{min} < \lambda < \infty. \tag{4.39}$$

Using (4.39), equation (4.37) can be solved using a numerical root-finding technique which starts its search at zero and "looks" in the positive direction. If, at λ, the left hand side of (4.37) is less than $\acute{P}$, then only a negative value of λ will solve the equation, and it becomes possible to solve (4.24) without the noise gain constraint.

Provided that the noise gain constraint is in effect ($\lambda > 0$), then the optimum noise gain and linearly constrained filter is

$$\mathbf{u} = \mathbf{B}\begin{bmatrix} \mathbf{v}_c \\ \mathbf{v}_a \end{bmatrix} = \mathbf{B}\begin{bmatrix} \mathbf{I}_C \\ -\left(\tilde{\mathbf{R}}_{22} + \lambda\mathbf{I}\right)^{-1}\tilde{\mathbf{R}}_{21} \end{bmatrix}\mathbf{b}, \tag{4.40}$$

where $\mathbf{v}_c = \mathbf{b}$ and $\mathbf{v}_a$ has been solved in terms of λ using (4.34).

To illustrate this technique, Figures 4.8 — 4.9 show the subarray and overall full array beampatterns for a "close" interferer, where the noise gain constraint is in effect. And Figure 4.10 shows the subarray beampattern for a "distant" interferer, when the noise gain constraint is not in effect. The signal is constrained, using the reduced-rank integral constraint approximation, over a narrow region at the top of the mainlobe. In this case, only 3 eigenvalues are needed to "span" the constraint matrix $\mathbf{D}_\theta$. It is unnecessary to constrain the entire mainlobe, because of the noise gain constraint. In these examples, the subarray noise gain constraint is $\mathrm{NG_{sa}} \leq kP_e \equiv 1.02P_e$.

Figure 4.8 shows the subarray beampattern for a close interferer. The subarray beamformer attenuates the interfering source slightly, at some expense in noise gain. In this case the noise gain constraint is in effect. And Figure 4.9 shows the overall beampattern for the close interferer. The source is clearly cancelled at the full array stage..

Figure 4.10 shows the subarray beampattern for a distant interferer. The subarray beamformer cancels the interferer with a subarray noise gain of $0.91P_e$, which is less than the constraint $1.02P_e$. Therefore, the noise gain constraint is not in effect.

Table 4.3 shows the power outputs, full array noise gains, and power increases for the close and distant interferer cases. The results are very similar to those of section 4.2.

The noise gain constrained solution of this section is computationally burdensome, and, because it attenuates proximate sources, it does not "act" in a manner analogous to the optimum, non-linear beamformer of section

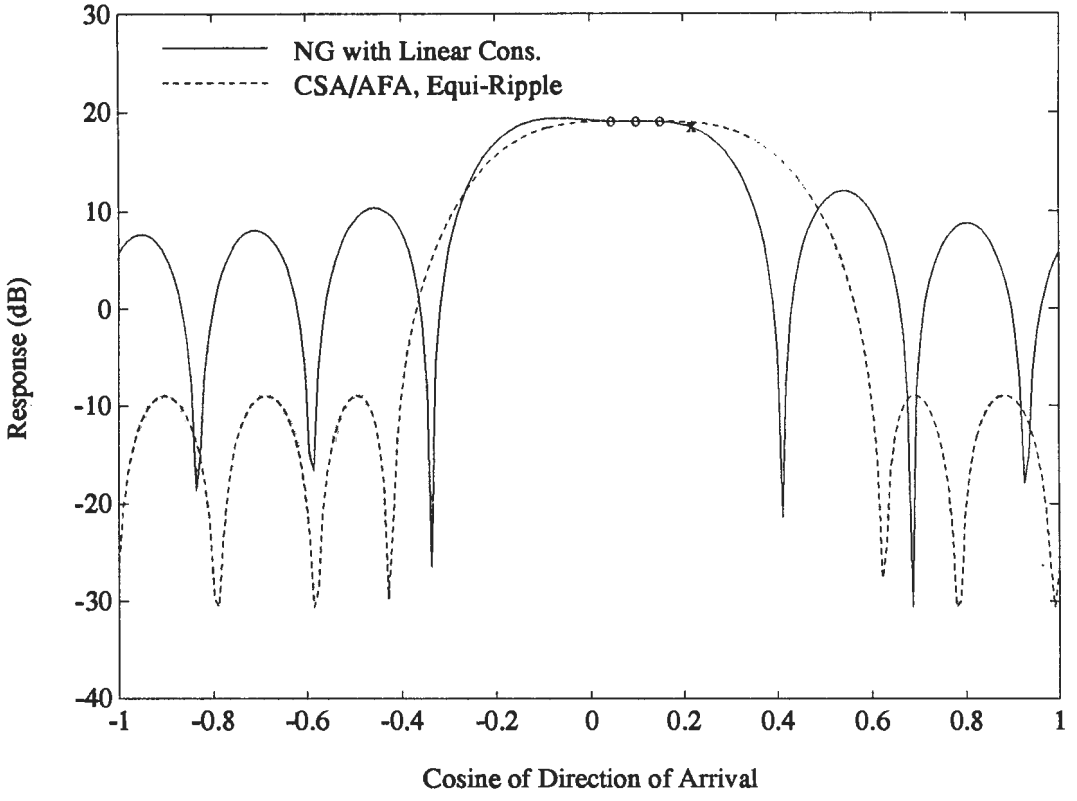

Figure 4.8: Noise Gain Constrained Subarray Beampatterns for one Close Interferer

Table 4.3: Power Outputs for Noise Gain Constrained Subarray Processor

Method	Beamform at 0.10			Beamform at -0.50		
	P_{out}	NG	PI (dB)	P_{out}	NG	PI (dB)
Fully Adaptive	21.73	21.72	0.00	21.05	21.05	0.00
NG Constrained SA	30.01	30.01	1.40	28.99	28.99	1.39
CSA/AFA	28.69	28.68	1.21	28.58	28.56	1.33

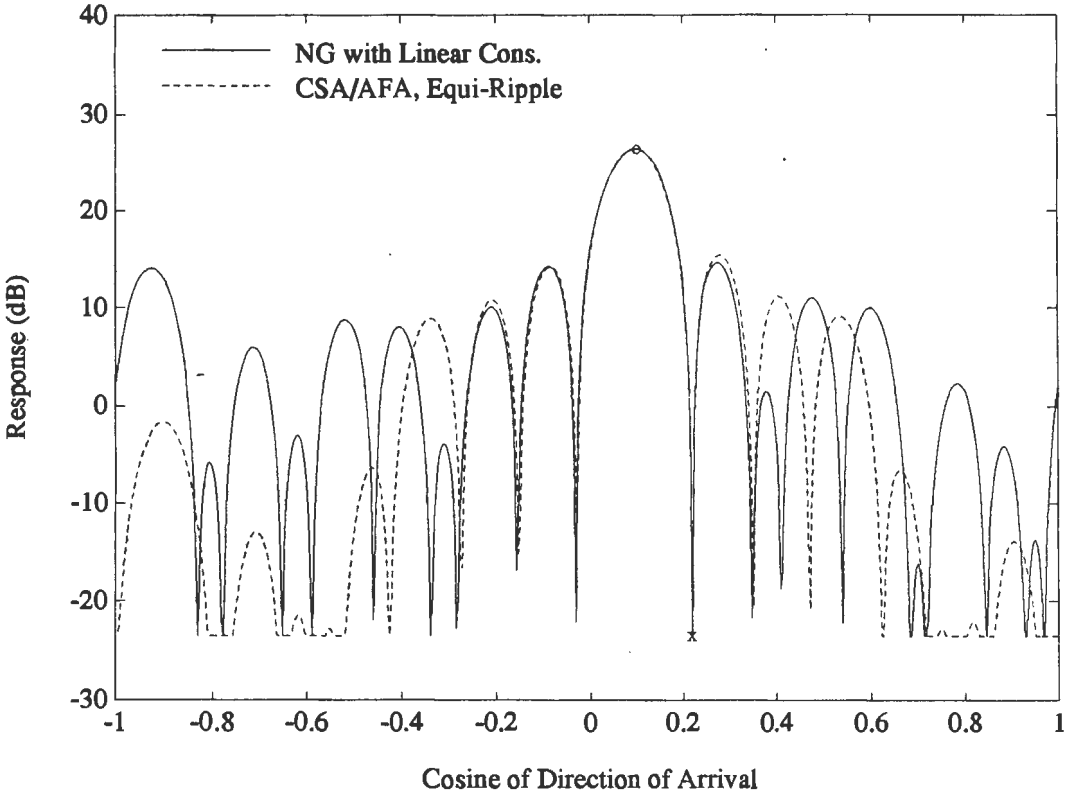

Figure 4.9: Noise Gain Constrained Overall Full Array Beampatterns for a Close Interferer

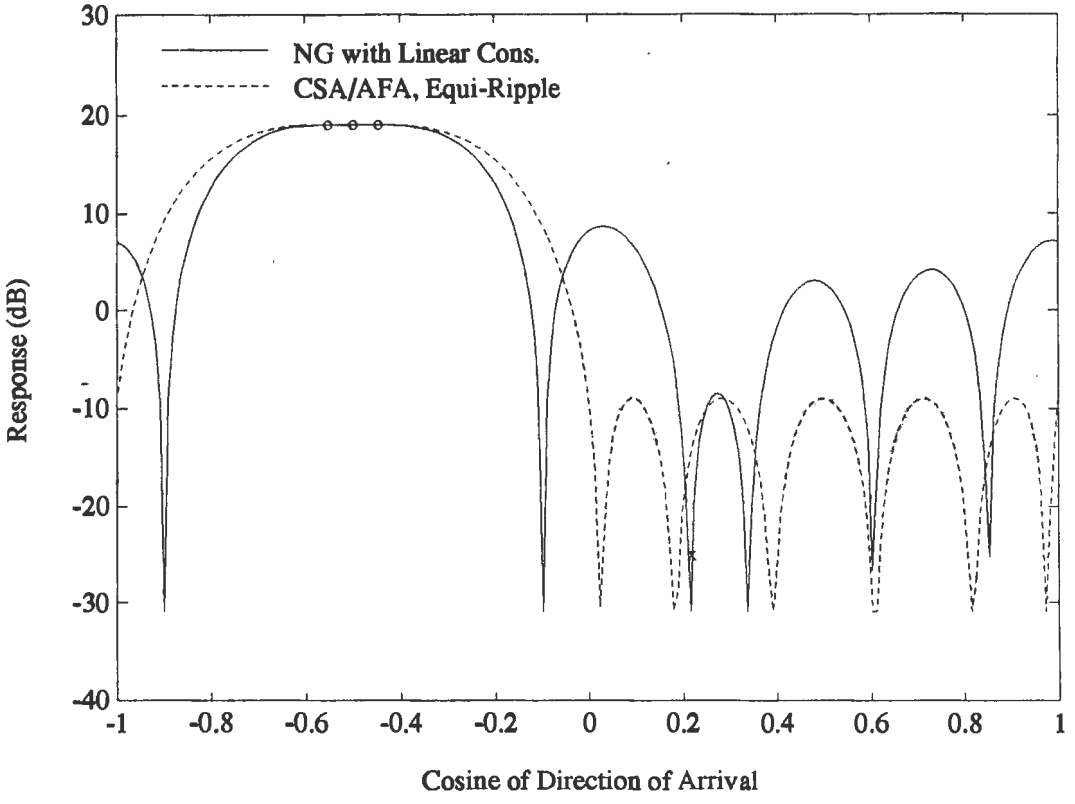

Figure 4.10: Noise Gain Constrained Subarray Beampatterns for a Distant Interferer

4.1. It does, however, illustrate an alternative formulation to the problem; one which can produce nearly equal results to the beamformer of section 4.2.

4.4 Mainlobe Constrained Subarray Processing using Penalties

In section 4.2, the mainlobe integrally constrained beamformer was introduced. This beamformer minimized output power, while achieving (exactly) a specified response in the subarray beam. The integrally constrained beamformer, however, requires two matrix inverses, as well as several matrix multiplications, leading to a computational burden which is significantly higher than, say, that of a point-constrained beamformer. In this section, a "penalty" method is introduced, which performs nearly identically to the integral constraint, but with much fewer calculations.

Minimum variance distortionless beamformers are often termed "hard" constrained solutions [5], because the Lagrangian multipliers ensure that the constraint is absolutely satisfied. An alternative formulation to this problem is to minimize (without constraints) the output power *plus* the error between the actual response and the desired response (in the subarray mainlobe). If the error is weighted more heavily than the objective function, then the optimum beamformer will cancel signals arriving outside of the mainlobe region, and tend to satisfy the "constraint," in the mainlobe. Such an approach is said to use a "soft" constraint, because the mathematics does not guarantee an exact response.

The soft constraint method minimizes the expected output power for the filter $\mathbf{u}$,

$$y(\mathbf{u}) = \mathbf{u}^H \mathbf{R} \mathbf{u}, \tag{4.41}$$

and the integrated mainlobe error term (see (4.13)),

$$e^2(\mathbf{u}) = e^2 = \mathbf{u}^H \mathbf{D} \mathbf{u} - \mathbf{u}^H \mathbf{D} \mathbf{e} - \mathbf{e}^H \mathbf{D} \mathbf{u} + \mathbf{e}^H \mathbf{D} \mathbf{e}, \tag{4.42}$$

subject to a weighting or penalty λ_p on the integrated error; that is, the soft constrained beamformer filter satisfies

$$y = \min_{\mathbf{u}} \left\{ y(\mathbf{u}) + \lambda_p e^2(\mathbf{u}) \right\}. \tag{4.43}$$

The solution to (4.43), in terms of the scalar penalty λ_p , is

$$\mathbf{u} = \lambda_p \left(\mathbf{R} + \lambda_p \mathbf{D}\right)^{-1} \mathbf{De}. \tag{4.44}$$

To ensure that the soft-constrained beamformer does not violate the constraint, it is necessary to penalize the error, caused by attenuating an interferer (even slightly), as heavily as the reduction in output power. A heuristic argument for the selection of the scalar penalty λ_p is now given.

The penalized integral error, for a slight attenuation a, can be approximated as

$$\begin{aligned} e_p^2 &\approx \lambda_p h^2 w \\ &\approx \lambda_p \left(P - aP\right)^2 \frac{1}{P}, \end{aligned} \tag{4.45}$$

where

$$\begin{aligned} a &\equiv \text{amount of interferer attenuation,} \\ h &\equiv \text{height of the error, and} \\ w &\equiv \text{assumed width of the attenuation.} \end{aligned}$$

Redefining the attenuation as

$$a = 1 - \epsilon, \tag{4.46}$$

the penalized integral error becomes

$$e_p^2 \approx \lambda_p P \epsilon^2. \tag{4.47}$$

The reduction in signal interference power output is

$$\Delta \mathrm{P}_{\mathrm{out}} = \sigma^2 P^2 - a^2 \sigma^2 P^2 = \left(2\epsilon - \epsilon^2\right) \sigma^2 P^2 \tag{4.48}$$

Now, assuming that the signal power reduction (4.47) is acceptable, the penalized, integral error (4.47) can be set equal to the power reduction (4.48). Solving for the scalar penalty λ_p, it is argued that

$$\lambda_p = \left(\frac{2}{\epsilon} - 1\right) P \sigma^2. \tag{4.49}$$

It is evident that the attenuation can not be set arbitrarily small, because λ_p will grow without bounds; hence, it is necessary to allow some attenuation. By experimentation, a value of

$$\epsilon \equiv \frac{1}{P^2} \tag{4.50}$$

has been found to be adequate.

Since the signal power σ^2 is not known, an upper bound on λ_p can be found using the trace of the CSDM and equation (4.50), giving

$$\lambda_p \equiv 2P^2 \text{trace}(R) > 2P^3\sigma^2. \tag{4.51}$$

If the value λ_p becomes much larger than the power of the sidelobe interferers, then this beamformer will not be capable of cancelling these interferers (due to numerical precision). For practical situations, where the dominant interferers are not hundreds of decibels above the "quieter" interferers, this is not a problem.

The argument given for selection of the penalty function λ_p assumed an interferer arriving at the top of the mainlobe. The same value has been found to work for all arrival locations in the mainlobe.

To evaluate the performance of the penalty method beamformer, the beampatterns, the integrated error terms, and power outputs will be calculated for three interference scenarios, as shown in Table 4.4. For comparison the responses for the subarray conventional filter vector $\mathbf{e}$, after which the constraints are modeled, are also shown. These scenarios are chosen to illustrate the following points:

- Scenario 1 shows that the penalty method works in a noise-only environment.
- Scenario 2 demonstrates that a strong mainlobe interferer does not (significantly) violate the constraint.
- Scenario 3 shows that a sidelobe interferer can be cancelled, in the presence of white noise and a mainlobe interferer.

Table 4.4: Interference Scenarios for Penalty Method

Scenario	Power (dB)		
	White Noise	Interferer @ 0.22	Interferer @ 0.90
1	0	OFF	OFF
2	0	5	OFF
3	0	5	0

For the examples that follow, the subarray setup variables are:

$$\begin{aligned} P &= 9 \quad \equiv \text{sensors per subarray,} \\ M &= 21 \quad \equiv \text{sensors in array, and} \\ S &= 7 \quad \equiv \text{number of subarrays.} \end{aligned} \tag{4.52}$$

Figure 4.11 plots the quiescent subarray beampattern for the penalty method, showing the response is equal to the desired response, in the "soft constrained" section of the mainlobe.

Figure 4.12 shows the subarray beampattern for scenario 2. The proximate interferer is not cancelled or attenuated, and the soft constraint is not violated. Note that there is a sidelobe at cosine $\theta = +0.9$; the interferer of scenario 3 is placed here, to show that the penalty method can "move" its sidelobes and cancel sources.

Figures 4.13 and 4.14 show the subarray and overall full array beampattern for interference scenario 3, respectively. Figure 4.13 shows the subarray beampattern. The soft constraint is obeyed in the region of interest and the distant (sidelobe) interferer is rejected. Figure 4.14 shows the overall full array beampattern. The proximate interferer is rejected at this stage

Table 4.5 shows the power outputs for the fully adaptive, the subarray integral penalty method, and the CSA/AFA beamformers. It is clear that the presence of one or both point interferers does not increase the output power above the quiescent beam power output; indicating that the penalty method can cancel (mainlobe and/or sidelobe) interferers and maintain the soft constraint, without an increase in power output. Note that the power output is identical to the power output of the mainlobe integrally constrained beamformer.

In Table 4.5, the integral error term (4.13) is also given. The error is

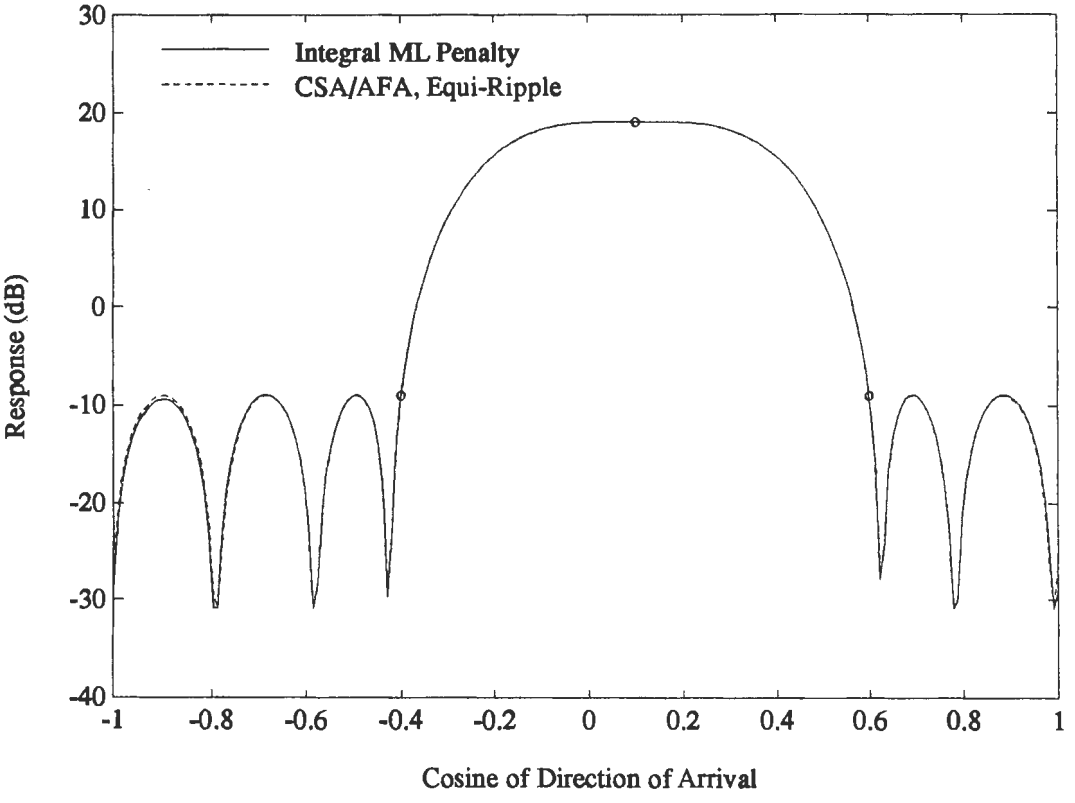

Figure 4.11: Mainlobe Penalty: Subarray Beampatterns for Scenario 1

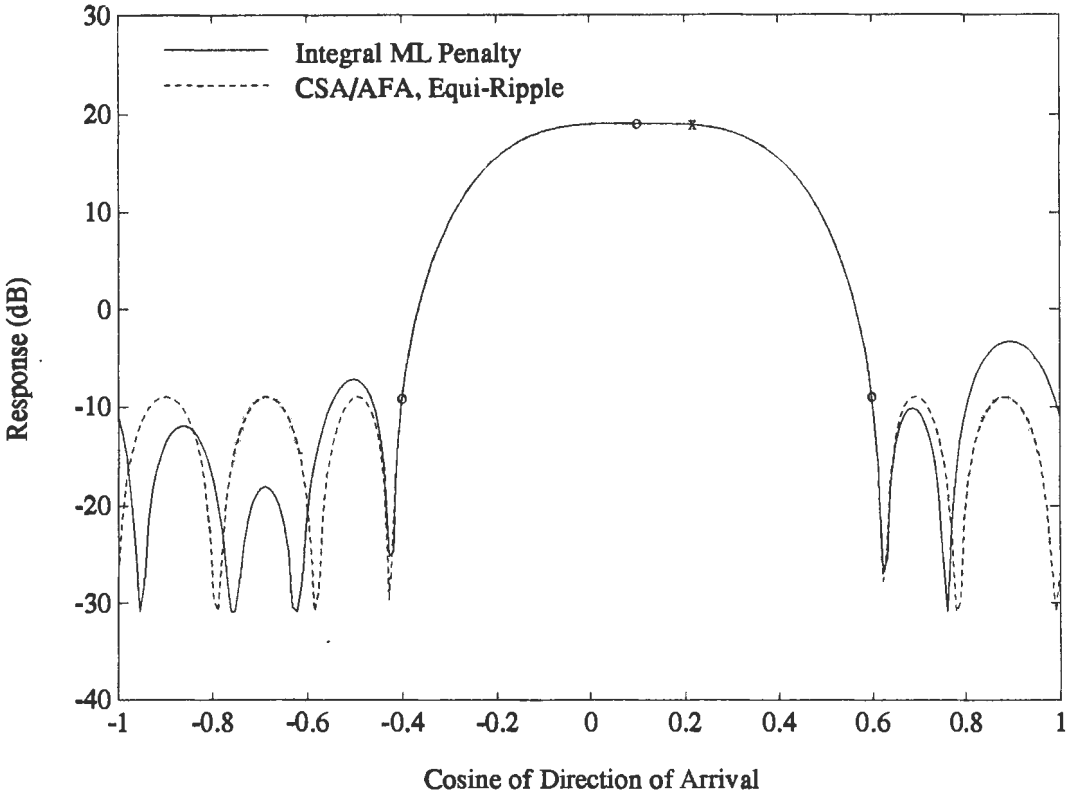

Figure 4.12: Mainlobe Penalty: Subarray Beampatterns for Scenario 2

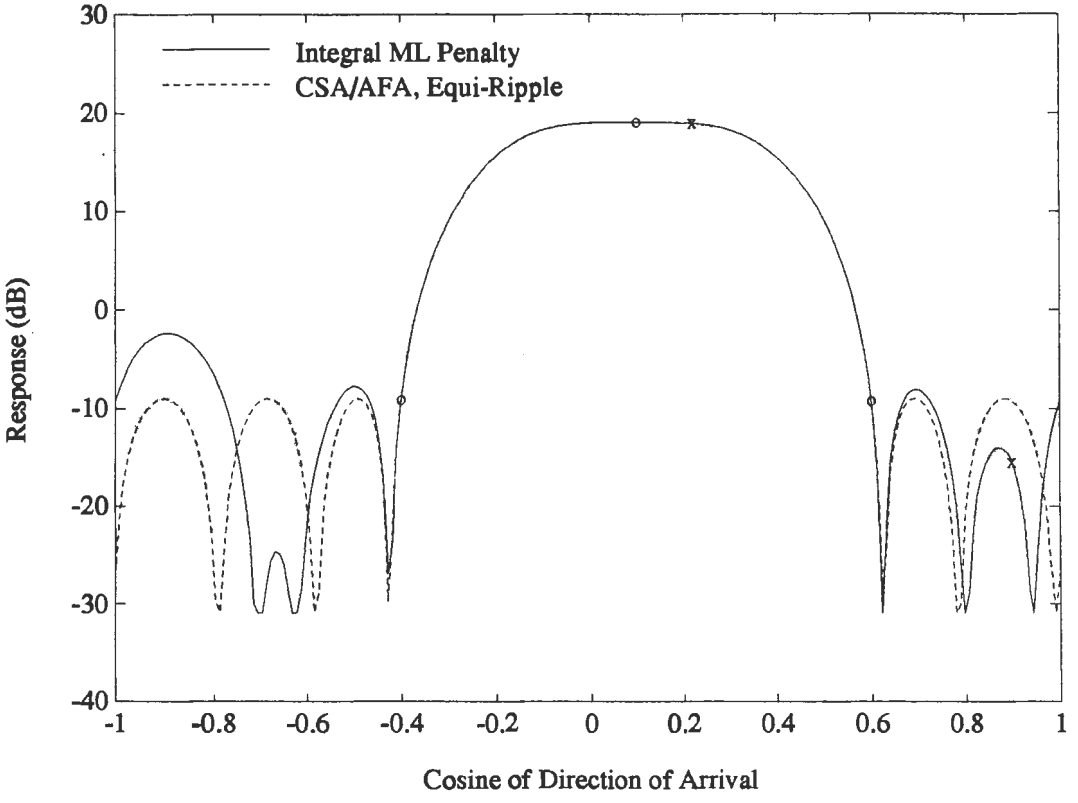

Figure 4.13: Mainlobe Penalty: Subarray Beampatterns for Scenario 3

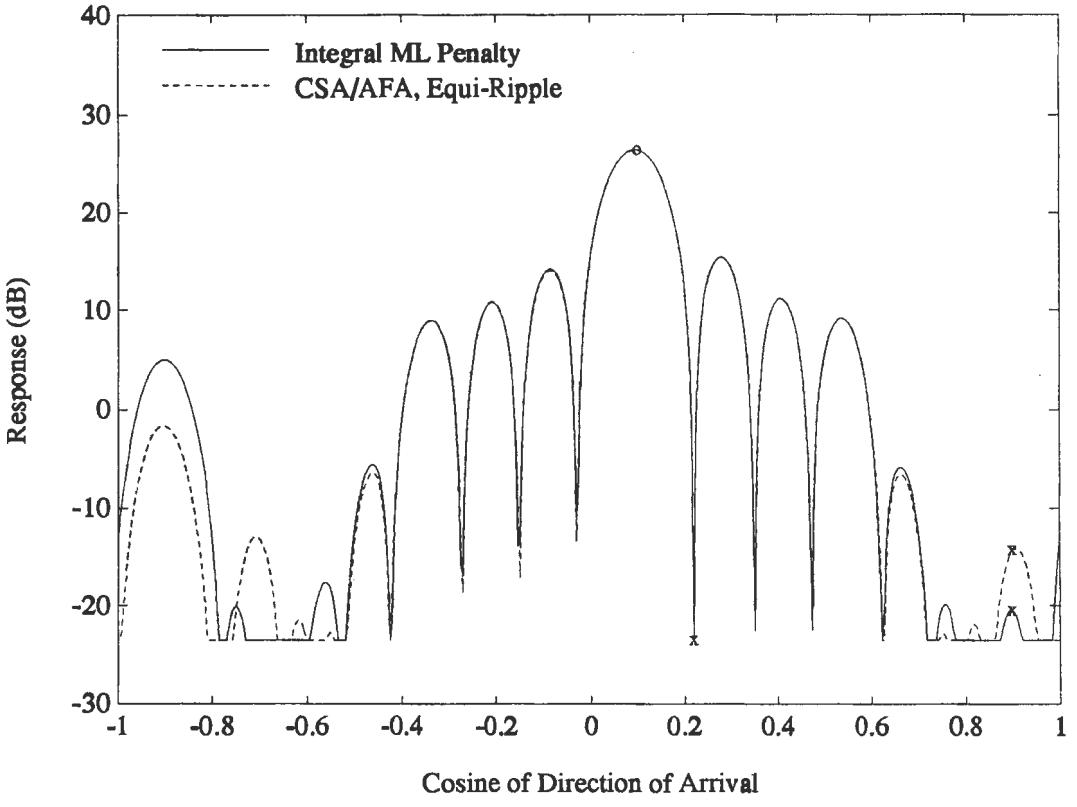

Figure 4.14: Mainlobe Penalty: Overall Full Array Beampatterns for Scenario 3

Table 4.5: Power Outputs and Errors for the Penalty Method

Scenario	Power Output (dB)			Relative Error (dB)
	MVDR	Mainlobe Penalty	Conv SA/ Adap FA	Mainlobe Penalty
1	21.00	28.54	28.56	-69
2	21.73	28.61	28.68	-55
3	21.77	28.76	28.72	-58

expressed in decibels, relative to the area of the constraint, as

$$e_r^2 \equiv 10 \log_{10} \left(\frac{e^2}{\mathbf{e}^H \mathbf{D} \mathbf{e}} \right). \tag{4.53}$$

It is seen that the relative integral error is very small, for all three scenarios.

The reduced computational load of the penalty method is now discussed, assuming that the subarray CSDM is complex Hermitian Toeplitz:

- The constraint matrix $\mathbf{D}$ is complex Hermitian Toeplitz, meaning that the matrix $\mathbf{R} + \lambda_p \mathbf{D}$ is also complex Hermitian Toeplitz; hence, the inverse can be calculated in $O[P^2]$ steps.
- The scalar penalty is simply a constant times the trace of the subarray CSDM estimate.
- The vector $\mathbf{De}$ can be calculated "off-line," since it does not change.
- The additional matrix multiplications and inverse (of the integrally constrained solution) have been avoided.

The soft constraint, integral penalty method is a very efficient method of calculating an adaptive subarray filter vector, and the performance of this beamformer is roughly equivalent to that of the mainlobe hard constrained beamformer. The soft constraint, integral penalty method is the preferred technique for calculating subarray beams.

Chapter 5

Analysis of Adaptive Subarray Processing

In section 4, three techniques for performing adaptive subarray beamforming were described. It was shown that each technique constrained a wide section of the subarray beam, while adaptively cancelling sources in the sidelobes. The performance of these techniques, in terms of calculation burden and dominant interference cancellation, and the details of implementation, in terms of subarray configuration, were not discussed. Accordingly, in this section, the following performance issues of the adaptive subarray beamformer are investigated:

- The calculation burden of an ASA beamformer is compared to that of a CSA beamformer.
- The resolution capability and array gain of the ASA beamformer are compared to that of the MVDR beamformer.
- The ramifications of subarray size, subarray overlap, and number of subarrays on the calculation burden and resolution capability are investigated.
- The capability of the ASA beamformer to cancel dominant interferers is compared to that of the CSA beamformer.

In order to discuss the specifics of implementation, such as subarray size and overlap, an array must be selected. In this section, a specific array will

be used: an equi-spaced linear array with 200 sensors. The results of this section are applicable to arrays with other geometries, provided that quasi-linear segments exist.

5.1 Calculation Burden of a Practical ASA/AFA System

In this section the practical issues of implementing a two-stage adaptive subarray beamformer are explored: the size, number and overlap of subarrays must be chosen according to a defined criterion, the subarray spatial window must be selected to avoid aliasing, etc. In making these decisions, the system designer must select from a set of parameters so as to minimize calculation burden, while maintaining a specified level of system performance. An approach is given for finding a subarray configuration (size, overlap, and number of subarrays) which meets these objectives. It is seen that, for the CSA beamformer, there is a basic tradeoff between calculation burden and system performance. Here system performance is measured in angular resolution; that is, subarray configurations with lower angular resolution tend to be computationally less expensive.

It is important to define the term "system performance," because there are several metrics which can be used. The most important performance metric is array gain. Array gain is defined as the ratio of signal gain to noise gain

$$\mathrm{AG} \equiv \frac{\mathrm{SG}}{\mathrm{NG}}. \tag{5.1}$$

This measure relates the signal gain of the array when focused *directly* at the signal to the white noise gain. As defined, array gain is related to the detectability of signals in white noise. In this section, signal gain loss will be limited by keeping the subarray filter scalloping loss below a specified threshold. Noise gain is also limited, by discarding subarray configurations with noise gain above a specified threshold. It is important to note that signal scalloping losses and noise power increases do not generally coincide. This is usually true because signal scalloping loss is at a maximum at the edge of the subarray beams, precisely where noise gain is at a minimum. The effect is to have nearly optimal, nearly flat array gain across the entire subarray beam, given limits on SG losses and NG.

In scenarios with two very close interferers, the noise gain term must include the interfering source and array gain will consequently decrease. Given that array gain is near optimum for the single source in white noise case, the ability to discriminate between the location of two proximate sources is a more direct measure of system performance. In summary, the definition of system performance used here is the resolution capability of the dual-stage adaptive beamformer, given near optimum array gain in white noise.

In order to maintain near optimal performance, it is also necessary to ensure that "spatial aliasing" is minimized. Spatial aliasing is here defined to be the leakage of sidelobe interferers in a subarray beam into the mainlobe at the full array stage. Aliasing is prevented by very low sidelobes in CSA and by steering nulls in the ASA. But in the presence of dominant interferers, significant leakage can occur in CSA.

The calculation and performance analysis is presented for a specific array: a linear array of 200 equi-spaced sensors. The intent is to design an adaptive system, for this array, which will not exhibit spatial aliasing in the presence of 20 dB interferers. The calculation burden and resolution performance of the ASA/AFA beamformer is then compared to a CSA/AFA system which *does* exhibit some spatial aliasing, and it is shown that the ASA and CSA beamformers are roughly equivalent in terms of calculation burden and resolution capability. A more costly conventional system could be designed to handle this interference scenario, but this example is chosen to demonstrate that a more capable ASA/AFA system can be implemented for the same cost. (These goals are achieved using adaptive subarray beams with quiescent sidelobe rejection of 30 dB and conventional subarray beams with 40 dB sidelobe rejection.)

Since the resolution of adaptive beamformers is signal-to-noise ratio and scenario dependent, the usage of the term "resolution" must be defined. An indication of a system's resolution capability is its response pattern peak width for a single source in white noise. Owsley [10] has derived the response peak widths for the direct conventional and adaptive beamformers:

$$\begin{aligned} \delta_C &\propto \frac{1}{Md}\sqrt{1+\frac{1}{M\sigma^2}} \\ \delta_A &\propto \frac{1}{Md}\sqrt{\frac{1}{M\sigma^2}}, \end{aligned} \tag{5.2}$$

where

$$\begin{aligned} d &\equiv \text{distance between sensors,} \\ \delta_C &\equiv \text{conventional peak width,} \\ \delta_A &\equiv \text{adaptive peak width, and} \\ \sigma^2 &\equiv \text{signal power (unity noise power assumed).} \end{aligned}$$

In (5.2), the second terms are dependent on the signal-to-noise ratio (σ^2) and can not be controlled by system design. The first term $\frac{1}{Md}$ is inversely proportional to the array's length or aperture

$$L = Md \tag{5.3}$$

and is directly proportional to the conventional beamwidth of the source. Since these are the only terms controllable by system design, the philosophy here is to maximize aperture to give maximum resolution capability. For indirect beamforming the effective aperture is dependent on the subarray configuration: the indirect "aperture" is equal to the number of subarrays times the spacing of the subarrays times the distance between sensors,

$$L_S = SQd. \tag{5.4}$$

Since the total number of sensors is

$$M = P + (S-1)Q, \tag{5.5}$$

then the product of number of subarrays S times the number of sensors between subarrays Q is

$$SQ = M - P + Q, \tag{5.6}$$

and it is clear that the effective aperture L_S is less than the total aperture L. The measure of resolution capability used here shall be the percentage of full aperture retained by the beamformer:

$$\rho_L = \frac{L_S}{L}. \tag{5.7}$$

As will be seen, roughly 90% of the effective aperture can be retained for the least costly ASA/AFA configurations.

In order to prevent spatial aliasing, it is necessary that the mainlobe bandwidth B_M of the subarray window be less than the principal non-aliasing full array bandwidth B_F. It is now shown that aliasing can be prevented provided that a certain minimum amount of subarray overlap is used. The mainlobe bandwidth is defined as the width which is higher than the highest sidelobe. For a conventional subarray window, the mainlobe bandwidth is roughly taken to be inversely proportional to the filter length P:

$$B_M = \frac{2\beta}{P}, \tag{5.8}$$

where

$$\begin{aligned} 2 &\equiv \text{the full sensor bandwidth,} \\ \beta &\equiv \text{proportionality constant, and} \\ P &\equiv \text{number of sensors per subarray.} \end{aligned}$$

Typical values of β are 2 and 4 for the rectangular and Hamming windows, respectively.

Note that the spatial bandwidth is expressed in cosine of arrival angle and that spatial Nyquist frequency is assumed. The full array bandwidth is equal to the full bandwidth at the sensor level divided by the number of sensors between subarrays ("desampling" the spatial signal):

$$B_F = \frac{2}{Q}, \tag{5.9}$$

where

$$\begin{aligned} 2 &\equiv \text{the full sensor bandwidth and} \\ Q &\equiv \text{skip between subarrays.} \end{aligned}$$

Since the subarray mainlobe width must be less than the full array bandwidth, equations (5.8) and (5.9) can be combined, defining a relationship between subarray size and skip between subarrays:

$$\begin{aligned} B_M &\leq B_F \\ \frac{2\beta}{P} &\leq \frac{2}{Q} \\ Q &\leq \frac{P}{\beta}. \end{aligned} \tag{5.10}$$

Equation (5.10) states that the skip between subarrays must be bounded by the width of the subarray mainlobe, as measured by the constant β. Recall that the overlap of the subarrays is defined as:

$$S_O \equiv 1 - \frac{Q}{P}. \tag{5.11}$$

Substituting Eqn (5.11) into Eqn. (5.10) and rearranging, the following relationship between subarray overlap and mainlobe width is found:

$$S_O \geq 1 - \frac{1}{\beta}. \tag{5.12}$$

Equation (5.12) establishes a lower bound on the amount of subarray overlap. By experimentation, the following approximate mainlobe width constants have been measured for sidelobe levels of 30 and 40 dB respectively:

$$\begin{aligned} \beta_{30} &\approx 2.7 \text{ and} \\ \beta_{40} &\approx 4.0. \end{aligned} \tag{5.13}$$

Using Equation (5.13) in Equation (5.12), minimum subarray overlaps for sidelobe levels of 30 and 40 dB respectively are:

$$\begin{aligned} S_{O_{30}} &\geq 0.637 \text{ and} \\ S_{O_{40}} &\geq 0.75. \end{aligned} \tag{5.14}$$

Equation (5.14) defines the minimum overlaps used here for the ASA and CSA beamformers, respectively.

The subarray spatial window used for the ASA and the CSA beamformers is the Parks-McClellan equi-ripple filter. The stop band is set equal to the full array bandwidth and the start of the transition bandwidth is offset from the stop band by one-half of the approximate mainlobe width of equation (5.8). The design of the filter is illustrated in Figure 5.1. Notice that the meaning of the conventional mainlobe width B_M of Equation (5.8) has been reinterpreted: here, the width B_M describes the required transition bandwidth on the rising and falling edges of the passband, to provide the specified stopband rejection; the passband is *not* included in the width B_M. This strategy uses the maximum available band width per subarray beam, while preventing spatial aliasing.

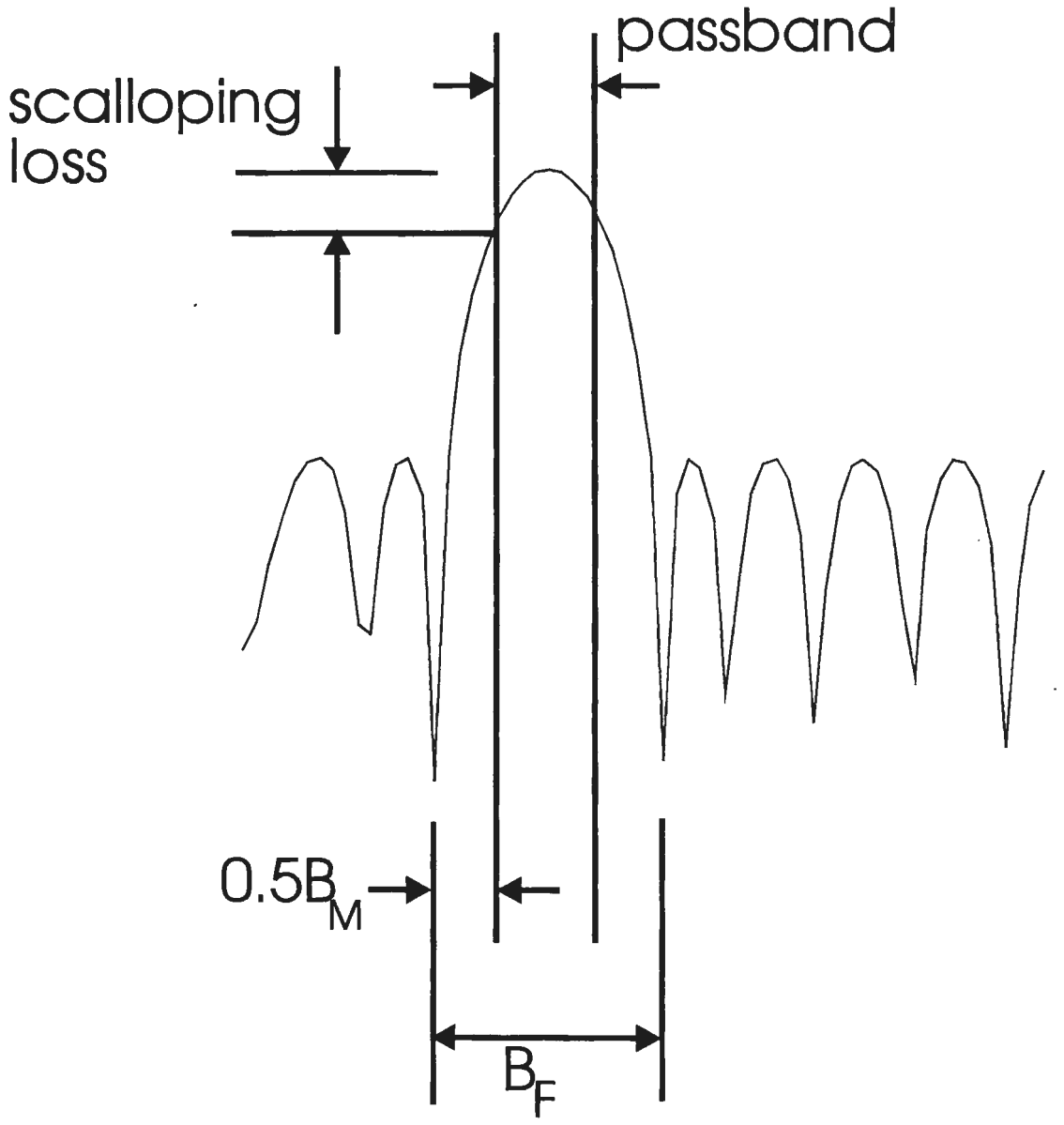

Figure 5.1: Design Parameters for Subarray Spatial Filtering Window

Besides the specification of stop band and pass band limits in the design of the Parks-McClellan spatial window, it is necessary to establish a limit on the in-band ripple or signal scalloping loss. The scalloping loss limit used here is

$$\rho_S \leq 0.5\text{dB}. \tag{5.15}$$

In order to meet specified scalloping loss limits and sidelobe levels, it is noted that, when using the Parks-McClellan filter, experimentation with specific pass band limits and relative weighting of pass band and stop band ripples was necessary.

For a given minimum subarray overlap, one must establish a set of rules for finding the set of realizable subarray configurations. To determine this set it is assumed that the subarrays will use the entire aperture (no sensors are left unutilized), and the number of sensors skipped between subarrays is uniform. The approach taken in this paper is outlined below:

1. Evaluate all possible skips (Q) between subarrays. This search starts with subarrays spaced two sensors apart and continues up to the maximum skip (associated with 2 subarrays per line).

2. For a particular skip between subarrays, find the minimum subarray length P_{min} and the corresponding maximum number of subarrays S_{max} as follows:

   (a) The minimum subarray length is

   $$P_{\text{min}} = \frac{Q}{1 - S_O}, \tag{5.16}$$

   where S_O is defined as the minimum required overlap.

   (b) The maximum number of subarrays per line is equal to

   $$S_{\text{max}} = \text{floor}\left(\frac{M - P_{\text{min}}}{Q} + 1\right). \tag{5.17}$$

   (c) And the integer minimum subarray length is recalculated as

   $$P_{\text{min}} = M - (S_{\text{max}} - 1)Q. \tag{5.18}$$

3. For each possible skip between subarrays, generate all possible subarray configurations. A list is created starting from the configuration with minimum subarray length and maximum number of subarrays. The list ends with a maximum subarray length and two subarrays.

4. For all configurations generated in step 3 above, test whether the following criteria are met:

   (a) Effective Aperture Test: Check that the effective aperture percentage ρ_L is greater than the specified threshold.

   (b) Noise Gain Test: Check that the noise gain is less than a specified threshold. Threshold is defined here to be the ratio of the ASA/AFA beamformer noise gain to the fully adaptive beamformer noise gain

   $$\rho_{\mathrm{NG}} = \frac{\mathrm{NG}_{\mathrm{ASA}}}{\mathrm{NG}_{\mathrm{MVDR}}} = \frac{\mathrm{NG}_{\mathrm{ASA}}}{N}. \tag{5.19}$$

   (c) Redundant Effective Aperture Test: If several configurations have identical effective apertures, then retain the configuration with the lowest calculation burden.

   (d) Effective Aperture Locally Maximum Test: If the calculation burden of a configuration is significantly higher than its neighbors (in terms of effective aperture), then discard the configuration. This is a "one-pass" operation.

   Note that steps (a) and (b) are performed so as to meet specified requirements, while steps (c) and (d) are necessary for presentation purposes only.

To evaluate the computational cost of the CSA/AFA and the ASA/AFA system, specific algorithms must be chosen to estimate CSDMs, calculate filter vectors and form beams— at both the subarray and full array stages. An outline of the algorithms used for this analysis is now given:

1. Subarray CSDM Estimation (SA CSDM), for ASA/AFA only: The array is assumed to be linear with equi-spaced sensors and far-field sources, giving a Hermitian Toeplitz subarray CSDM. A single subarray CSDM is estimated, by use of FFT convolution techniques, because all subarrays are assumed to have identical statistics.

2. Subarray Filter Vector Calculation (SA FV), for ASA/AFA only: Subarray adaptive filters are found by solution of a Hermitian Toeplitz linear system [7]. One filter vector is calculated per subarray beam, on a periodic basis.

3. Subarray Beam Output Calculation (SA Beams):

   (a) ASA/AFA outputs are calculated via complex vector inner products. One subarray output is calculated for each beam for each subarray.

   (b) CSA/AFA outputs are calculated using composite-N FFTs [19], where the FFT length (number of beams per subarray) is found which minimizes the combined cost of subarray beam output calculation and full array CSDM estimation (while maintaining the minimum number of subarray beams).

   For subsequent use, the cost of Z_b-point FFT is taken as:

$$C_F(Z_b) = Z_b \sum_{i=1}^{P_b} \alpha(p_i)(p_i - 1), \tag{5.20}$$

   where

$$\begin{aligned} \{p_i\}_{i=1}^{P_b} &\equiv \text{a set of prime numbers, satisfying} \\ \prod_{i=1}^{P_b} p_i &= Z_b, \text{ and} \\ \alpha(p_i) &= \begin{cases} 5 & p_i = 2, \\ 8 & \text{otherwise} \end{cases} . \end{aligned}$$

   It is noted that, in a practical system, the cost of composite-N FFTs is most likely higher than the simple count of multiplies and adds, used in this section. Therefore, the CSA/AFA cost is biased low.

4. Full Array CSDM Estimation (FA CSDM): Full array CSDMs are calculated using a reduced-rank eigen-signal subspace technique [2, 20]. A full array CSDM is required for each subarray beam look direction.

5. Full Array Filter Vector Calculation (FA FV): Full array filter vectors are found via "back solution" of the eigen-signal subspace mentioned above. A full array filter is calculated for each full beam look direction, on a periodic basis.

6. Full Array Beam Outputs (FA Beams): Full array outputs are calculated via complex vector inner products. To allow for sufficient sampling of strong sources, typically, three times as many full array beams are required as sensors in the array.

The philosophy used in selecting these algorithms was to choose the most efficient methods possible, for both the ASA and the CSA systems; for example: in the ASA case, the Hermitian Toeplitz assumption is convenient, but may not apply in all cases, and in the CSA case, the cost function for the subarray beam formation is certainly biased low, as mentioned above.

Table 5.1 summarizes the variables and assumptions pertinent to the cost analysis of the beamformer described above and Table 5.2 presents the computational cost of each step in the beamformer. The cost is measured in terms of the total number of multiplies and adds in the operation, and the term floating point operation (FLOP) is used to describe either a multiply or an add.

To aid in the cost versus performance analysis of the CSA and ASA systems, several tables summarize the set of subarray setups and the detailed calculation cost figures considered here. The purpose of these tables is to present the computational cost of each system as a function of effective aperture. As mentioned, there is a tradeoff between computation cost and performance, but, for ASA/AFA, this tradeoff does not occur until the system attempts to get more than 90% of the total aperture; that is, systems yielding less than 85% effective aperture are more costly and are not reasonable alternatives. Results have been calculated for systems with more than 75% of the total aperture and having a skip between subarrays of two or more sensors.

Tables 5.3 and 5.4 give a detailed accounting of the subarrays setups for the CSA/AFA and ASA/AFA, respectively. Each table lists the skip between subarrays, the number of subarrays, the sensors per subarray, and the number of beams required per subarray. From these figures, the overlap percentage, effective aperture and total FLOPS have been calculated, as listed in the tables.

Table 5.1: Beamformer Cost Analysis: Variable Definition and Values

Name	Value	Description
$S_{O_{40}}$	≥ 0.75	CSA Subarray overlap
$S_{O_{30}}$	≥ 0.63	ASA Subarray overlap
ρ_S	0.5 dB	Scalloping loss
ρ_L	≥ 0.75	CSA/CFA Effective Aperture
ρ_{NG}	≤ 0.5 dB	Noise Gain Ratio
M	200	Number of sensors in the array
P		Number of sensors per subarray
S		Number of subarrays per line
Q		Skip between subarrays
Z_b		Number of beams per subarray
U	Z_b	Number of full array CSDMs
N_F	$2^{\text{ceil}(\log_2 M)+1}$	SA CSDM convolution length
D	4	Dimension of eigen-signal subspace
N_B	$3M+1$	Number of full array beams
I	20	Period of SA FV and FA FV updates

Table 5.2: Beamformer Cost Analysis: FLOP Count, by Sub-Operation

Operation	FLOP count
SA CSDM	$5N_F \log_2 N_F + 3N_F + 5\frac{1}{2}N_F \log_2 \frac{1}{2}N_F + 18P$
SA FV	$\frac{1}{I}Z_b(16P^2)$
SA Beams, ASA	$SZ_B(8P)$
SA Beams, CSA	$SC_F(Z_b)$
FA CSDM	$U(36SD)$
FA FV	$\frac{1}{I}N_B(18DS)$
FA Beams	$N_B(8S)$

Table 5.3: Analysis of Subarray Setups for CSA/AFA Processing

Config.	Subarrays	Skip	Sensors per SA	Overlap %	Eff. Aper. %	Beams	FLOPS
1	11	14	60	77	77	96	272047
2	15	11	46	76	83	80	339774
3	17	10	40	75	85	72	352301
4	19	9	38	76	86	64	344044
5	29	6	32	81	87	20	310056
6	35	5	30	83	88	16	335846
7	44	4	28	86	88	9	376446
8	59	3	26	88	89	6	469734
9	89	2	24	92	89	3	663192
10	36	5	25	80	90	20	384897
11	91	2	20	90	91	4	690471
12	61	3	20	85	92	8	502859
13	46	4	20	80	92	16	441397
14	37	5	20	75	93	36	505701
15	62	3	17	82	93	9	530447
16	47	4	16	75	94	32	581841
17	63	3	14	79	95	18	644464
18	95	2	12	83	95	6	756352
19	96	2	10	80	96	9	821337
20	97	2	8	75	97	16	930773

Tables 5.5 and 5.6 list the computational cost for each stage of the beamformer and the total cost for each subarray setup for the CSA/AFA and ASA/AFA beamformers, respectively. The figures given in the above mentioned tables were calculated using the general formulas found in Table 5.2.

Figure 5.2 graphs the cost of selected subarrays setups as a function of resolution. Note that each setup, whether it is used with conventional or adaptive subarrays, gives identical resolution, meaning the cost of equivalent CSA/AFA and ASA/AFA setups appear at the same place on the horizontal axis.

Referring to Tables 5.1—5.6 and Figure 5.2, the following observations

Table 5.4: Analysis of Subarray Setups for ASA/AFA Processing

Config.	Subarrays	Skip	Sensors per SA	Overlap %	Eff. Aper. %	Beams	FLOPS
1	6	25	75	67	75	152	1440523
2	7	22	68	68	77	133	1217362
3	8	20	60	67	80	121	1044180
4	7	23	62	63	81	137	1119795
5	9	18	56	68	81	108	944942
6	11	15	50	70	83	84	783059
7	14	12	44	73	84	59	634285
8	13	13	44	70	85	71	694011
9	10	17	47	64	85	103	822999
10	22	8	32	75	88	32	496581
11	30	6	26	77	90	16	422044
12	26	7	25	72	91	37	565955
13	61	3	20	85	92	6	573627
14	46	4	20	80	92	10	498909
15	37	5	20	75	93	21	536053
16	62	3	17	82	93	7	590499
17	47	4	16	75	94	18	596567
18	63	3	14	79	95	7	588272
19	38	5	15	67	95	32	626790
20	48	4	12	67	96	25	660548
21	97	2	8	75	97	11	933704
22	98	2	6	67	98	13	963123

Table 5.5: Detailed FLOPS Analysis for CSA/AFA Processing

Config.	SA Beams	SA CSDM	SA FV	FA CSDM	FA FV	FA Beams	Total Total
1	43296	0	0	152064	23800	52888	272048
2	62400	0	0	172800	32454	72120	339774
3	57528	0	0	176256	36781	81736	352301
4	36480	0	0	175104	41108	91352	344044
5	24360	0	0	83520	62744	139432	310056
6	11200	0	0	80640	75726	168280	335846
7	12672	0	0	57024	95198	211552	376446
8	7434	0	0	50976	127652	283672	469734
9	4272	0	0	38448	192560	427912	663192
10	30240	0	0	103680	77890	173088	384898
11	3640	0	0	52416	196888	437528	690472
12	7320	0	0	70272	131980	293288	502860
13	14720	0	0	105984	99526	221168	441398
14	55944	0	0	191808	80053	177896	505701
15	17856	0	0	80352	134143	298096	530447
16	37600	0	0	216576	101689	225976	581841
17	41958	0	0	163296	136307	302904	644465
18	11970	0	0	82080	205542	456760	756352
19	27648	0	0	124416	207706	461568	821338
20	31040	0	0	223488	209869	466376	930773

Table 5.6: Detailed FLOPS Analysis for ASA/AFA Processing

Config.	SA Beams	SA CSDM	SA FV	FA CSDM	FA FV	FA Beams	Total Total
1	547200	36166	684000	131328	12982	28848	1440524
2	506464	36040	491994	134064	15145	33656	1217363
3	464640	35896	348480	139392	17309	38464	1044181
4	475664	35932	421302	138096	15145	33656	1119796
5	435456	35824	270950	139968	19472	43272	944943
6	369600	35716	168000	133056	23800	52888	783060
7	290752	35608	91379	118944	30290	67312	634286
8	324896	35608	109965	132912	28127	62504	694012
9	387280	35662	182022	148320	21636	48080	823000
10	180224	35392	26214	101376	47599	105776	496582
11	99840	35284	8653	69120	64908	144240	422045
12	192400	35266	18500	138528	56254	125008	565956
13	58560	35176	1920	52704	131980	293288	573628
14	73600	35176	3200	66240	99526	221168	498910
15	124320	35176	6720	111888	80053	177896	536053
16	59024	35122	1618	62496	134143	298096	590500
17	108288	35104	3686	121824	101689	225976	596568
18	49392	35068	1098	63504	136307	302904	588272
19	145920	35086	5760	175104	82217	182704	626791
20	115200	35032	2880	172800	103853	230784	660549
21	68288	34960	563	153648	209869	466376	933704
22	61152	34924	374	183456	212033	471184	963123

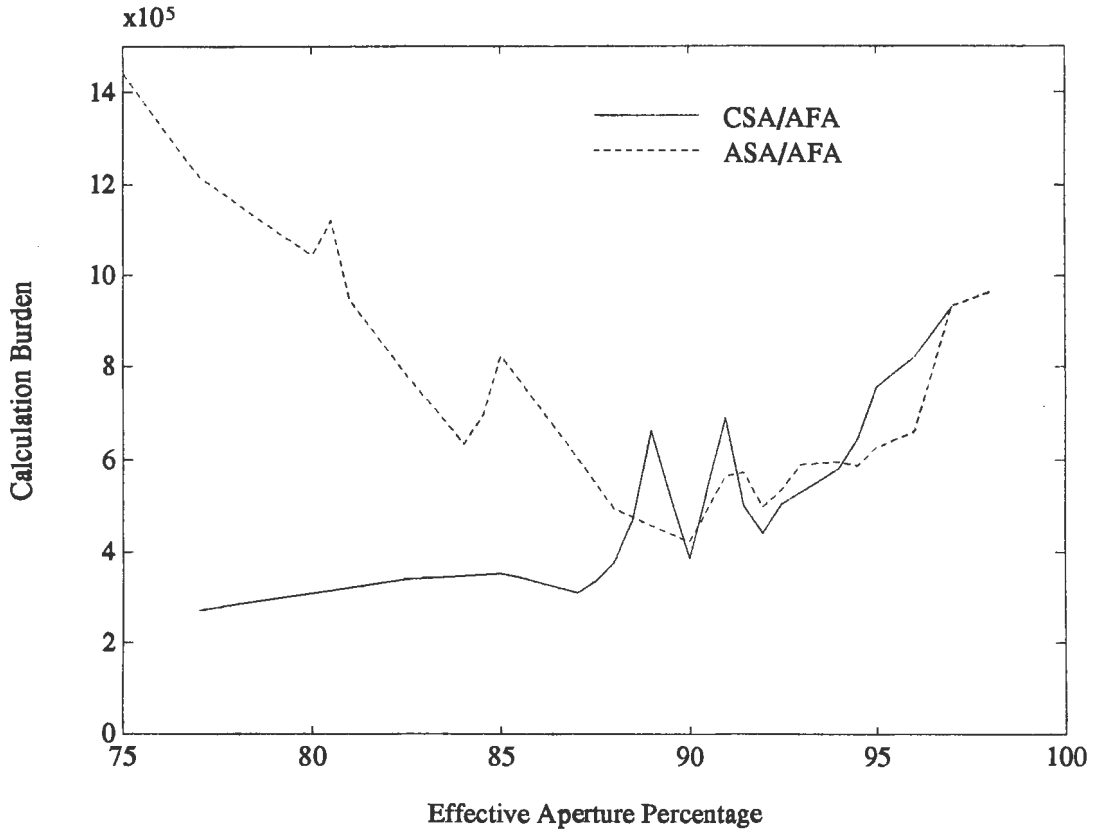

Figure 5.2: Calculation Burden vs Percentage of Aperture for ASA and CSA

can be made:

- The FA FV and FA Beam costs are identical for the CSA/AFA and ASA/AFA systems, because the number of beams and sensors per subarray are identical for each subarray setup.
- The ASA/AFA SA FV cost is low for subarrays with few sensors and becomes prohibitive for the largest subarray sizes.
- The number of beams required for an adaptive subarray is approximately one half that of the conventional subarray.
  - The reduced number of ASA beams does not give a reduction in SA Beams cost because conventional subarray beams can be calculated very efficiently.
  - The reduced number of ASA beams does, however, reduce the cost of FA CSDM estimation.
  - The reduction in FA CSDM cost and the increase in cost of SA Beams, SA CSDM, and SA FV for the ASA/AFA beamformer, relative to CSA/AFA, are even tradeoffs for configurations ranging from 88% to 97% of the full aperture, where the subarrays are the shortest.
- The efficiency of the composite-N FFT allows very long subarrays to be calculated. For the CSA/AFA beamformer, this leads to a strict tradeoff between calculation burden and resolution.
  - It is noted that when CSA beams are calculated using vector inner products, as contrasted with composite-N FFTs, then there is a large penalty for longer subarrays. This penalty applies to the shorter subarrays as well, and leads to the ASA beamformer being more efficient than the CSA beamformer, in all cases.
- For ASA/AFA, systems with either low resolution (long subarrays) or high resolution (short subarrays) are most costly. It is interesting that there is no tradeoff between calculation cost and resolution below 85%, as in CSA/AFA.

In summary, this section has addressed the practical issues of calculation burden and system performance, measured in effective aperture, for the CSA and ASA beamformers. For the systems with the best resolution, it has been shown that ASA and CSA are roughly equivalent in cost. In section 5.3, it will be shown that, in the presence of dominant interferers, the particular ASA systems considered here are very resistant to spatial aliasing effects, while the CSA systems are not.

5.2 Response Patterns of Closely-Spaced Low-Level Sources

In section 5.1, it was noted that signal and noise gain vary with angular position within a subarray beam, and that the aperture of a dual-stage beamformer is reduced from that of the full array. It was claimed that signal loss and noise gain increase do not generally coincide, and that effective aperture is a measure of resolution capability. In response to these claims, several examples are given to demonstrate that:

- Signal gain and noise gain tend to follow each other, resulting, fortunately, in nearly constant array gain.
- Resolution of two sources is diminished with decreased aperture.

In order to verify that array gain is nearly uniform across a subarray, it is desired to normalize either the signal or the noise gain to a constant, and then check for a near-constant response of the unnormalized quantity. In this section, the philosophy is to scale the response so as to achieve constant signal gain. For emphasis, it is noted that constant signal gain is not a requirement when the ripple is only 0.5 dB— it is done only to investigate the array gain response within a subarray beam.

Signal gain variations are the result of ripple in the passband of a subarray beam. As a function of angular position within the subarray beam, there is a predetermined loss or gain in signal— as compared to the desired P^2 signal gain. Since the signal variation is known, it can easily be removed by scaling the response pattern by the measured subarray passband ripple. This procedure is referred to as "signal gain compensation."

Table 5.7: Source Scenario for Low-Level, Closely-Spaced Sources

Source	Cosine of Arrival Angle	Power (dB)
1	-0.057	-19
2	-0.046	-19

The subarray signal gain equalization gives uniform signal gain, but it does not guarantee equal noise gain in the subarrays's beam-space. This is an important consideration because unequal noise gain means unequal array gain. Intuitively, the noise gain ought to correlate highly with signal gain for the following reasons: noise gain is the integral of the noise centered about the signal of interest, and signal and noise have approximately equal ripple in one region of the subarray beam. If subarray noise and signal gains are highly correlated, then correcting signal gain, for example, will tend to correct noise gain. To verify this intuition– in at least one case – the response pattern to white noise-only is measured before and after signal gain compensation. Figure 5.3 shows the uncompensated and compensated ASA responses to white noise. In this figure, configuration 11 from Table 5.4 is used with mainlobe constrained ASA processing. The MVDR solution is also shown for comparision purposes. In the compensated case it is clear that noise gain is uniform to within 0.1 dB across the subarray beam-space. It is recalled that configurations from Table 5.4 were specified to have a maximum normalized noise gain of 0.5 dB. It is evident that the actual noise gain is somewhat less than 0.5 dB above the MVDR solution.

Figure 5.4 illustrates the effect of signal gain compensation in the presence of two equal interferences. In this figure, subarray configuration 11 from Table 5.4 is used with mainlobe constrained ASA processing and the source scenario used is given in Table 5.7. The MVDR solution is also shown for comparision purposes. It is evident that the peak signal responses are unequal without compensation. With compensation the peaks are equal but slightly higher than the MVDR solution. This bias is due to ASA noise gain which is higher than the MVDR noise gain.

Referring to Figure 5.4 again, the resolution capability of the ASA beamformer can be compared to the MVDR beamformer by comparison of the "notch depth." Notch depth is here defined to be the depth of the response pattern between the two sources. It is clear that the ASA notch depth is not

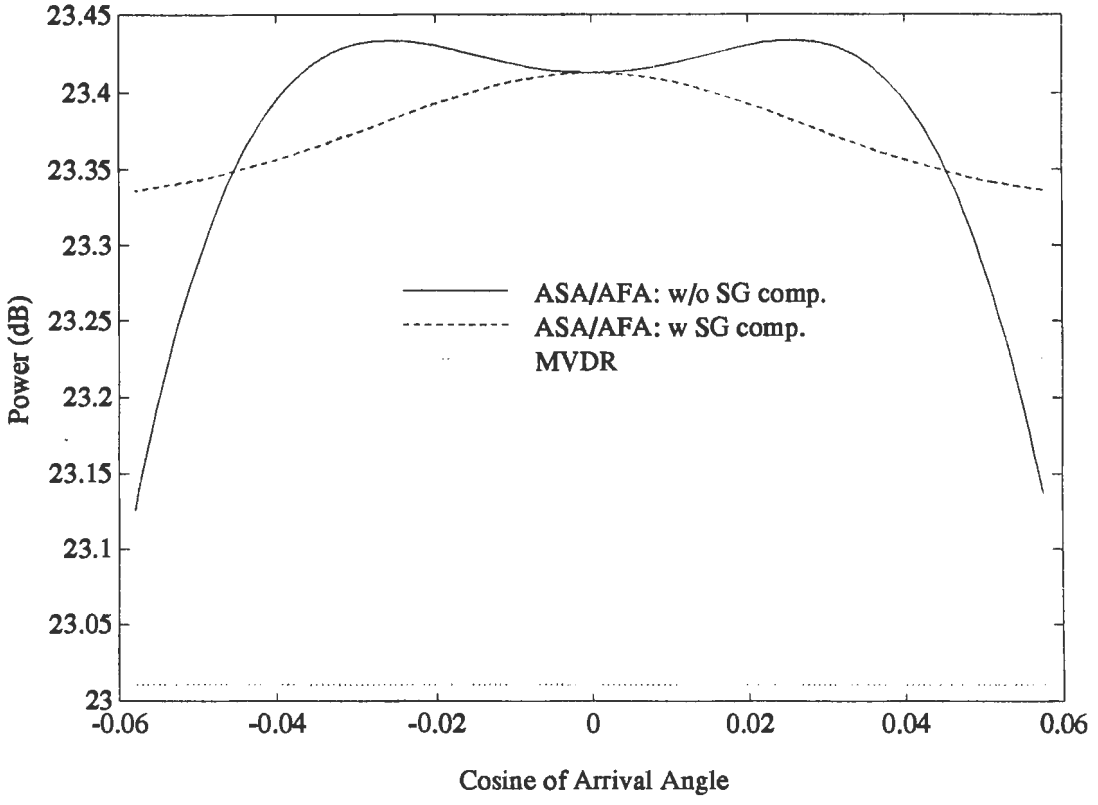

Figure 5.3: Response Pattern in a Subarray Beam to White Noise

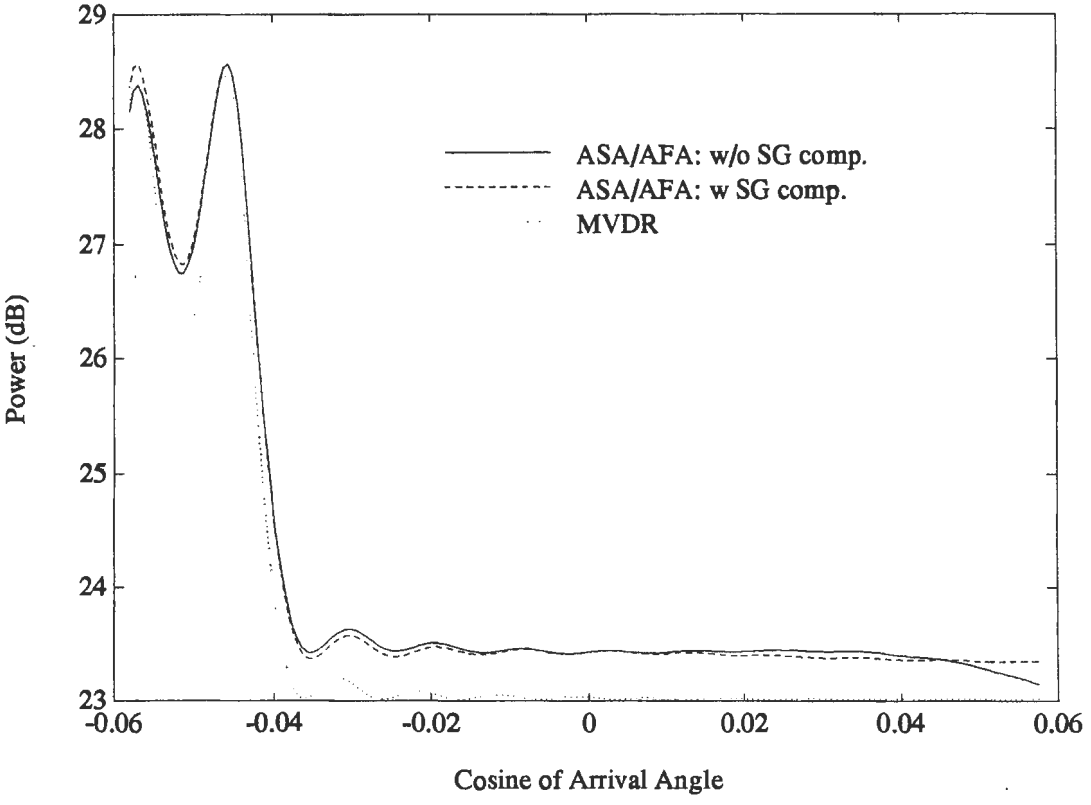

Figure 5.4: Response Pattern in A Subarray Beam to Two Low-Level Sources

as deep as the MVDR, meaning that some loss in resolution has occurred. (Note that this is true despite the noise gain bias of the ASA response: the ASA noise gain causes a 0.5 dB deflection at 23 dB and only a 0.2 dB deflection at 27 dB, and the notch depth differences are greater than 0.2 dB.)

In summary, the examples used in this section have shown the following:

- Signal gain compensation removes signal response bias.
- Signal gain compensation smooths out the noise gain response.
- Noise gain can be kept reasonably close to the the optimum found with MVDR, yielding near-optimum array gain.
- Resolution capability decreases slightly with slight decreases in effective aperture.

5.3 Response Patterns for Worst Case Dominant Interferers

In this section, the anti-aliasing properties of the mainlobe and noise gain constrained ASA beamformers are compared to the CSA beamformer. It has been claimed that ASA beamformers can steer sidelobe nulls in the subarray beam to "cancel out" interferers, while the CSA must rely solely on low sidelobes to attenuate interferences. To verify these claims, it is important to not only pick interferences of sufficient strength, but also to investigate the importance of source position (within a subarray beam) and the number of sources present. Accordingly, the following objectives are pursued in this section:

- Establish the relationship between a single source's location and (response pattern) performance, when using mainlobe constrained ASA (ML ASA) beamformer.
  - Establish the performance with source position when there are one or two additional, fixed sources.
- From above, pick a "worst case" scenario for one, two, and three sources and compare the performance of the ML ASA beamformer, the noise

gain constrained ASA (NG ASA) beamformer, and the CSA beamformer.

As mentioned above, it is the goal of this section to establish the performance of the ASA beamformers in some "worst case" scenarios. In order to define what is a worst case, it important to note how performance can be impacted. The performance of an ASA beamformer, as measured by the response pattern, is degraded by either of two effects:

- Excessive Subarray Noise Gain: High noise gain in a subarray beam leads to high full array noise gain. This is exhibited by the response pattern being "biased" high in the region of a subarray beam.

  Empirically, it has been observed that excessive subarray noise gain can occur in the ML ASA beamformer. The mainlobe constraint imposes no limit on the noise gain, allowing for maximum non-mainlobe interference cancellation.

- Insufficent Sidelobe Cancellation: When inadequate nulls are steered at sources outside of the full array non-aliasing bandwidth, then spatial aliasing occurs. This is exhibited by "false peaks" in the response pattern.

  Empirically, it has been observed that this tends to occur when there is a noise gain limit imposed on the subarray beamformer. The noise gain limit restricts the beamformer's "freedom" to shift location— and more importantly —the level of the sidelobes, leading to partial interference cancellation.

From the above comments, it is clear that a worst case for the ML ASA beamformer will not be the worst case for the NG ASA beamformer and vice versa. It is the philosophy here to seek a worst case for the "best" ASA beamformer, because it is desired to show how well this beamformer performs in the most difficult situation. Since the ML ASA beamformer is considered the most efficient (and will be shown to have the best performance), it is selected as the algorithm of choice. Thus "worst case" scenarios shall be ones which maximize subarray noise gain.

As mentioned in the introduction to this section, it is desired to find worst case scenarios for one, two, and three sources. To do this a sequential procedure is adopted here: the worst location of a single source is first found,

and then, fixing the location of the first source, the location for the second interferer is determined, etc. The procedure used is outlined below:

1. Find the worst location for a single source:
   (a) Pick a subarray configuration and one subarray beam focussing direction.
   (b) Evaluate the subarray noise gain as a function of arrival angle. Vary the location through all possible angles.
   (c) Place the single source at the location where subarray noise gain is maximized.
2. Find the worst locations for two sources:
   (a) Repeat step (1a).
   (b) Fix a single source at location found in step (1c).
   (c) Evaluate noise gain for all possible arrival angles.
   (d) Place the second source where maximum noise gain occurs, omitting from consideration the "neighborhood" of the single fixed source. The "neighborhood" of the single fixed source is defined as the peak area of the subarray noise gain plot of step (1b).
3. Find the worst locations for three sources:
   (a) Repeat steps (2a) — (2d) except that there are two fixed sources.

It is noted that this procedure does not maximize subarray noise gain by simultaneously moving all three sources. It is therefore likely that an absolute maximum has *not* been found.

Figure 5.5 plots the subarray noise gain versus arrival angle for one, two, and three sources. In this figure, subarray configuration 11 from Table 5.4 is used, the subarray beam is focussed at $\cos(\theta) \approx 0.07$, and the mainlobe constraint limits are at approximately -0.1 and $+0.23$. The worst case scenarios, as taken from this plot, are noted in Table 5.8.

Referring to Figure 5.5, the following observations can be made for the *single* interferer case:

- The subarray noise gain is highest in the first sidelobes on the left and right of the mainlobe. Evidently, the adaptation has the most difficulty when cancelling sources close to the constraint region.

- The subarray noise gain is also sensitive in the second sidelobes.

- In the subarray mainlobe and outside of the first and second sidelobes, the subarray noise gain is nearly equal to that of the CSA beamformer.

Referring to Figure 5.5, the following observations can be made for the *double* interferer case:

- With a first sidelobe interferer, the next worst case is in the second sidelobe on the opposite side of the mainlobe.

- Subarray noise gain is nearly constant at 0.4 dB in the subarray mainlobe and outside of the first and second sidelobes.

Referring to Figure 5.5, the following observations can be made for the *triple* interferer case:

- With a fixed interferer in the first left sidelobe and another interferer in the second right sidelobe, the worst place for the third interferer is in the third right sidelobe.

- Subarray noise gain is nearly constant at 0.65 dB in the subarray mainlobe and outside of the first three sidelobes.

It is noted that these worst case scenarios are subarray configuration and frequency dependent. Any change in subarray configuration, subarray focussing direction or frequency will cause the response to be very different (due to shifting subarray beam sidelobe locations).

To evaluate the performance of the ASA and CSA beamformers for the three worst cases of Table 5.8, refer to Figures 5.6 — 5.8 for scenarios 1, 2 and 3, respectively. From these figures, the following observations can be made:

- In the targetted subarray beam ($\cos(\theta) \approx 0.06$), the ML ASA beamformer exhibits a 1 — 2 dB excess in noise gain, for all three scenarios.

- The NG ASA beamformer exhibits a single spatial alias at $\cos(\theta) \approx 0.2$ in the two and three source scenarios. This is the result of the proximate source at $\cos(\theta) \approx 0.31$: the subarray beamformer must cancel this close mainlobe interferer, and, consequently, can not sufficiently null the interferer at $\cos(\theta) = -0.14$.

  A full mainlobe constraint in conjunction with the noise gain constraint would correct this particular alias, but, from experimentation, it has been found that such a combined ML/NG ASA beamformer will exhibit aliases when dominant interferers occur in the first and second sidelobes; the ASA beamformer must allow noise gain in order to prevent spatial aliasing.

- The CSA beamformer exhibits many large spatial aliases. The spatial aliases can be alleviated by use of a subarray window with 10 dB lower sidelobes, but this would drive the calculation burden significantly higher.

It is noted that the ML and NG ASA beamformers would both benefit from an optimization technique which omits the subarray transition band from power minimization. In the ML ASA beamformer this would allow the limits of the constraint to be eased, allowing easier cancellation of the first and second sidelobe interferers. And in the NG ASA beamformer, this would prevent the cancellation of transition band interferers, which lead to spatial aliases in the above examples. Since it was not apparent how to perform such an optimization, this modification to the ASA beamformer could not be implemented.

In summary, the following conclusions can be made:

- In the presence of "worst case" first, second and third sidelobe interferers, the ML ASA beamformer exhibits some extra noise gain.

- In the presence of dominant transition band interferers, the NG ASA beamformer exhibits an occasional spatial alias.

- In the presence of sufficiently powerful interferers, the CSA beamformer exhibits spatial aliasing. The subarray sidelobe levels can be decreased, at a cost in calculation burden.

Table 5.8: Source Scenario for Worst-Case, Dominant Interferers

Source	Cosine of Arrival Angle	Power (dB)
1	-0.1394	20
2	+0.3125	20
3	+0.3870	20

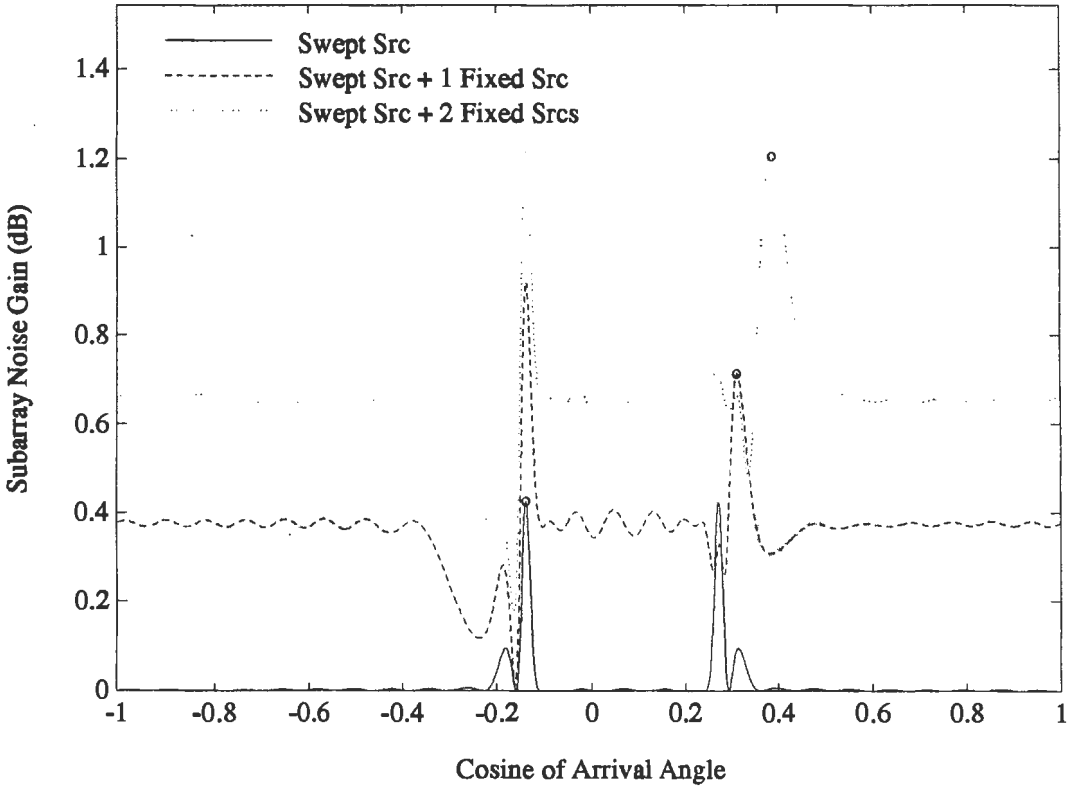

Figure 5.5: Subarray Noise Gain for Three Swept, Dominant Interferers

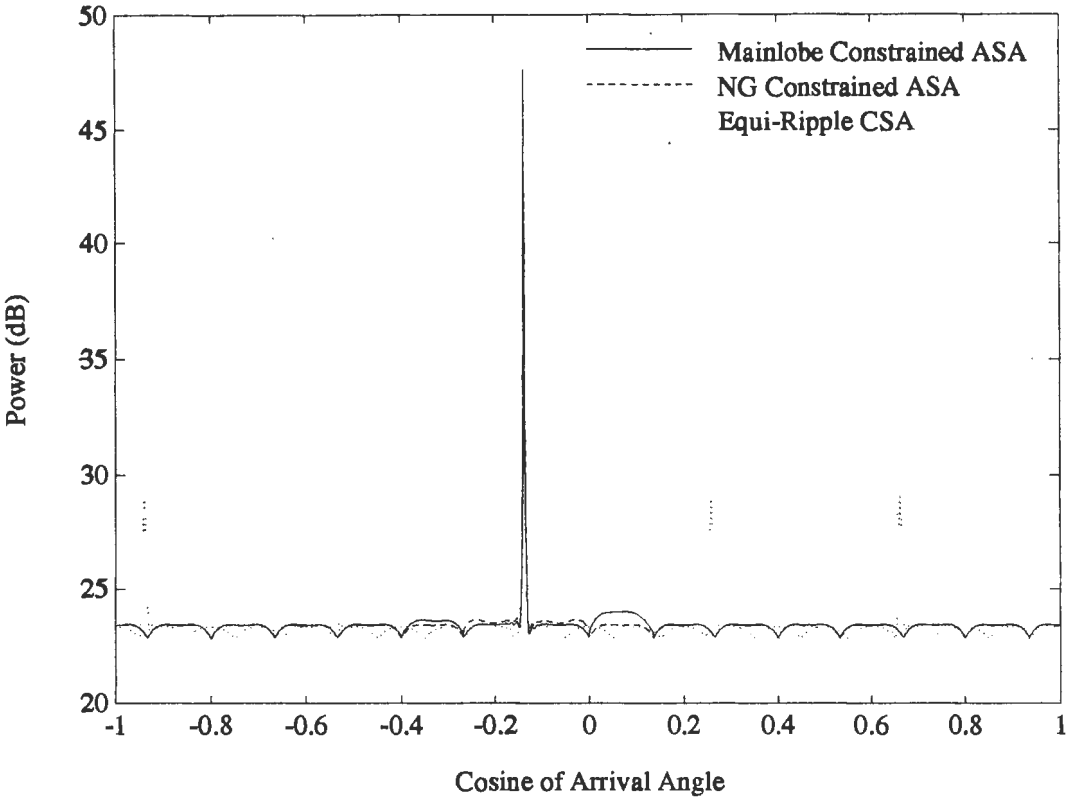

Figure 5.6: Response Patterns for One Dominant Interferer

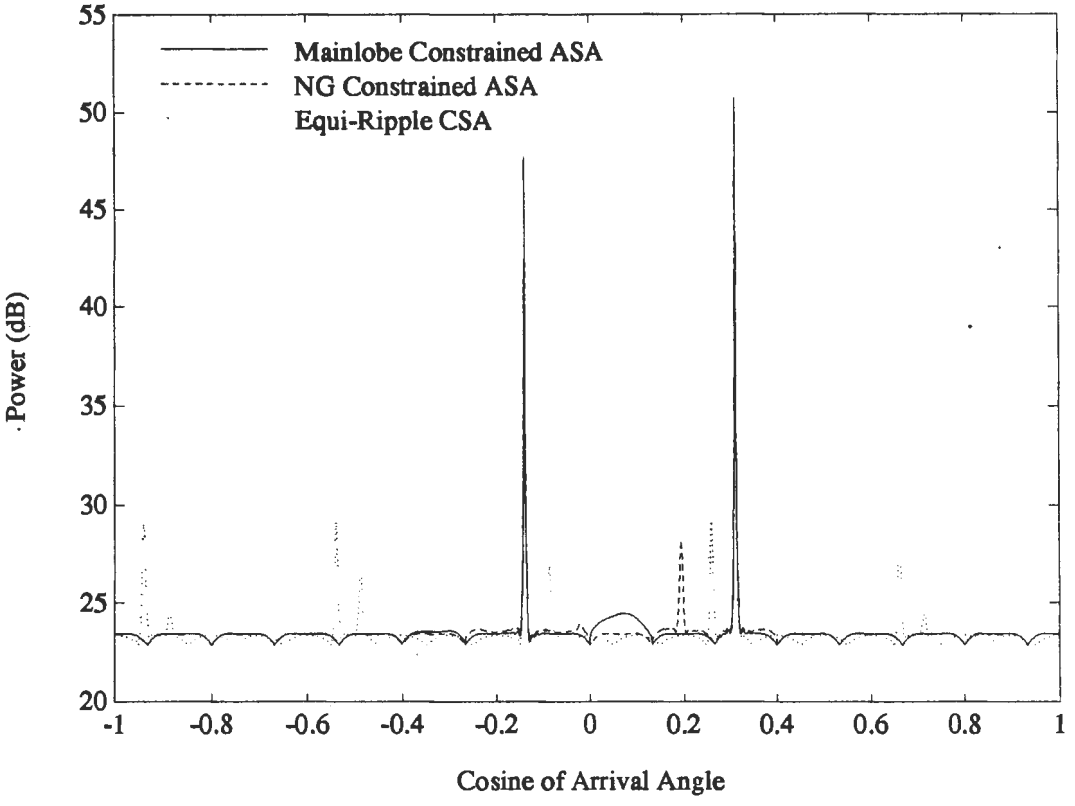

Figure 5.7: Response Patterns for Two Dominant Interferers

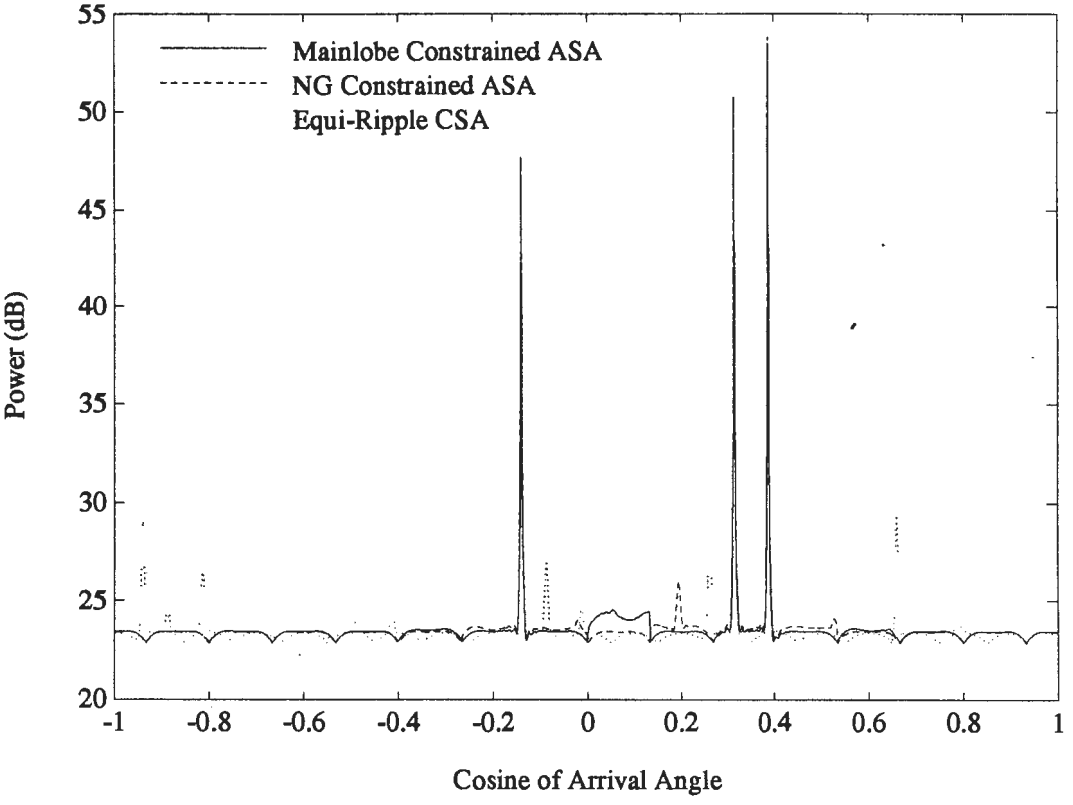

Figure 5.8: Response Patterns for Three Dominant Interferers

Chapter 6

Conclusions

This thesis has introduced the two-stage adaptive-adaptive subarray beamformer (ASA/AFA) and has addressed whether there is an advantage in using this beamformer over the conventional-adaptive subarray beamformer (CSA/AFA). Additionally, it has described practical methods of configuring subarrays, for either the ASA/AFA or CSA/AFA beamformers, to achieve near optimum array gain and effective aperture, while minimizing calculation burden of the overall beamforming system.

Finding the best method to calculate adaptive subarray beams required careful consideration. Viewing the subarray beam as a "directional hydrophone," it was clear that the subarray beam had to be constrained so as to achieve a fixed angular passband, otherwise signals of interest would be cancelled. To achieve the fixed passband a variety of techniques to constrain the subarray beam were proposed; these included derivative, multiple point, and unity gain integral constraints. These methods, termed here subarray passband constraint methods, would pass the subarray beam passband and allow adaptation to cancel interference and noise everywhere else. This strategy satisfied the minimal requirement of creating a subarray beam passband, but the question remained whether these ASA/AFA beamformer would outperform, or even perform as well as, the CSA/AFA beamformer.

To answer whether the subarray passband constraint ASA/AFA beamformer could outperform the CSA/AFA beamformer, the extreme case of a "point" subarray passband constraint (point ASA/AFA) was considered; that is, the subarray and the full array beamformers are constrained at only a single point, termed the look direction. It was discovered that the point

ASA/AFA beamformer cancelled interferers which arrived close to the beamformer look direction, and that the resultant subarray beampattern distortion and noise gain resulted in poorer performance than the CSA/AFA beamformer: it was clear that the strategy of constraining only one point in the subarray passband was not acceptable and needed modification. The question now arose: what is the optimum way to form an adaptive subarray beam?

To find the optimum way to form adaptive subarray beams would require a difficult non-linear, joint optimization of the subarray and full filter vectors. To avoid this difficulty and still gain insight into the optimum strategy, a near-optimum iterative solution of the subarray and full array filter vectors was proposed. It was seen that the behavior of this iterative solution varied with the location of an interferer relative to the beamformer look direction. If the interference arrived in the mainlobe of the subarray beam, the subarray beamformer passed the interference and the full array beamformer cancelled it; conversely, if the interference arrived in the sidelobes of the subarray beam, the subarray beamformer cancelled the interference. These observations established that an adaptive subarray beam must not attempt to cancel interferers arriving in the mainlobe of the subarray beam.

After observing that the near-optimum adaptive subarray beamformer does not cancel interferers arriving in the subarray mainlobe, a sub-optimum approach to forming adaptive subarray beams was suggested: constrain the entire subarray mainlobe and allow adaptation only in the subarray sidelobes. This strategy divided the work between the subarray and full array beamforming stages and allowed each stage to do the work that it did best: the subarray beamformer is best at cancelling interferers in the sidelobes and the full array beamformer is best at cancelling interferers in the mainlobe.

After establishing this strategy for the ASA/AFA beamformer the issue of the relative performances and calculation burdens of the ASA and CSA beamformers was addressed. To do this a practical method of selecting subarray configurations, which met specified requirements in terms of attaining near maximum array gain and alleviating spatial aliasing, was presented. It was shown that the ASA and CSA beamformers have nearly equal calculation burden for configurations with near full effective aperture, and that the CSA beamformer has a lower calculation burden for configurations with less than 80% effective aperture.

Since the ASA beamformer adapts its subarray sidelobes to null interfer-

ences and the CSA can only attenuate these same interferences, it is claimed that the ASA beamformer is a better choice in a dominant interference scenario. Although it was clear that the ASA beamformer could cancel a single dominant interferer placed in the subarray sidelobes, it was not clear how well it could cancel multiple interferers placed in arbitrary locations. The behavior of the ASA beamformer in scenarios with worst-case placements of one, two, and three interferers was then investigated. It was discovered that this worst-case noise gain could become quite large in a subarray beam if sources were placed in certain worst-case locations relative to the subarray beam. It was noted, however, that this undesirable feature could probably be avoided by shifting the positioning and number of subarray beams when the noise gain in a particular subarray beam became too high.

In summary, it has been shown that the ASA beamformer can prevent spatial aliasing in the presence of dominant interferers better than the CSA beamformer, and that the ASA beamformer is roughly equivalent to the CSA beamformer in calculation burden for configurations with near full effective aperture. Because the computational burden of ASA is not less than that of CSA, it is therefore concluded that only in scenarios with dominant interferences is there any advantage to using the ASA beamformer over the CSA beamformer.

Bibliography

[1] Norman Owsley and Douglas Abraham. Preprocessing for high resolution beamforming. In *Proceedings on 23rd Asilomar Conference*, November 89.

[2] M. Kaveh and J. Yang. Adaptive eigensubspace algorithms for direction or frequency estimation and tracking. *IEEE Transactions on Acoustics, Speech, and Signal Processing*, 36(2), February 88.

[3] Ronald D DeGroat. Noniterative subspace tracking. *IEEE Transactions on Signal Processing*, 40(3):571–577, March 92.

[4] M. H. Er and A. Cantoni. An alternative formulation for an optimum beamformer with robustness capability. *IEE Proceedings*, 132(pt. F):447–460, October 85.

[5] Barry D. Van Veen. Minimum variance beamforming with soft response constraints. *IEEE Transactions on Signal Processing*, 39(9):1964–1972, September 91.

[6] J. Justice, N. Owsley, J. Yen, and A. Kak. *Array Signal Processing.* Prentice-Hall, Inc., 87.

[7] S. Lawrence Marple, Jr. *Digital Spectral Analysis with Applications.* Prentice-Hall, Inc., 87.

[8] M. Rendas and J. Moura. Cramer-Rao bound for location systems in multipath environments. *IEEE Transactions on Signal Processing*, 39(12):2593–2610, December 91.

[9] Norman L. Owsley. A standardized test case (STC) for sensor array processing evaluation. Technical Report 8981, Naval Underwater Systems Center, November 91.

[10] Norman L. Owsley. Modern space-time signal processing. University of Connecticut (EE300) Class Notes, January 1991.

[11] Barry D. Van Veen. An analysis of several partially adaptive beamformer designs. *IEEE Transactions on Acoustics, Speech, and Signal Processing*, 37(2):192–203, February 89.

[12] D. A. Gray. Formulation of the maximum signal-to-noise ratio array processor in beam space. *J. Acoust. Soc. Am.*, 72(4):1195–1201, October 82.

[13] Albert H. Nuttall. An approximate FFT technique for vernier spectral analysis. Technical Report 4767, Naval Underwater System Center, 74.

[14] Jeffrey L. Krolik and William S. Hodgkiss. Matched field source localization in an uncertain environment using constraints based on sound speed perturbations. In *OCEANS Proceedings*, pages 771–778, 91.

[15] Sidney P. Applebaum and Dean J. Chapman. Adaptive arrays with main beam constraints. *IEEE Transactions on Antennas and Propagation*, AP-24(5):650–662, September 76.

[16] Henry Cox, Robert M. Zeskind, and Mark M. Owen. Robust adaptive beamforming. *IEEE Transactions on Acoustics, Speech, and Signal Processing*, ASSP-35(10), October 87.

[17] Lloyd J. Griffiths and Kevin M. Buckley. Quiescent pattern control in linearly constrained adaptive arrays. *IEEE Transactions on Acoustics, Speech, and Signal Processing*, ASSP-35(7):917–926, July 87.

[18] David G. Luenberger. *Linear and Nonlinear Programming.* Addison-Wesley Publishing Company, 89.

[19] Alan V. Oppenheim and Ronald W. Schafer. *Digital Signal Processing.* Prentice-Hall, Inc., 75.

[20] Douglas A. Abraham. Reduced dimension adaptive beamforming. Technical Report 8747, Naval Underwater System Center, July 90.

DISTRIBUTION LIST, INTERNAL

New London

D. Abraham	2121
T. Anderson	2152
W. Bernecky	2153
R. Choma	2123
G. Connolly	2192
M. Gouzie	2121
S. Greineder	2121
J. Hall	2152
J. Law	2123
T. Luginbuhl	2121
M. Maguire	2123
A. Nuttall	302
J. Nuttall (5)	2121
N. Owsley	2123
R. Stahl	2121
R. Turner	3314
Library (2)	

Newport

Library (2)